

Investigation of Thorax Response
and Potential for Injury in Side Impacts
Using Integrated Detailed Human
and Vehicle Finite-Element Models

by

Donata Gierczycka

A thesis
presented to the University of Waterloo
in fulfillment of the
thesis requirement for the degree of
Doctor of Philosophy
in
Mechanical and Mechatronics Engineering

Waterloo, Ontario, Canada, 2018

© Donata Gierczycka 2018

Examining Committee Membership

The following served on the Examining Committee for this thesis. The decision of the Examining Committee is by majority vote.

External Examiner	MATTHEW P. REED Research Professor
Supervisor(s)	DUANE S. CRONIN Professor
Internal Member	NAVEEN CHANDRASHEKAR Associate Professor
Internal Member	KAAN INAL Associate Professor
Internal-external Member	JACK P. CALLAGHAN Professor

Author's Declaration

This thesis consists of material all of which I authored or co-authored: see Statement of Contributions included in the thesis. This is a true copy of the thesis, including any required final revisions, as accepted by my examiners.

I understand that my thesis may be made electronically available to the public.

Statement of Contributions

Some of the thesis content has been previously published in the following journal articles:

Gierczycka, D., Watson, B., & Cronin, D. (2015). Investigation of occupant arm position and door properties on thorax kinematics in side impact crash scenarios—comparison of ATD and human models. *International Journal of Crashworthiness*, 20(3), 242-269. © 19 Jan 2015 – <https://www.tandfonline.com/10.1080/13588265.2014.998000>

Brock Watson initially validated the vehicle finite element model used in the study and provided the occupant models pre-set in three positions (30%). Duane Cronin served as a PI and a reviewer of the pre-print of the manuscript (15%). Donata Gierczycka contributed to 55% of the published work.

Gierczycka, D., & Cronin, D. (2017). Occupant thorax response variations due to arm position and restraint systems in side impact crash scenarios. *Accident Analysis & Prevention*, 106, 173-180. © 14 Jun 2017 – <https://doi.org/10.1016/j.aap.2017.05.017>

Duane Cronin served as a PI and a reviewer of the pre-print of the manuscript (10%). Donata Gierczycka contributed to 90% of the published work.

Gierczycka, D., & Cronin, D. (2018). Influence of the chest compression measurement method on assessment of restraint performance in side-impact crash scenarios. *Journal of Biomechanics*, 75, 53-57. © 26 Jun 2018 – <https://doi.org/10.1016/j.jbiomech.2018.04.044>

Duane Cronin served as a PI and a reviewer of the pre-print of the manuscript (10%). Donata Gierczycka contributed to 90% of the published work.

Co-authors agree with the evaluation of the roles and contributions:

Brock Watson




(signature)

June, 19, 2018

(date)

Duane Cronin



(signature)

JUNE 19, 2018

(date)

Abstract

Car accidents are amongst the most common causes of fatalities for a younger population in developed countries and world-wide. While research using Anthropometric Test Devices (ATDs) has led to improvements in frontal impact occupant protection, epidemiological data on the effectiveness of devices for side impact protection remains inconclusive. Current regulatory physical side impact tests are limited to standardized full-vehicle Moving Deformable Barrier and rigid pole impacts, only one seating position of the occupant, and a unidirectional occupant surrogate (side impact ATD). To address some limitations of the existing research methods, and expand the understanding of the occupant response and potential for injury, numerical Human Body Models (HBMs) have been developed as repeatable, biofidelic, omni-directional, and frangible occupant surrogates. The overall goal of this study was to improve the understanding of the underlying sources of conflicting epidemiological and physical test data on thoracic response in side impacts.

This study applied two highly detailed HBMs in parametric investigations with simple to complex impact scenarios ranging from a pendulum, rigid-wall side sled, to a full-vehicle lateral impact and an accident reconstruction. Subsequently, a thoracic side airbag and three-point seatbelt models were developed and integrated with the vehicle model to study the effect of occupant pre-crash position on the potential for injury. Occupant response assessment included global criteria (chest deflection and viscous criterion), local measurements at different thorax levels, spine kinematics, and prediction of rib fracture locations and lung response.

This research identified limitations in current analysis methods, demonstrating effects on occupant response of pre-crash arm position, which is known to vary widely among occupants. The magnitude of the arm effect was dependent on the lateral impact scenario, where the occupant response demonstrated the highest sensitivity to arm orientation in the full vehicle impact. The arm position effect was more significant than changes in response to four restraint combinations, where the assessment of the restraint performance was also dependent on the thoracic response measurement locations and method. A parametric study using detailed HBM, vehicle and restraint models provided new understanding of occupant response in side impact crash scenarios.

Acknowledgements

I would like to sincerely thank my supervisor, Professor Duane Cronin, for being a great role model of academic integrity and high research standards. I greatly appreciate his guidance, encouragement, patience, and trust. The last five years spent at the University of Waterloo have been the greatest challenge and opportunity to grow I could have ever wished for.

Thank you goes to my previous academic supervisor, Professor Cezary Rzymkowski, from the Warsaw University of Technology, and to Dirk Meißner and all colleagues from Takata-Petri AG R&D Center in Berlin, for introducing me to the field of injury biomechanics and mentoring me on my way from undergraduate student to (junior) researcher.

I would also like to express my gratitude for support and motivation I received from Elaine and Murray Mackay, and from the IRCOBI community over the last 13 years. It means a lot to me.

I greatly appreciate financial support from the Natural Sciences and Engineering Research Council of Canada, the Global Human Body Model Consortium, and the Toyota Canada Automotive Safety Graduate Scholarship from the University of Waterloo. I would like to acknowledge Honda R&D Americas for valuable feedback, the Global Human Body Model Consortium for use of the HBM, the National Crash Analysis Center for use of the vehicle model, DYNAmore and Humanetics for the use of the ATD model, the National Highway Traffic Safety Administration for the reference data, and Compute Canada and Sharcnet for the computational resources.

I want to take this opportunity to thank all the people who helped me during my first months in Canada. Many thanks to the Sibiga family, my Unit 95 roommates and friends, and to my co-workers.

A special thank you goes to my parents, for their support and care, and to my siblings, for constantly challenging me to refine my sense of humor.

Dedication

To my best friend.

Table of Contents

Examining Committee Membership	ii
Author's Declaration	iii
Statement of Contributions	iv
Abstract	v
Acknowledgements.....	vi
Dedication	vii
Table of Contents.....	viii
List of Figures	xii
List of Tables	xvii
List of Abbreviations	xix
Chapter 1 Introduction	1
1.1 Motivation for Research.....	4
1.2 Research Objective and Scope	6
1.3 Organization of the Thesis by Chapter.....	6
Chapter 2 Background	9
2.1 Thoracic Injuries Resulting from Automotive Side Crashes	9
2.1.1 Thorax Anatomy.....	9
2.1.2 Thoracic Injury Types in Side Impacts.....	10
2.1.3 Thoracic Injury Criteria in Side Impacts	13
2.2 Occupant Surrogates	16
2.2.1 History of PMHS Tests and Developments.....	16
2.2.2 History of ATD Developments.....	17
2.2.3 History of Human Body Model developments.....	24
2.2.4 The University of Waterloo Human Body Model	25
2.2.5 Summary of the GHMBC-HBM Development.....	31
2.3 Side Impact Safety Assessment.....	34
2.3.1 Occupant Kinematics and Sources of Injury in Side Impacts	36
2.3.2 Side Impact Restraint Systems	38

2.3.3 Side Impact Modeling Using a Full Vehicle Finite Element Model	41
2.4 Limitations of the Existing Research Methods in Predicting Occupant Response	44
2.4.1 Differences in Occupant Surrogates Sensitivity to Pre-Crash Parameters	45
2.4.2 One Standardized Pre-Crash Arm Orientation to Model Driver Position	45
2.4.3 Lateral Impact Type to Represent Side Crash	47
2.4.4 Occupant Response Measurement Method	48
Chapter 3 Verification of Vehicle and Occupant Surrogate Models	50
3.1 Methodology	50
3.1.1 UW-HBM and ATD Model Thoracic Response	50
3.1.2 GHBMCM-HBM Response Assessment	53
3.2 Results	55
3.2.1 UW-HBM Response to Pendulum and Sled Impacts	55
3.2.2 ATD and UW-HBM Chest Compression Response in a Rigid-Wall Sled Test.....	58
3.2.3 Comparison of the UW-HBM and ATD Models Responses to Full-Vehicle Experimental Data	59
3.2.4 Examination of GHBMCM-HBM Occupant and Vehicle Response for a Reconstructed Side Crash Event.....	60
3.3 Discussion	62
Chapter 4 Occupant Surrogate Sensitivity to Door Compliance and Pre-Crash Position	64
4.1 Methodology	65
4.1.1 Variation of the Door Trim Material Properties	66
4.1.2 Arm Position and Door Compliance Interactions.....	69
4.1.3 Arm Position Effect for ATD and UW-HBM Responses	69
4.1.4 UW-HBM and GHBMCM Sensitivity to Arm Position	70
4.2 Results	72
4.2.1 Change of Occupant Response Due to Door Compliance Variation.....	73
4.2.2 Interaction between the Arm Position and Door Compliance	77
4.2.3 Arm Position Effect on Occupant Thorax Response.....	79
4.2.4 GHBMCM and UW-HBM Thorax Response to Varying Arm Position	82
4.3 Discussion	83

4.3.1 Influence of the Door Trim Material Properties	83
4.3.2 Influence of Arm Position in Side Impact	84
Chapter 5 Human Body Model Sensitivity to Lateral Impact Type	89
5.1 Methods	89
5.1.1 Lateral Impact Scenarios	89
5.1.2 Occupant Pre-Crash Position	91
5.1.3 Occupant Response Assessment	92
5.2 Results	92
5.2.1 Concentrated Versus Distributed Load	92
5.2.2 Free-Flight versus Velocity-Pulse	95
5.2.3 Prediction of Lung Contusion Severity and Pattern	96
5.3 Discussion	97
Chapter 6 Occupant Thorax Response Variations Due to Arm Position and Restraint Systems in Side Impact Crash Scenarios	100
6.1 Methods	101
6.1.1 Arm Position, tSAB Location and Pressure Effect for UW-HBM Response	102
6.1.2 GHBMHC-HBM Response to Varying Arm Position and Restraint Combinations	104
6.2 Results	107
6.2.1 Interaction with tSAB Depending on Arm Position Predicted by the UW-HBM	107
6.2.2 Interaction with tSAB Depending on Arm Position Predicted by the GHBMHC- HBM	113
6.2.3 GHBMHC-HBM Spine Kinematics Change Due to Arm Position and Restraints Configuration	115
6.2.4 Side Restraint Combination Effect Assessed with Two Chest Compression Measurement Methods	117
6.3 Discussion	120
Chapter 7 Conclusions	125
7.1 Recommendations and Future Work	127
Letter of Copyright Permission	128

Bibliography	129
Appendix A Supplementary figures for Chapter 4	148

List of Figures

Figure 1.1: (a) Near-side impact location (Otte 2009), (b) road accident fatalities for different impact directions, side category includes near-side and far-side impacts (IIHS 2017), (c) fatal injuries in side impacts by body region (NHTSA 2001) presented with a Human Body Model.....	1
Figure 1.2: Flow chart summarizing the structure and contents of this thesis.....	8
Figure 2.1: (a) Thoracic cage, (b) central left rib (adapted from Gray 1918).....	10
Figure 2.2: (a) Lungs (Gray 1918), (b) alveolar structure (adapted from OpenStax 2013)....	11
Figure 2.3: Calculation of the Viscous Criterion (from Lau 1986). D – initial chest breadth. $D(t)$ – time-history of the chest deflection in mm. $C(t)$ – chest compression, $V(t)$ – chest deformation velocity in m/s.....	14
Figure 2.4: Instrumented PMHS prepared for a rigid-wall sled test (adapted from Pintar 2007).....	17
Figure 2.5: Anthropometric Test Devices representing a 50th percentile male occupant for: (a) frontal – Hybrid III (adapted from humaneticsatd.com), (b) side – ES-2re (adapted from humaneticsatd.com), (c) side – WorldSID (adapted from Hitech.com.sg), and (d) rear – BioRID II (adapted from IIHS.org) impact testing.	18
Figure 2.6: ATD integrated with: (a) a rigid wall sled, (b) pendulum impactor. Measurement of: (c) external forces exerted by the occupant on the impacted wall, (d) internal response of the occupant in terms of displacements and accelerations (adapted from Kuppala 2004).....	19
Figure 2.7: (a) Computational model of the ES-2re ATD (DYNAmore 2015) integrated with a rigid-wall sled model, (b) physical component test utilizing the ES-2re ATD (Aekbote 2007).	21
Figure 2.8: (a) Computational model of the side impact ES-2re ATD thorax, (b) ES-2re rib potentiometer (Stricklin 2009).....	22
Figure 2.9: Calibration tests of the ES-2re ATD: (a) isolated rib module impact, (b) exposed thorax pendulum impact, (c) shoulder pendulum impact (adapted from Watson 2010, Gierczycka et al. 2015).	22
Figure 2.10: Chest deflection in: (a) isolated rib module test for four impact velocities, (b) exposed thorax pendulum impact, (c) pendulum acceleration in the shoulder pendulum impact. Dotted lines: experimental corridors, solid lines: simulated response (Watson 2010, Gierczycka et al. 2015).	23
Figure 2.11: Rib deflection responses of the ES-2re ATD model in the full vehicle FMVSS 214 test (NHTSA #3522, #3482, adapted from Watson 2010, Gierczycka et al. 2015).	23
Figure 2.12: Early developments: (a) finite element model by Huang (1994) under a side sled impact, (b) multibody model by Cheng (1994), (c) finite element THUMS model by Oshita (2001), integrated with a pendulum impactor.	24
Figure 2.13: Thoracic section of the UW HBM, pendulum impact test: (a) front view, (b) lateral view (Forbes 2005).	25

Figure 2.14: Lateral impact scenarios for the UW-HBM model assessment: (a) oblique pendulum, (b) lateral pendulum, (c) WSU-type rigid-wall sled impact, (d) NHTSA-type rigid-wall sled impact.....	26
Figure 2.15: Comparison of the UW-HBM and PMHS kinematics in a 6.67 m/s NHTSA rigid sled impact (Forbes 2005, adapted from Gierczycka et al. 2015).	26
Figure 2.16: Comparison of distances between upper, middle, and lower rib levels of the: (a) UW-HBM, (b) ATD model. Outer layers removed for clarity.....	27
Figure 2.17: UW-HBM chest compression and VC response in 6.7 m/s NHTSA-type rigid-wall sled impact measured at: (a)(b) upper chest band, (c)(d) middle chest band, (e)(f) lower chest band (Yuen 2010, Gierczycka et al. 2015).	29
Figure 2.18: Comparison of the UW-HBM numerical and ATD experimental response at three rib levels in a FMVSS 214 MDB impact (Campbell 2009, 2014).	30
Figure 2.19: Examples of full body model validation setups of the GHBMC-HBM: (a) frontal pendulum, (b) lateral pendulum, (c) full vehicle MDB impact, (d) frontal sled-test (Wang 2014).....	33
Figure 2.20: (a) Location of the pre-defined chest bands in the GHBMC-HBM, (b) lateral breadth of the thorax at one chest band level prior to the crash, (c) change in length due to crash.	34
Figure 2.21: Configuration of the standardized lateral impact tests: (a) Moving Deformable Barrier (adapted from NCAP 2016), (b) pole impact (adapted from EuroNCAP 2018).	36
Figure 2.22: Human Body Model in a side impact scenario: (a) Moving Deformable Barrier test setup (NHTSA 1996), (b) the Human Body Model coupled with the vehicle, showing occupant motion during a side impact event.....	37
Figure 2.23: (a) Ford Taurus model and physical vehicle intrusion, (b) comparison of the vehicle model right front sill velocity to experimental results of 66 mid-sized sedan from MY 1996-1999 range (Watson 2010).	41
Figure 2.24: Deformation time histories of five different location of the vehicle and corresponding physical test results. Simulation results are presented with red solid line, physical test results with dashed line (Watson 2010, from Gierczycka et al 2015).	42
Figure 2.25: (a) Vehicle model integrated with the MDB model, (b) MDB force-displacement response in two validation scenarios, from Watson (2010).	43
Figure 2.26: Numerical models of the: (a) seat (gray) and a three-point seatbelt (red), (b) UW-HBM integrated with the vehicle. Side door removed for clarity.	44
Figure 3.1: Validation scenarios of the occupant surrogate models re-assessed in this thesis.	50
Figure 3.2: (a) The CIREN side crash scenario schematic (CIREN 2018), (b) reconstruction of the crash with the vehicle and Moving Deformable Barrier models.....	54
Figure 3.3: (a) Moving Deformable Barrier test configuration, (b) GHBMC Human Body Model integrated with the vehicle, seat and the restraints.....	55
Figure 3.4: UW-HBM response (blue) for an oblique pendulum impact at 6.7 m/s, PMHS results in gray.....	55
Figure 3.5: UW-HBM response (blue) in a WSU-type rigid-wall sled at 6.7 m/s, compared to PMHS data (gray).	56

Figure 3.6: UW-HBM response (blue) in a NHTSA-type rigid-wall sled test at 6.7 m/s, compared to PMHS data (gray).	57
Figure 3.7: Comparison of the ATD and UW-HBM chest compression and VC responses in a NHTSA-type rigid sled impact at 6.67 m/s at the three rib levels. Experimental corridors and averages are based on PMHS experiments (Pintar et al. 1997).....	59
Figure 3.8: Computational model of the (a) Moving Deformable Barrier impact scenario, (b) ES-2re ATD model integrated with vehicle and restraints, (c) UW-HBM integrated with vehicle and restraints (Gierczycka et al. 2015).....	59
Figure 3.9: Deformation pattern (a) of the physical vehicle (CIREN 2018), (b) predicted by the computational model.....	60
Figure 3.10: Locations of severe thoracic injuries predicted by the GHBMCM-HBM, in agreement with the physical data: (a) rib fractures, (b) diaphragm rupture, (c) spleen laceration.	62
Figure 4.1: Location of the three rib levels in the: (a) UW-HBM model, (b) ATD model, with respect to the vehicle door.	66
Figure 4.2: Vehicle side door, the highlighted door trim section indicates location of the modified elements.....	67
Figure 4.3: Three pre-crash arm positions: (a) vertical, (b) driving, (c) horizontal for the ATD (upper row) and the UW-HBM (bottom row).	70
Figure 4.4: Two Human Body Models integrated with the vehicle in a driving position, unbelted: (a) UW-HBM, (b) GHBMCM-HBM, (c) comparison of the ribcage position with respect to the door, oblique view: UW-HBM (blue), GHBMCM-HBM (red).	71
Figure 4.5: Two Human Body Models integrated with the vehicle: (a) driving position, lateral view, (b) vertical arm position, front view, (c) vertical arm position, lateral view, UW-HBM (blue), GHBMCM-HBM (red).....	71
Figure 4.6: Comparison of the HBM and ATD kinematics in the full vehicle MDB impact.	72
Figure 4.7: Marginal means plots visualizing mean factor effects of and two-factor interactions between the Young's modulus, density, and yield strength for rib deflection, predicted by the UW-HBM at the (a) upper, (b) middle, and (c) lower rib level.	74
Figure 4.8: Half-normal probability plots of the effects at each rib level, for the chest deflection response (mm). E – Young's modulus, rs – interaction between the Young's modulus and density, Es – interaction between the Young's modulus and yield strength. Distinguishable effects marked in red.....	75
Figure 4.9: Pareto charts of effects, for the three rib levels. E – Young's modulus, s – yield strength, r – density. Er – interaction between the Young's modulus and density, Es – interaction between the Young's modulus and yield strength, Ers – interaction between the three factors.	75
Figure 4.10: Pareto charts of effects at three rib levels. A – arm, E – Young's modulus, s – yield strength, AE – interaction between the arm position and Young's modulus, As – interaction between the arm position and yield strength, AEs – interaction between the three factors.	78

Figure 4.11: Marginal means plots visualizing mean factors effects and two-factor interactions between the arm position, Young’s modulus and yield strength, predicted by the UW-HBM at the three rib levels.	79
Figure 4.12: (a) maximum chest deflection, (b) VCmax, predicted by the ATD and UW-HBM models for the three arm positions.	81
Figure 4.13: Comparison of the UW-HBM (blue) and GHBMC-HBM (red) chest compression at three rib levels in a full vehicle side impact in a: (a) standard driving position, (b) vertical arm position.	83
Figure 5.1: Lateral impact scenarios: (P-F) free-flight pendulum, (WSU-F) free-flight WSU rigid sled, (NHTSA-F) free-flight NHTSA rigid sled, (P-V) velocity-pulse pendulum, (NCAP-V) velocity-pulse full vehicle NCAP (Gierczycka and Cronin 2015a).	90
Figure 5.2: Examples of the two arm positions for the lateral impact conditions: <i>arm up</i> in orange, <i>arm down</i> in blue, (a) pendulum impacts, (b) rigid-wall sled impacts, (c) full vehicle impacts.	91
Figure 5.3: Patterns of the peak values of chest compression at three rib levels, two arm positions: arm up (orange) and arm down (blue); (a) free-flight pendulum (P-F), (b) WSU-type rigid-wall sled (WSU-F), (c) NHTSA-type rigid-wall sled (NHTSA-F), (d) velocity-pulse pendulum (P-V), (e) full-vehicle impact. Chest compression patterns reflect the lateral impact direction, according to experimental standards (left for rigid-wall sled and vehicle, right for pendulum).	94
Figure 5.4: Maximum (a) chest compression, (b) VC (m/s) for free-flight and velocity-pulse impacts.	95
Figure 5.5: Predicted total contused lung volumes for two arm positions, for all loading types.	96
Figure 5.6: Predicted contused lung volumes for (a) WSU-F scenario, (b) NCAP-V scenario, for the two arm positions.	97
Figure 6.1: Restraint models: (a) inflated tSAB, (b) seat with a three-point seatbelt.	102
Figure 6.2: (a) four considered tSAB locations; UW-HBM with varying arm positions: (b) horizontal, (c) vertical.	102
Figure 6.3: Restraint system configurations for vehicle side-impact scenario (Gierczycka et al. 2018).	104
Figure 6.4: GHBMC-HBM pre-crash position: (a) arms in driving position, (b) arms in vertical position.	105
Figure 6.5: Chest compression measurement location: (a) tissue outer contour with chest-band locations marked with respect to the ribcage, (b) chest-band (CB) method, (c) rib-deflection (RD) method (Gierczycka et al. 2018).	106
Figure 6.6: Predicted locations of rib fractures, left view, and contused lung pattern: (a) horizontal, and (b) vertical arm position.	108
Figure 6.7: Normal plots of the effects at each rib level and maximum overall value, for the UW-HBM model chest deflection response (upper row) and the Viscous Criterion (lower row). Magnitude of the effect plotted on the abscissa for each metric, distinguishable effect marked in red.	109

Figure 6.8: UW-HBM response at three rib levels for the horizontal arm position (H), with a tSAB combination that reduced (green) and increased (red) the injury metrics with respect to a case with no tSAB (gray).	110
Figure 6.9: UW-HBM response at three rib levels for the vertical arm position (V), with a tSAB combination that reduced (green) and increased (red) the injury metrics with respect to a case with no tSAB (gray).	111
Figure 6.10: Normal plots of the effects, magnitude of the effect plotted on the abscissa for each of the metrics, distinguishable effects marked in red.	112
Figure 6.11: Marginal means plots visualizing mean factor effects of two-factor interactions predicted by the UW-HBM.	113
Figure 6.12: Thoracic side airbag (tSAB) effect for a driving (aD) versus vertical (aV) arm position for an unbelted occupant, measured at three chest band (CB) levels: (a) chest compression, and (b) Viscous Criterion (VC). The highest increase in chest compression and VC due to vertical arm position indicated by arrows. Injury criteria threshold values marked with a red dashed line.	114
Figure 6.13: Kinematics and visualization of spine tracking of the GHBMCM-HBM during the lateral MDB impact. Unbelted, no tSAB, vertical arm position case (aV-B-tSAB).	115
Figure 6.14: Spine kinematics (T1, T6, T11, L3, and pelvis) for four unbelted cases: drive no thoracic side airbag (tSAB), drive with tSAB, vertical no tSAB, vertical with tSAB. Vertical distance was measured from the ground, lateral distance from body centerline (0 at time=0).	116
Figure 6.15: Spine kinematics (T1, T6, T11, L3, and pelvis) for driving arm position cases and different restraint combinations: unbelted no tSAB, unbelted with tSAB, belted no tSAB, and belted with tSAB. Vertical distance was measured from the ground, lateral distance from body centerline (0 at time=0).	117
Figure 6.16: Chest compression for unbelted and belted configurations without the tSAB, measured with RD and CB methods.	117
Figure 6.17: Rib fracture locations for the: (a) unbelted, no tSAB, (b) belted, no tSAB. Frontal and lateral view of the GHBMCM-HBM ribcage post-crash. Eroded elements marked as black solid.	118
Figure 6.18: Chest compression values for unbelted and belted configurations with the tSAB, measured with RD and CB methods on the GHBMCM-HBM.	119
Figure 6.19: Rib fracture locations for the: (a) unbelted, no tSAB, (b) belted, no tSAB. Frontal and lateral view of the GHBMCM-HBM ribcage post-crash. Eroded elements marked as black solid.	119
Figure A.1: Marginal means plots visualizing mean factors effects and two-factor interactions between the Young's modulus, density, and yield strength, predicted by the ATD at the three rib levels.	148
Figure A.2: Comparison of chest deflection time histories of the UW-HBM and ATD at three rib levels.	149
Figure A.3: Comparison of Viscous Criterion time histories of the UW-HBM and ATD at three rib levels.	150

List of Tables

Table 2.1: Thoracic injury with a corresponding AIS scale (adapted from Cavanaugh 2002).	12
Table 2.2: Biofidelity scores of three side impact ATDs (Scherer 2009) [scale 0-10; 10 is best].	19
Table 2.3: A rating scale describing the correlation.	20
Table 2.4: A rating scale describing sensitivity.	20
Table 2.5: UW-HBM model biofidelity assessment method (from Yuen 2010).	28
Table 2.6: Assessment of the UW-HBM chest compression response in a NHTSA 6.67 m/s rigid sled impact, by loading phase (from Yuen 2010).	28
Table 2.7: Number of rib fractures observed in PMHS rigid sled experiments compared to UW-HBM simulations (adapted from Yuen 2010).	31
Table 2.8: Number of test configurations to verify body region level response (GHBMC 2014).	32
Table 2.9: Test configurations to verify full body model response (GHBMC 2014).	33
Table 2.10: Summary of experimental studies on tSAB effectiveness (adapted from Gierczycka and Cronin 2017).	40
Table 3.1: The UW-HBM response verification and verification scenarios simulated in previous studies (Forbes 2005, Campbell 2009, Yuen 2010), and repeated for the purpose of this thesis (bold font).	51
Table 3.2: The ES2-re ATD model response verification and verification scenarios simulated during previous studies and repeated for the purpose of this thesis (bold font).	52
Table 3.3: Comparison of rib deflection values (mm) at three rib levels for the physical and computational test surrogates (NHTSA 2000) subjected to a FMVSS 214 MDB impact in a Ford Taurus vehicle.	60
Table 3.4: Injuries sustained by the physical occupant in a side crash (CIREN 2018).	61
Table 4.1: Baseline and extreme values for the door trim ABS material properties.	67
Table 4.2: Coded (Table 4.3) experimental design for the eight runs of the factorial design.	68
Table 4.3: Description of the experimental factors and variable codes.	68
Table 4.4: Coded experimental design for the eight runs of the factorial design.	69
Table 4.5: Description of the experimental factors and variable codes.	69
Table 4.6: Comparison of rib deflection values for the computational occupant surrogates subjected to a NCAP (61 kph) impact.	73
Table 4.7: Average CORA rating for the occupant responses compared at three rib levels between baseline-low, and baseline-high material properties setting.	76
Table 4.8: Percentage change of the maximum global response with respect to the baseline case for both occupant surrogates and all modified material properties.	77
Table 4.9: Chest deflection responses predicted by the ATD and UW-HBM at all three rib levels for three pre-crash arm positions (maximum values shown in bold).	80
Table 4.10: Average cross-correlation rating for the occupant responses compared at three rib levels between driving-horizontal, driving-vertical, and vertical-horizontal arm positions.	80

Table 4.11: Viscous Criterion responses predicted by the ATD and UW-HBM at all three rib levels for three pre-crash arm positions (maximum values shown in bold).....	81
Table 5.1: Summary of standard lateral impact conditions.	90
Table 5.2: Relative changes in occupant metrics due to <i>arm down</i> pre-crash position.	93
Table 6.1: Description of the experimental factors and variable codes.	103
Table 6.2: Coded experimental design for the eight runs of the fractional factorial design.	103
Table 6.3: Simulation configurations (aD = arms in driving position, aV = arms in vertical position, -B = unbelted, +B = belted, -tSAB = without tSAB, +tSAB = with tSAB deployed).	105
Table 6.4: Maximum chest compression and Viscous Criterion results (aD = arms in driving position, aV = arms in vertical position, -B = unbelted, +B = belted, -tSAB = without tSAB, +tSAB = with tSAB deployed) normalized with respect to injury criteria thresholds.	114
Table 6.5: Effect of the restraints on chest compression for the two measurement methods	121
Table 6.6: Two-factor interactions aliased due to the experimental design of the fractional factorial experiment.	124
Table A.1: Chest deflection and VC response on different chest band levels. Base – baseline material properties. Low – lower boundary for material properties. High – upper boundary for material properties.	151
Table A.2: Correlation ratings on three rib levels: d – driving position, h – horizontal position, v – vertical position. Base – baseline material properties, low – lower boundary for material properties, high – upper boundary for material properties.	152

List of Abbreviations

1-D	One-dimensional
2-D	Two-dimensional
ABS	Acrylonitrile Butadiene Styrene
AIS	Abbreviated Injury Scale
ARDS	Acute Respiratory Distress Syndrome
ATD	Anthropometric Test Device (crash test dummy)
BioRID	Biofidelic Rear Impact Dummy
C, C(t)	Chest compression
CB	Chest band
CDCP	Centers for Disease Control and Prevention
CG	Centre of Gravity
CII	Crash Induced Injury
CIREN	Crash Injury Research
CORA	Correlation and Analysis
CT	Computer Tomography
D(t)	Chest deflection
ECE	Economic Commission for Europe
ES2-re	European Side Impact Dummy with rib extensions
EuroNCAP	European New Car Assessment Program
FE	Finite Element
FMVSS	Federal Motor Vehicle Safety Standard
GHBMC	Global Human Body Models Consortium
HBM	Human Body Model
HUMOS	Human Model for Safety
IIHS	Insurance Institute for Highway Safety
IRCOBI	International Research Council on Biomechanics of Injury
ISO	International Standards Organization
LSTC	Livermore Software Technology Company

MDB	Moving Deformable Barrier
MY	Model Year
NBDL	Naval Biodynamics Lab
NCAP	New Car Assessment Program
NHTSA	National Highway Traffic Safety Administration
PC	Pulmonary Contusion
P-F	Free-flight pendulum
PMHS	Post-Mortem Human Surrogate
P-V	Velocity-pulse pendulum
R&D	Research and Development
RD	Rib deflection
SAB	Side airbag
SUV	Sport utility vehicle
THUMS	Total Human Model for Safety
tSAB	Thoracic side airbag
USSID	United States Side Impact Dummy
UW-HBM	University of Waterloo Human Body Model
V, V(t)	Chest compression velocity
VC	Viscous Criterion
VCmax	Maximum Viscous Criterion
WHO	World Health Organization
WorldSID	World Side Impact Dummy
WSU	Wayne State University

You cannot hope to build a better world without improving the individuals.
To that end, each of us must work for our own improvement.

-Maria Skłodowska-Curie

Chapter 1

Introduction

Although heart disease and cancer comprise the leading causes of death in developed countries (128,588 deaths in Canada and 1,229,772 in the United States in 2015) (Statistics Canada 2018; Heron 2017), car accidents remain the leading cause of death amongst young people (15-30 years old) and are the 8th significant cause of fatalities for all ages worldwide (WHO 2018). In 2016 there were 23,793 passenger vehicle fatalities in the United States (IIHS 2017) and 1,858 in Canada (Transport Canada 2017), constituting 16% of accidental deaths in both countries (Statistics Canada 2018; Heron 2017). Vehicle drivers constituted 74% of fatally injured occupants (IIHS 2017). The introduction of advanced safety systems has reduced the number of road deaths in recent years in mostly highly motorized countries; however, the number of injured occupants remains high (Schmitt 2014). Within Canada, 115,956 occupants were injured in motor vehicle traffic collisions in 2017 (Transport Canada 2017).

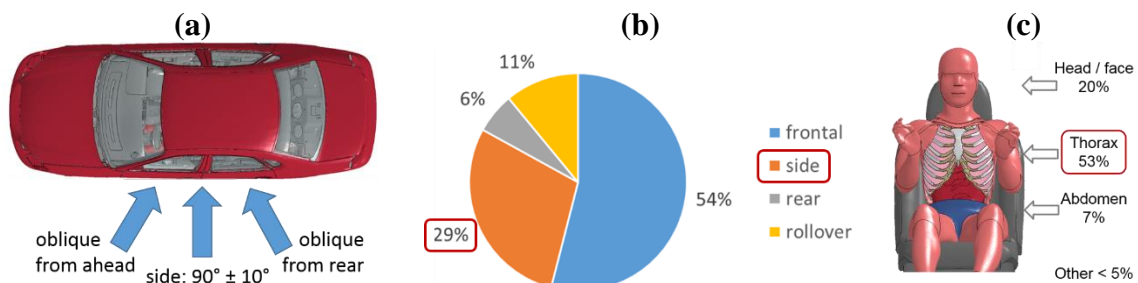


Figure 1.1: (a) Near-side impact location (Otte 2009), (b) road accident fatalities for different impact directions, side category includes near-side and far-side impacts (IIHS 2017), (c) fatal injuries in side impacts by body region (NHTSA 2001) presented with a Human Body Model.

Although frontal impact protection has been a high priority for many years, side impacts have only received serious attention over the last couple of decades and remain a challenge, due to a limited structural crush zone and space for the restraint systems such as side impact airbags and curtains to operate. Vehicle-to-vehicle side impact in this context

encompasses collisions where a striking vehicle impacts a target vehicle at $90^\circ \pm 10^\circ$, at the location of the driver (near-side) or the passenger (far-side) door (Otte 2009) (Fig.1.1a). In 2016, 29% of road deaths in North America (IIHS, 2017) were attributed to side crashes (Fig.1.1b).

Side impacts were estimated to be 2.26 more likely to result in fatal injury compared to frontal impacts (Bedard et al. 2002), based on the Fatal Accident Reporting System (FARS) data from 1975-1988. Severe to fatal injuries to the thorax were observed in 53 to 58% of front seat occupants in near-side impacts (NTHSA 2001, Kahane 2007) (Fig.1.1c), and pulmonary contusion (PC), which is a serious injury resulting from thoracic blunt trauma, was sustained by 26.9% occupants in near-side impacts, where the PC frequency for occupants injured in frontal impacts was 15% (O'Connor 2009). Therefore, injury mechanisms to the thorax, defined as mechanical interaction with the human body that results in injury to the human body (Schmitt 2014), require further research in the side impact scenarios.

Countermeasures have been implemented to reduce the relative velocity between the intruding vehicle door and occupant to mitigate injury severity in side impacts. In addition to side door padding (Strother et al. 1984), the introduction of side impact airbags has resulted in an overall reduction of injuries in side impacts, but to a smaller extent than was expected (Aldaghlis 2010, Gaylor and Junge 2015, Griffin 2012, Kahane 2014, Maltese 2002, Tencer 2005, Weber 2004, Viano and Parenteau 2016, Welsh 2007, Yoganandan 2005, Yoganandan 2007). While side curtain air bags were estimated to reduce fatalities by 25-37% for driver and front passenger due to a reduction of head injuries, the inclusion of torso airbags in vehicles has only reduced thoracic injuries in near-side impacts by 8% on average (Kahane 2014, McCartt and Kyrychenko 2007). However, in far-side impacts, tSABs were associated with an increase of fatal injury risk for driver and passenger (+4.9%), attributed to a wide range of potential impact forces and directions, and occupant pre-crash position (Kahane 2014). Furthermore, experimental tests by Viano and Parenteau (2016) demonstrated a negative outcome of tSABs for predicted thoracic injury (+22% increase).

Welsh (2007) suggested that proper representation of the load transfer in the side impact by the occupant surrogate is essential for realistic prediction of real-world occupant

injuries. Human volunteers can participate in non-injurious tests only; therefore, impact tolerance testing requires representative surrogates. Injurious experimental tests utilize animals, Post Mortem Human Subjects (PMHSs), and standardized reusable mechanical human models or Anthropometric Test Devices (ATDs). To date, most of the focus has been on the mid-sized male, often termed the 50th percentile male. More recently side impact testing has been conducted with an ATD with reference dimensions based on the 5th percentile female stature and body weight. Current regulatory tests use ATDs in specific loading scenarios and seating positions (McNeill 2005, NHTSA 2006, NHTSA 2012). ATDs are designed to represent the human body in terms of dimensions and impact response, and to provide a repeatable response to test impact conditions for which they were designed (frontal, side, rear impact). For vehicles sold in the United States and Canada, occupant restraints, protective systems and vehicle structures are tested for side impact compliance (e.g. FMVSS 214) (NHTSA 2012a) and performance (e.g. NCAP) (NHTSA 2012a) with use of a Side Impact Dummy (SID-II) or the Euro-SID (ES-2re) ATDs. In both cases a stationary vehicle is impacted with a moving deformable barrier (MDB) representing a striking mid-sized sedan vehicle, at 61 kph/38 mph (NCAP) or 54 kph/33.5 mph (FMVSS and CMVSS 214). The ATDs are equipped with load cells and accelerometers that measure the occupant kinematic and kinetic response during the test impacts. However, ATDs are not frangible, which means that they are not capable of demonstrating failure of tissues that may occur in the human body, corresponding to traumatic injury. In contrast, HBMs are biofidelic, frangible human occupant surrogates that can be used in parametric studies and side impact testing in a range of seating positions.

Human Body Models (HBMs) represent important structural and life-sustaining tissues in the human body in detail. HBMs began with simple spring-mass-damper models in the 1970's (Lobdell 1971) and progressed to multi-body models in 1990's (Cheng 1994). More recently, advances in computational power have led to the development of detailed human body models, including the University of Waterloo Human Body Model (UW-HBM) (Forbes 2005, 2006; Yuen 2008, 2010), Total Human Model for Safety (THUMS) (Oshita et al. 2001), and the Global Human Body Models Consortium HBM (GHBMC-HBM) (GHBMC 2014).

HBM s include high-resolution representation of hard and soft tissues, nonlinear material properties, and in some cases, the ability to directly simulate injury in impact scenarios through material failure. HBM s enhance analysis capability, providing the ability to evaluate non-traditional load scenarios or different initial body positions. HBM s are suitable for impacts from any direction, whereas most ATDs are designed specifically for frontal, side or rear impacts. Further, new scientific knowledge obtained through biomechanical testing can be applied directly to detailed HBM s, as they explicitly include important structural tissues. This knowledge cannot be used directly in physical ATDs without re-designing, calibrating and validating with respect to physical ATD test data (Wismans 2005). Experience has shown that incorporating new human response data into ATDs may take several years or even several decades (Albert et al. 2018).

1.1 Motivation for Research

Researchers have highlighted a need to understand injury mechanisms and sources of differences between the field data and laboratory test results and injury predictions (Aldaghl as 2010, Hallman 2008, Loftis 2011, Luzon-Narro 2014, McNeill 2005, Samaha 2003, Tencer 2005a, Yoganandan 2007). Several studies have compared the responses of ATD and HBM models and the corresponding injury predictions. Baudrit et al. (1999) evaluated the response of the frontal impact ATD (Hybrid III), side impact ATD (EuroSID), and an HBM (Lizee 1998) in a side impact. Comparison of the thoracic deflection and VC varied depending upon the model used, and the differences were related to a relatively coarse mesh and limited material properties in the early finite element models, a consequence of limited computational capacity. Pyttel et al. (2007) found large differences in predicted deformations and accelerations comparing the EuroSID ATD and an early finite element HBM response in side impact (ESI H-model, Choi et al. 1999), and suggested that the injury criteria calculated with the ATD model may not represent individual characteristics of the human body, such as geometry of the thorax, arm, and the pelvis segment. Importantly, HBM allow for loading on individual ribs and the injury risk to be assessed directly; whereas the ATD models can only infer the potential for thoracic injury through a response metric such as chest deflection.

Depending on the occupant's posture at the time of impact, the arm can be a primary load transmission interface between the door and the occupant thorax. Consequently, investigators have examined the effect of the arm position and compliance on the thoracic response (Tencer 2005ab, Yoganandan 2013). However, minimal data are available regarding the effect of initial occupant arm position on injury response in side impact crash scenarios (Viano 1991, 1994, Watson and Cronin 2011). Several authors investigated the effect of arm position with different results, depending on the occupant model chosen (ATD or PMHS) and on the test scenario (free-flight, velocity pulse, distributed or concentrated load). In most cases, the PMHS were observed to be sensitive to arm position while ATD tests did not show a significant effect. For free-flight impacts, the kinetic energy of the impactor is absorbed by body of the occupant body until the impactor and body move at a common velocity, the PMHS arm in the loading path was observed to reduce the number of rib fractures. Experiments included concentrated load impacts (pendulum) (Kemper 2008), and showed similar results when the PMHS was dropped from a height of 1 m on a rigid surface with arms above the head or in the driving position (Stalnaker 1979). Other researchers did not identify the effects of arm position on injury in free-flight pendulum tests (Cesari 1981). Studies on the ATD response to lateral impact with different arm positions demonstrated no sensitivity of the ES-2re ATD to the test configuration (Trosseille 2010), and Dalmotas (1991) suggested that effect of the arm in the loading path investigated with use of the ATDs could mask the effect of different restraint designs on the injury response.

Although physical tests using PMHS provide important insights into impact response, they are costly and sensitive to variance introduced by test subjects. Tests involving ATDs have led to improvements in occupant safety, but many investigators have suggested that further improvements in safety systems could be achieved by introducing new computational analysis tools (Aldaghlis 2010, Hallman 2008, Klaus 1983, Loftis 2011, Lorenzo 1996, Luzon-Narro 2014, McNeill 2005, Samaha 2003, Tencer 2005ab, Yoganandan 2007). Information collected during the physical tests is limited to pre-arranged measured parameters, such as displacements, forces, and accelerations, and many desired variables are difficult to measure without unacceptable levels of tissue disruption. Numerical models with relevant verification

and validation (ASME 2006) enable in-depth analysis, covering not only the global responses but also component, material or tissue level responses, to bridge the gap between the ATDs and human occupants, as more anatomically accurate and biofidelic surrogates. HBMs enable detailed parametric on occupant response in complex impact scenarios, providing repeatable test conditions that reduce variance associated with physical experiments.

1.2 Research Objective and Scope

This thesis provides a new understanding of occupant response in side impact scenarios and identifies underlying sources of conflicting epidemiological and physical test data with respect to the effectiveness of thoracic restraints. A range of impact scenarios, from simple pendulum and rigid-wall side sled tests to a full-vehicle side crash and accident reconstruction, were investigated in parametric studies with two state-of-the-art HBMs. The effect of occupant pre-crash position and interaction with door padding, a three-point seatbelt, and thoracic side airbag on the potential for thoracic injury was assessed in terms of global criteria (chest deflection, VC), local measurements at different thorax levels, spine kinematics, predicted rib fracture locations, and lung strain, strain rate, or pressure response. Limitations of current side impact research methods were identified through a demonstration of occupant response variation due to pre-crash position, where the highest sensitivity to arm orientation was observed in full vehicle impacts. Side restraint effectiveness assessment was demonstrated to be dependent on the thoracic response measurement method and location. However, the arm effect was significantly more pronounced than the differences among the four restraint combinations considered in this thesis.

1.3 Organization of the Thesis by Chapter

This thesis is organized into seven chapters, including the introduction (Chapter 1) (Fig.1.2). Chapter 2 provides background information on side impact kinematics, and statistics related to automotive injuries types, severity, and criteria with focus on the thoracic anatomy and trauma relevant to side impact crash scenarios. An overview of occupant surrogates used in side impact testing is provided, including a summary of development of the two HBMs used in this thesis. The advantages and limitations of each occupant surrogate are discussed. Lateral impact testing

scenarios used to represent vehicle side crashes are presented along with the processes for verification and validation processes of computational vehicle, seat, and restraint models with respect to experimental data. The epidemiological and experimental studies on thoracic side airbags (tSABs) effectiveness are reviewed. Lastly, limitations of existing research methods are highlighted.

Chapter 3 summarizes a lead-in study to investigate and verify the thorax response for the HBM in impact scenarios using the UW-HBM and GHBMC-HBM. The process of integrating the occupant with vehicle, seat, and restraints is explained. Simulation results are compared to existing experimental and real-world crash data on occupant injury.

Chapter 4 presents the results of a study on occupant surrogate response sensitivity to door compliance and arm pre-crash position. Occupant response was evaluated using both global and local rib-level response. Interactions between the arm position and door trim material properties were analyzed. This chapter demonstrates high sensitivity of the UW-HBM injury response to parametric changes, where the arm position effect is the most significant.

Chapter 5 details an evaluation of the effect of arm position on occupant response, depending on the side impact loading type. The UW-HBM response in full vehicle scenario discussed in Chapter 4 is compared to standardized biomechanical pendulum and rigid-wall sled tests. The UW-HBM response is discussed with respect to past hypotheses on the arm position effect in side impacts, and recommendations for a side impact scenario to represent vehicle side crash are outlined.

Chapter 6 discusses the effect of variations of restraints parameters and combinations in interaction with two pre-crash arm positions for occupant response. The contribution of four thoracic side airbag (tSAB) locations, two tSAB pressure settings and two seatbelt configurations (belted / unbelted) for predicted occupant injury severity are compared, considering the effect of occupant arm position. Chest compression methods specific for PMHS and ATDs are compared to examine the occupant response and interaction with the seat belt system and tSAB. The dependence of restraint performance assessment on the response measurement method used are demonstrated.

Chapter 7 summarizes the overall conclusions, demonstrating the potential of HBM to improve understanding the underlying sources of conflicting epidemiological and physical test data on thoracic response in side impacts. This thesis enabled an identification of limitations in current methodology, demonstrating a variation in occupant response due to the pre-crash arm position. Future research directions and recommendations for application of the HBMs for the improvement of occupant protection are discussed.

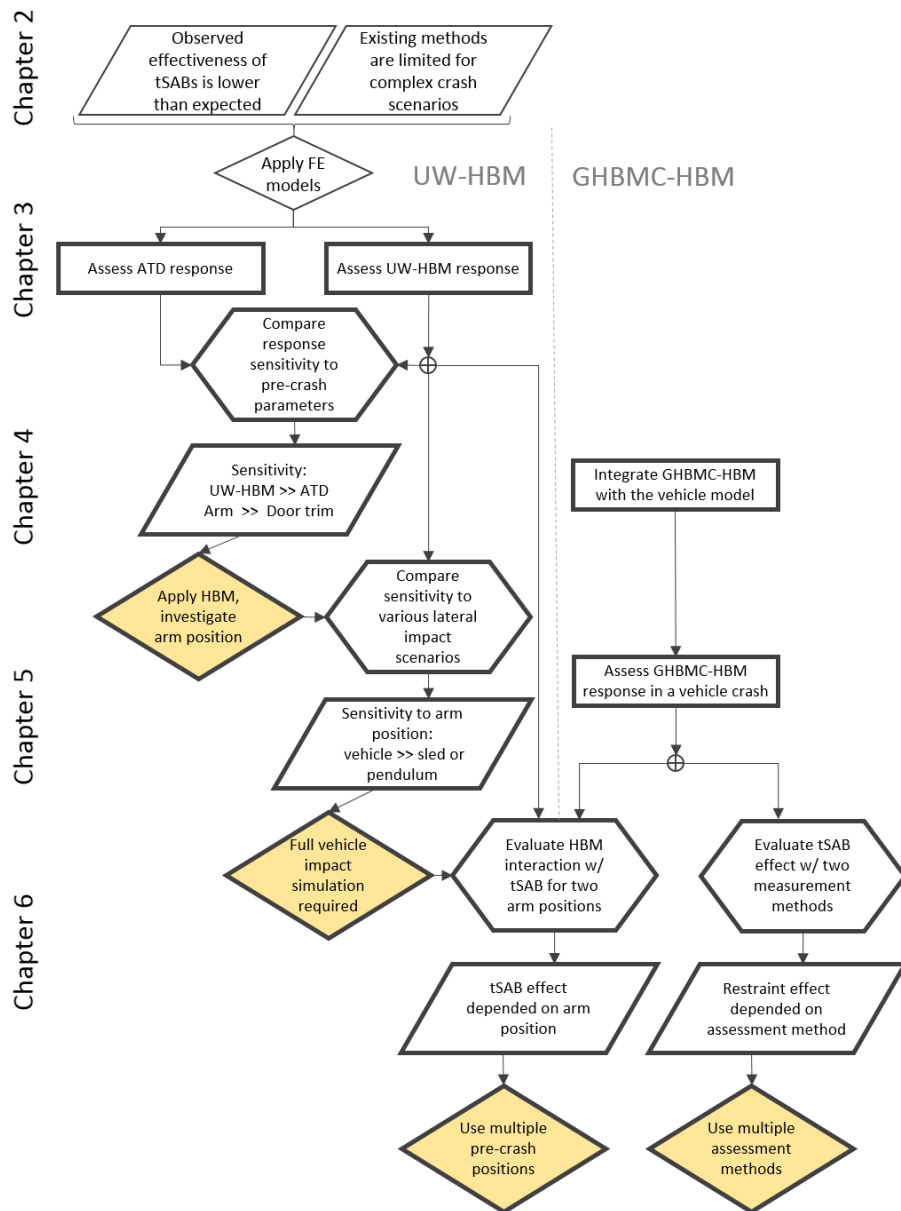


Figure 1.2: Flow chart summarizing the structure and contents of this thesis.

Chapter 2

Background

2.1 Thoracic Injuries Resulting from Automotive Side Crashes

Blunt chest trauma is associated predominantly with vehicle crashes (60-70% of chest injuries) (Weaver et al. 2013), and injuries to the thorax are responsible for 58% of fatalities in side impacts (Kahane 2007). More specifically, pulmonary contusion (PC) is a common blunt trauma injury resulting from side impact loading. PC accounts for over 35% of serious thoracic injuries (Danelson et al. 2015) and is the most significant contributor to the development of potentially fatal acute respiratory distress syndrome (ARDS) (Becher 2012). A brief overview of thoracic anatomy and injury is presented in this chapter, followed by an introduction to the physical and numerical human surrogates used in vehicle development and testing.

2.1.1 Thorax Anatomy

The upper part of the human trunk between the abdomen and neck is referred to as thorax. The thoracic cage comprises hard tissues, namely ribs, vertebrae, and sternum, connected by costal cartilage and intervertebral disks (Fig.2.1a), and supports soft tissues: muscles, fascia, vessels, nerves, and skin. This combination of hard and soft tissues, referred to as the thoracic wall, protects the internal organs (Fig.2.2a) in the thoracic and abdominal region from external and internal loads, and provides structure to enable breathing. The thorax also provides attachment points for the musculature of the upper body, including the upper extremities.

Ribs are considered as long bones, because their length significantly exceeds the transverse dimensions (Fig.2.1b), and comprise a dense cortical bone shell filled with trabecular bone. Ribs 1-7 are called vertebrocostal (true) ribs, and connect thoracic vertebrae with the sternum through a costal cartilage extension. Ribs 8-10, called vertebrochondral (false) ribs, indirectly connect thoracic vertebrae with the sternum, attaching to costal cartilage of ribs immediately superior to them. Free (floating) ribs, 11-12, originate at the thoracic vertebra and connect at the end to posterior muscles of the abdomen.

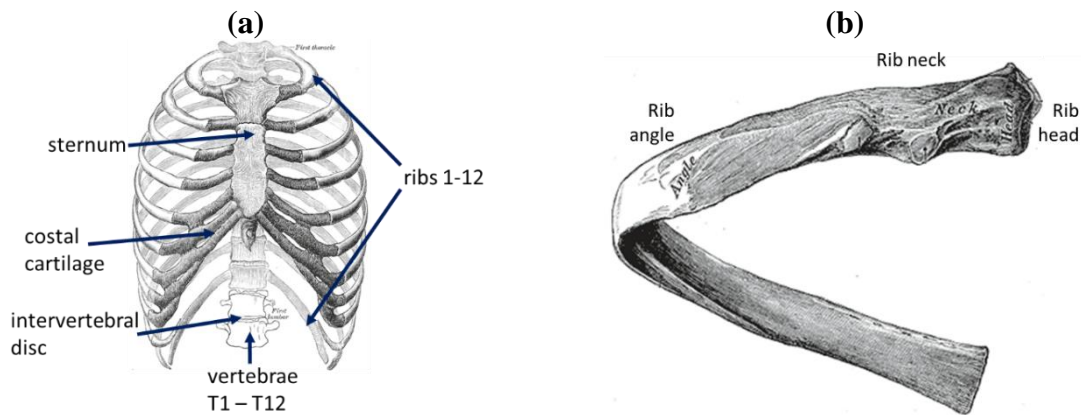


Figure 2.1: (a) Thoracic cage, (b) central left rib (adapted from Gray 1918).

Internal organs enclosed within the thoracic cage comprise the heart, lungs, and vessels (aorta, pulmonary artery, and smaller vasculature) (Fig.2.2a). The lungs are divided into lobes, two for the left lung, three for the right lung, and their primary function is to transfer oxygen and carbon dioxide between air and blood. The exchange occurs during a diffusion process at the level of the alveoli, which are microscopic air sacs (0.2-0.3 mm in diameter, Weibel 1977) wrapped in capillaries (Fig.2.2b). Clusters of alveoli form alveolar sacs, which then connect to respiratory bronchioles through alveolar ducts. Respiratory bronchioles connect to terminal bronchioles that run to higher order bronchi, and eventually to the main bronchi and trachea.

The heart fits in the space between the lungs (Fig.2.2a), pumping blood in two circuits: first, drawing oxygenated blood from the pulmonary circuit (lungs) and pumping it to the systemic circuit, i.e., throughout the body, and second, pushing venous, deoxygenated blood to the pulmonary circuit.

2.1.2 Thoracic Injury Types in Side Impacts

Injuries to the thorax can be classified as either hard tissue (ribcage) injuries or soft tissue injuries. Rib fractures occur most often at the mid-thorax level, at the greatest curvature of the rib (Fig.2.1b) as a result of direct blunt impact or indirect compressive loads (Moore et al. 2011). A rib fracture or discontinuity of the connection between sternum and cartilage or cartilage and rib can lead to penetrating injuries of underlying soft tissues. Perforation of the

thoracic wall, where the space between the lung and thoracic wall fills with air, is referred to as pneumothorax. In a case where the cavity between the lung and thoracic wall filled with blood due to internal bleeding is referred to as hemothorax. The lung subjected to external pressure from the fluid in chest cavity may collapse, which leads to breathing impairment.

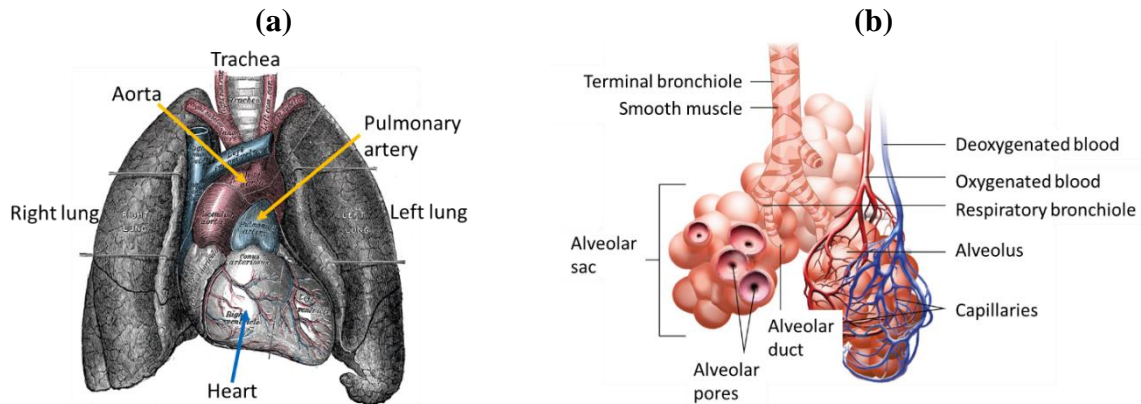


Figure 2.2: (a) Lungs (Gray 1918), (b) alveolar structure (adapted from OpenStax¹ 2013).

Lung injury at a large scale or tearing is referred to as pulmonary laceration. A ruptured or punctured lung releases air or blood, which may accumulate in the chest cavity and cause closed pneumo- or hemothorax. Pulmonary laceration is one of the injury mechanisms leading to pulmonary contusion (PC) (Wagner et al. 1988), where damage and bleeding occur at alveolar level. Alveoli fill with fluid and collapse, impairing the breathing process and potentially leading to an inflammatory reaction. If more than 24% of the total lung volume is contused, the risk of ARDS onset rapidly increases (Becher 2012).

Heart injury types include laceration and contusion. Cardiac laceration can be caused by severe deformation of the heart between hard tissues, such as between the sternum and vertebrae, or contact with fractured ribs. Laceration or its extreme form, heart rupture, can cause high volume internal bleeding or heart failure. Aside from laceration and rupture, cardiac

¹ Download for free at <http://cnx.org/contents/ccc4ed14-6c87-408b-9934-7a0d279d853a@4> (required by Creative Commons license permission for the image).

contusion can impair the functionality of the muscular fibers resulting in defective heart rhythm and cardiac arrest (Moore et al. 2011). Similar injury types are observed in side impacts for the aorta and large vessels. Rupture of the aorta is a severe injury commonly leading to fatal blood loss (Thomas and Frampton 1999).

Classification of Thoracic Injury Severity

A variety of injuries scales have been developed to facilitate triage at a crash scene, at a trauma centre, and during the assessment of restraint effectiveness during vehicle design process. The Abbreviated Injury Scale (AIS) (AAAM 2015) is the injury scale most widely used by the automotive industry and crash response teams. The simplified AIS scale (Table 2.1) provides a number that translates to a potential threat to life as a result of certain injury, on a scale from 0 (no injury) to 6 (fatal). The detailed AIS scale provides a code sequence that describes location, type, and severity of the injury, based on body regions: 1 – head, 2 – face, 3 – neck, 4- thorax, 5 – abdomen, 6 – spine, 7 – upper extremity, 8 – lower extremity, 9 – unspecified (AAAM 2015).

Table 2.1: Thoracic injury with a corresponding AIS scale (adapted from Cavanaugh 2002).

	AIS	Rib cage injury	Soft tissue injury
Minor	1	Single rib fracture	Skin abrasion, contusion, laceration
Moderate	2	2-3 rib fractures, sternum fracture	Major skin laceration, partial thickness tear, bronchus
Serious (not life threatening)	3	>4 rib fractures, 2-3 rib fractures with haemothorax or pneumothorax	Minor heart contusion, unilateral lung contusion
Severe (life threatening but survivable)	4	>4 rib fractures with hemothorax, pneumothorax, or flail chest	Severe heart contusion, intimal tear of aorta
Critical	5	Bilateral flail chest	Major aortic laceration, heart perforation, ventricular heart rupture
Fatal	6		Aortic laceration with haemorrhage

2.1.3 Thoracic Injury Criteria in Side Impacts

Translation of the kinematic response of an occupant surrogate to the probability of injury of certain severity for a human occupant is performed with use of injury criteria. The injury risk curves, providing a link between laboratory predictions and experimental data, have been developed for each body region separately. Thoracic injury criteria for side impacts were based on PMHS tests conducted over the last 30 years (Viano et al. 1989a, Cavanaugh et al. 1991, 1993, Pintar et al. 1997, ECE-R95 1995, Kuppaa 2004, NHTSA 2012). A correlation between kinematic responses, such as displacements and accelerations, and injury assessed during a post-test autopsy, has been established and referred to as injury criteria (Mertz 2003). The PMHS results are often normalized for the anthropometry of an average, 50th percentile male or scaled to other statures (Kuppaa 2004) and implemented in vehicle test standards. After the kinematic response of the ATD is measured during an impact test, a probability of injury of certain severity to a human occupant is inferred based on the injury criteria (Kuppaa 2004).

Currently used thoracic injury criteria for side impact include thoracic lateral compression (NHTSA 2012) and the Viscous Criterion (Lau and Viano 1986, NHTSA 2012). Thoracic compression is measured as change of thorax breadth normalized with respect to initial thorax breadth (Viano et al. 1989). Compression levels of 33.9% correspond to a 50% probability of AIS 3+ injury (Viano et al. 1989). The FMVSS 214 injury threshold for an ES2-re ATD is 44 mm (NHTSA 2012a), and a good side impact rating with IIHS requires 34 mm or less of lateral chest deflection of a SID-II_s ATD (IIHS 2017).

The Viscous Criterion is calculated using the normalized compression $C(t)$, defined as the chest deflection at a given time $D(t)$ divided by initial chest breadth, multiplied by the velocity obtained by differentiating the time history of the rib deflection, $V(t)$ (Fig.2.3, Lau 1986). Test standards usually report only the maximum of the VC values measured at all rib levels, referred to as VC_{max} (ECE R 95 1995). A VC_{max} value of 1.0 m/s corresponds to a 50% probability of AIS 3+ injury (Lau 1986, IIHS 2017).

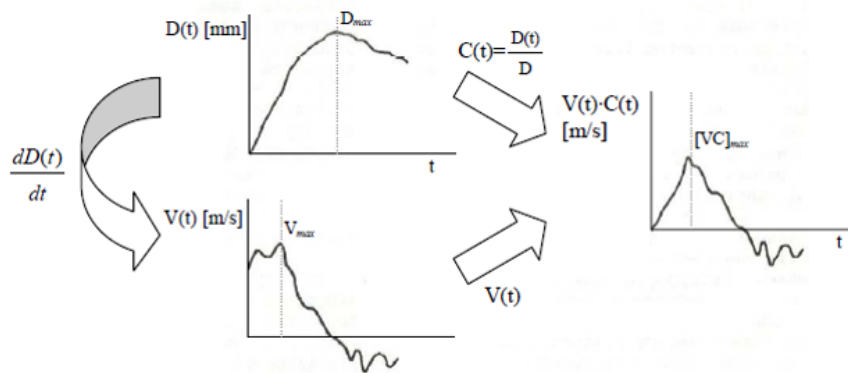


Figure 2.3: Calculation of the Viscous Criterion (from Lau 1986). D – initial chest breadth. D(t) – time-history of the chest deflection in mm. C(t) – chest compression, V(t) – chest deformation velocity in m/s.

The Thoracic Trauma Index (TTI) is a historic side impact injury criterion based on lateral accelerations measured at three thoracic vertebrae levels and normalized depending on the occupant age (where applicable) and weight. The TTI is calculated as a mean of the T12 and either T4 or T8 acceleration, depending which is higher (Kuppa 2004). Although TTI was reported to correlate with thoracic injury (Kallieris 1994), it is not used in current safety standards.

Spine curvature, namely a relative lateral distance between the vertebrae, was described by Kaneko et al. (2007) as a potential metric that correlates with chest compression in side impacts. Consistent spine curvature during the side impact was associated with lower chest deflection and VCmax values in ATD tests. However, up to date the criterion has not been quantified or formalized.

Rib Fracture Location Prediction

Human Body Models incorporate tissue level injury criteria, which enable prediction of specific injury types and locations. Rib fractures in the University of Waterloo Human Body Model (UW-HBM) are predicted based on element erosion with a von Mises based failure criterion, embedded as a function of the effective strain rate in the linear elastic-plastic cortical and trabecular bone material (138.3 MPa for strain rate of 1/s) (Forbes 2005, Yuen 2010) as a

strain rate dependent linear elastic-plastic material incorporating a failure definition based on von Mises stress at failure as a function of the effective strain rate.

The Global Human Body Models Consortium (GHBMC) Human Body Model predicts locations of rib fracture locations based on a plastic strain failure criterion embedded in cortical and trabecular bone material definition. The rib bone materials follow an elastic-plastic material definition (piecewise linear plasticity), and rate effects are accounted for through the Cowper-Symonds model that scales yield stress (LS-Dyna User's Manual 2002). Within the model, elements that exceed the threshold effective plastic strain value of 0.018 for the cortical bone and 0.13 for the trabecular bone erode and are virtually removed from the rib (GHBMC 2014). Eroded elements can be located during graphical post-processing of the results and classified as a rib fracture location.

The Total HUMAN Model for Safety (Oshita 2001, Iwamoto 2002) also includes a strain-based criterion for the cortical bone, and the threshold values proposed for element erosion varied between 0.0203-0.0238 (Mendoza-Vazquez et al. 2014).

Internal Organ Injury Risk

The GHBMC HBM was described as sufficiently validated to predict potential for pulmonary contusion (PC) and diaphragm injuries (GHBMC 2014). However, no Crash Induced Injury (CII) criterion and threshold was provided for PC.

The UW-HBM lung material model was developed by Yuen (2010), based on in-vivo impact experiments performed on rats, pressure-volume experiments performed on dog lungs, and human lung tissue biaxial experiments. Yuen (2010) examined a variety of previously proposed criteria (Gayzik 2007; 2008) to predict PC onset: first principal strain (Yuen's proposed threshold value: 0.78), strain rate (threshold value: 243 1/s), instantaneous product of strain and strain rate (threshold value: 103 1/s), and his own criterion of threshold dynamic pressure (52.4 kPa). The dynamic pressure criterion was correlated to tensile deformation of the lung tissue and demonstrated a capacity to capture the spalling effect, observed to result in hemorrhagic lung injury (Yen 1988). Although different criteria for PC prediction have been proposed in the last decade (Gayzik 2011, Danelson 2015), Yuen's study emphasized

contribution of the hydrostatic lung material response and evaluating response locally. Using the pressure criterion, Yuen predicted patches of contused lungs in the UW-HBM similar to PC patterns in trauma patients (Yuen 2010).

2.2 Occupant Surrogates

One of the first volunteer studies on the effects of abrupt decelerations on human body in interaction with restraints was conducted by Col. Stapp's group for the purpose of evaluation of military ejection seat design (Stapp 1947, 1949). The National Biodynamics Lab (NBDL) further investigated occupant response using a rigid sled accelerated and decelerated in different directions to mimic a frontal or lateral crash pulse (Wismans 1986, Thunnissen 1995). Although volunteer tests have provided important data on living human response under crash conditions, experiments at relatively high energies have not been repeated in modern times due to ethical concerns and a possible risk of injury to the volunteer. Therefore, Post Mortem Human Surrogates (PMHSs) and ATDs have been utilized as human surrogates in biomechanical experiments at impact severities and decelerations which could potentially exceed physiological pain and injury thresholds. Both ATD and PMHS-based research has a long history of development, and a number of updates have been proposed over the past several decades to improve the response measurement and post-processing.

2.2.1 History of PMHS Tests and Developments

PMHSs have been widely used in biomechanical research since the 1950s due to the anatomical accuracy in representing the human body. PMHS testing is widely used to determine impact response and tolerance. Test scenarios utilizing PMHSs include pendulum impacts, sled-impacts (Fig. 2.4), and investigation of interaction with passive restraints (door design, seatbelts, and airbags). Experiments assessing PMHS response in full vehicle impacts are very limited (Klaus and Kallieris 1983, Berg et al. 1998).

To measure occupant response during side impacts, instrumented metallic bands, referred to as *chestbands*, are placed around the PMHS thorax, usually at two anatomical locations: at the level of 4th sterno-costal joint, and at the level of xiphoidal process of the

sternum (Pintar et al. 1997). Deformation of the chestbands during impact is used to calculate chest deflection magnitude and pattern. However, interpreting chestband contours can present challenges due to the complex deformations of soft tissues, particularly for higher-BMI subjects. Additional accelerometers or load cells can be fixed directly to hard tissues at certain anatomical landmarks to measure displacements, accelerations, and forces (Baudrit 2005). Recent studies (Trosseille et al. 2011) measured strain-time histories using strain gauges bonded directly to PMHS ribs to track strain measurements directly. However, measurements are limited to a few locations, and installation of the strain gauges prior to the test requires a surgical procedure, which can affect the structural thoracic response.



Figure 2.4: Instrumented PMHS prepared for a rigid-wall sled test (adapted from Pintar 2007).

2.2.2 History of ATD Developments

ATDs were first developed to study loading due to deployment of aircraft ejection seats. The first ATDs were designed to represent the height and weight of a mid-sized male aviator, and the use of the so-called 50th-percentile male as the reference body size eventually became a standard in automotive testing (NHTSA 2012a). Most current ATDs are designed for one standard driving seating position and specific impact directions and are validated with respect to measurements performed on PMHSs under the same loading conditions. Different ATDs are used for frontal (Fig. 2.5a), side (Fig. 2.5b,c), and rear (Fig 2.5d) impact tests.

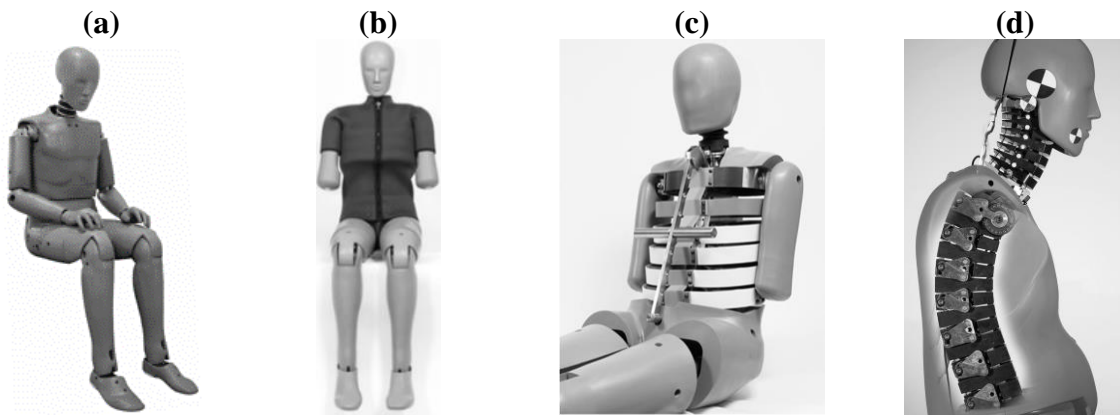


Figure 2.5: Anthropometric Test Devices representing a 50th percentile male occupant for: (a) frontal – Hybrid III (adapted from humaneticsatd.com), (b) side – ES-2re (adapted from humaneticsatd.com), (c) side – WorldSID (adapted from Hitech.com.sg), and (d) rear – BioRID II (adapted from IIHS.org) impact testing.

The accuracy of a surrogate such as an ATD in replicating PMHS response for the same impact scenario (Fig.2.6a,b) is referred to as biofidelity. ATD and PMHS impact responses can be compared using gross kinematics, segment accelerations, and forces measured at external loading surfaces (Fig. 2.6c). For concentrated load impacts, such as pendulum impacts, force and displacement time histories of impactors are compared between the ATD and PMHS. Internal responses can be compared using displacements and accelerations measured at certain anatomical landmarks (Fig.2.6d). The ATD response needs to fall within a biomechanical corridor, namely a range of responses predicted by PMHSs (Scherer 2009). The biofidelity index of two side impact ATDs, USSID and ES-2re, compared by Scherer (2009) is presented in Table 2.2, where scores 8.7-10 indicate excellent, 6.6-8.6 good, 4.5-6.5 fair, 2.7-4.4 marginal, and below 2.6 is considered an unacceptable biofidelity rating (ISO 9790).

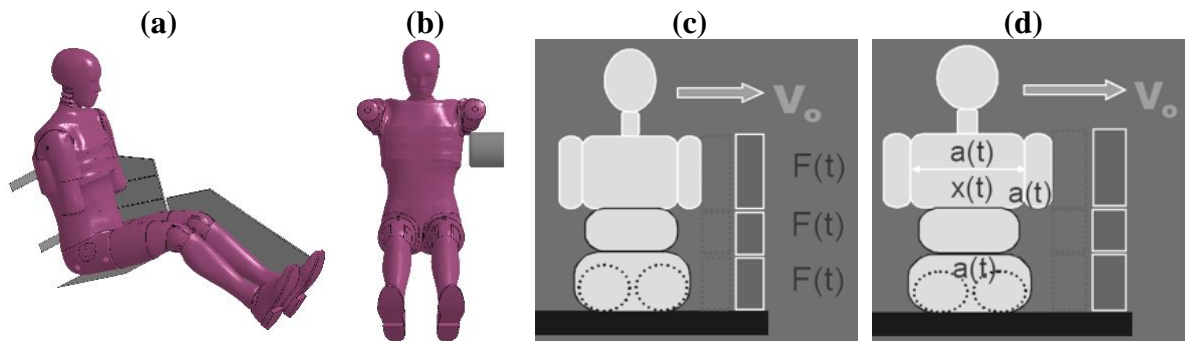


Figure 2.6: ATD integrated with: (a) a rigid wall sled, (b) pendulum impactor. Measurement of: (c) external forces exerted by the occupant on the impacted wall, (d) internal response of the occupant in terms of displacements and accelerations (adapted from Kuppa 2004).

Table 2.2: Biofidelity scores of three side impact ATDs (Scherer 2009) [scale 0-10; 10 is best].

	USSID	ES-2re	WorldSID
head	0	5	10
neck	2.5	4.2	5.3
shoulder	0	4.5	10
thorax	3.1	4	8.2
abdomen	4.4	4.1	9.2
pelvis	2.5	3.2	5.1
overall	2.3	4.2	8

Objective Rating Methods

ATD response agreement with PMHS experimental data is also assessed with an objective rating method such as Correlation and Analysis (CORA) developed by the Partnership for Dummy Technology and Biomechanics (PDB 2012) (Thunert 2012). CORA evaluation can consist of corridor rating, cross-correlation rating, or both, with weight for the rating importance subjectively chosen by user. For the corridor component, CORA compares the fit

of evaluated signals to experimental or user-set corridors. The cross-correlation component provides a score rating based on shape, phase shift, and area calculated below two compared signals. A CORA score equal to 1.0 corresponds to overlapping, identical curves, while a CORA score of 0.0 would mean no correlation between the model response and data. A rating scale used for the purpose of this thesis was adapted from the existing biofidelity rating (ISO 1999) to qualitatively describe the correlation between two responses (Table 2.3). Correlation values of 0.86 and above indicate good match between the compared curves. Reasonable correlation corresponds to rating between 0.65 and 0.85, and rating below 0.65 indicates poor correlation. Cross-correlation was also used to assess the sensitivity of the response for different impact scenarios (e.g. horizontal and vertical arm positions for the HBM). A cross-correlation rating over 0.86 corresponds to small effect of the varied parameter, 0.66-0.85 to moderate effect, and 0.65 to 0.0 indicates large effect size (Cohen 1988) (Table 2.4).

Table 2.3: A rating scale describing the correlation.

poor	$0.0 \leq \text{rating} \leq 0.65$
reasonable	$0.66 \leq \text{rating} \leq 0.85$
good	$0.86 \leq \text{rating} \leq 1.0$

Table 2.4: A rating scale describing sensitivity.

large	$0.0 \leq \text{rating} \leq 0.65$
moderate	$0.66 \leq \text{rating} \leq 0.85$
small	$0.86 \leq \text{rating} \leq 1.0$

Side Impact ATD Model Used in This Study

Computational models of ATDs have been developed over the last four decades (Fig.2.7a), in parallel with the increasing computational capacity of modern computers (Cronin 2011). These models evolved from simplified multibody representations (rigid bodies connected through kinematic joints) (Wismans 2005) to finite-element (FE) models (DYNAmore 2015, Humanetics 2017) capturing geometry and material properties in more detail (Fig.2.7a,b).



Figure 2.7: (a) Computational model of the ES-2re ATD (DYNAmore 2015) integrated with a rigid-wall sled model, (b) physical component test utilizing the ES-2re ATD (Aekbote 2007).

Although the physical WorldSID ATD biofidelity rating was higher compared to other side impact ATDs (Scherer 2009), the overall performance of the numerical WorldSID ATD model evaluated by Park et al. (2014) in comparison to three PMHS responses demonstrated cross-correlation rating (CORA) comparable to the ES-2re ATD model. Moreover, the ES-2re ATD model demonstrated the highest correlation with PMHS experimental data for rib deflection responses (WorldSID=0.13, ES-2re=0.63). Therefore, due to application in standardized vehicle testing (NHTSA 2012a) and performance comparable to other side impact occupant surrogates, the ES-2re ATD was used in this thesis.

The ES2-re ATD thorax consists of three metal bands (“ribs”) encapsulating three rib deflection potentiometers that reach from a spine box mounted on the ATD spine towards ribs on the impacted side of the thorax (Fig.2.8a). Deformations of the three ribs are intended to correspond to deformations of the upper and lower thorax, and of the abdominal area, of a mid-sized human occupant, respectively. For the numerical ES-2re ATD model, the chest compression was defined as the change in length of a discrete element connecting two nodes located on the rib modules (Fig.2.8a). The location of the nodes corresponded to the physical potentiometer attachment points (Fig.2.8b); therefore, thorax compression was measured in the same manner as in the physical ATD.



Figure 2.8: (a) Computational model of the side impact ES-2re ATD thorax, (b) ES-2re rib potentiometer (Stricklin 2009).

Verification of the ES-2re side impact ATD FE model was conducted through simulations of calibration tests (United States Code of Federal Regulations 2008) and comparing the responses to standards for physical ATD results by the model developer (DYNAmore 2014). The calibration tests were repeated by Watson (2010).

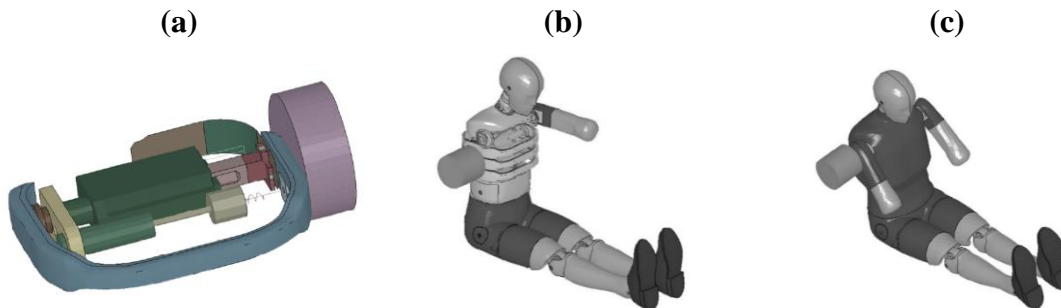


Figure 2.9: Calibration tests of the ES-2re ATD: (a) isolated rib module impact, (b) exposed thorax pendulum impact, (c) shoulder pendulum impact (adapted from Watson 2010, Gierczycka et al. 2015).

Thoracic calibration at a component level included a drop test performed for each rib, where a 7.78 kg (7.8 lbs), 150 mm (5.9”) impactor was dropped from different heights (Fig.2.9a, 2.10a). Full thorax response assessment included a 5.5 m/s lateral rigid pendulum impact to the middle of the second rib, where the ATD arm and jacket were removed (Fig.2.9b, 2.10b). The same impactor (152.4 mm, 6” diameter, and 23.4 kg, 51.6 lbs in weight) was used

to evaluate shoulder response in a lateral impact of 4.3 m/s. The ATD model was found to meet the Federal Code (2008) requirements for all the simulated impact scenarios (Fig.2.9c, 2.10c) (Watson 2010).

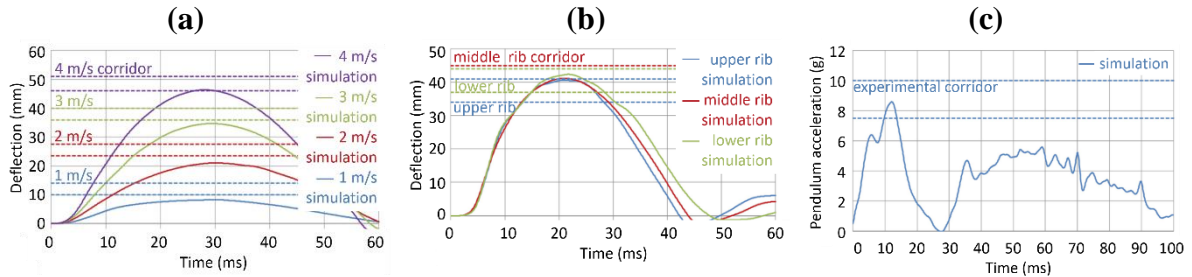


Figure 2.10: Chest deflection in: (a) isolated rib module test for four impact velocities, (b) exposed thorax pendulum impact, (c) pendulum acceleration in the shoulder pendulum impact. Dotted lines: experimental corridors, solid lines: simulated response (Watson 2010, Gierczycka et al. 2015).

After integration of the ATD model with the vehicle and restraint models, the vehicle was subjected to a 54 kph (33.5 mph) MDB impact replicating a FMVSS 214 side impact test to facilitate a direct comparison with the available ES2-re ATD results of a physical MDB tests of the same vehicle make and generation, namely the 1996-1999 MY Ford Taurus impact tests (NHTSA 2000), achieving a good match (Fig.2.11) (Watson 2010).

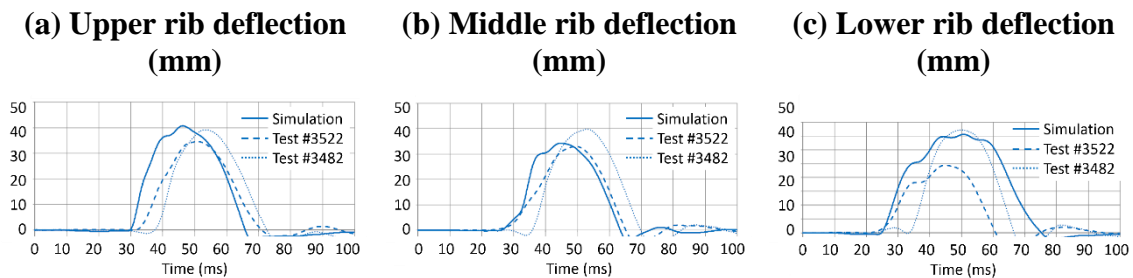


Figure 2.11: Rib deflection responses of the ES-2re ATD model in the full vehicle FMVSS 214 test (NHTSA #3522, #3482, adapted from Watson 2010, Gierczycka et al. 2015).

2.2.3 History of Human Body Model developments

Advancements of computational technology and the recognition of the biofidelity limitations of ATDs led to development of numerical models of the human body, to bridge the gap between the ATDs and real occupants. Initial Human Body Models (HBMs), such as the lumped thorax model (Lobdell 1973), and finite-element (FE) thorax models, including Huang (1994) (Fig.2.12a), Wang (1995), Lizee (1998), and El-Jawahri (2010), represented isolated body segments. Full-body models originated as multibody representations (Cheng 1994) (Fig.2.12b), facet HBMs (Wismans 2005), and combinations of the FE thorax with simplified multibody representations of other body parts (Plank et al. 1998). Within the following decade, first facet and full-body FE models were developed: Total HUMAN Model for Safety (THUMS) by Oshita et al. (2001) (Fig.2.12c), HUMOS by Robin (2001), occupant models by Ruan et al. (2003), and the THUMS elderly occupant model (Tamura et al. 2005). The FE models were deformable and had the potential to simulate tissue failure.

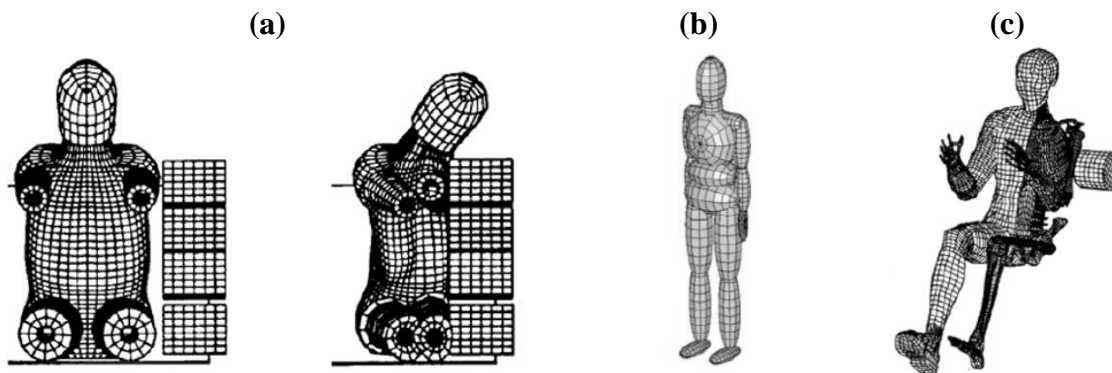


Figure 2.12: Early developments: (a) finite element model by Huang (1994) under a side sled impact, (b) multibody model by Cheng (1994), (c) finite element THUMS model by Oshita (2001), integrated with a pendulum impactor.

Current HBMs provide detailed anatomical representation of a mid-sized male or of a small female, reflecting the automotive safety standards (NHTSA 2012a) and can be morphed to a wide range of body sizes and shapes (Hwang et al. 2016). HBMs enable parametric studies through a repeatable, fully controllable environment, combining advantages of both PMHS and ATDs in a numerical environment (Wismans 2005, Cronin 2011).

2.2.4 The University of Waterloo Human Body Model

The UW-HBM originated from a thorax model developed by Deng et al. (1999), and further enhanced at the University of Waterloo (Forbes 2005, 2006; Campbell 2009, 2014; Yuen 2009) (Fig.2.13) through a refinement of material properties and adding simplified pelvis, abdomen, head, and lower and upper extremities. The models comprises 159,159 elements and 180,655 nodes.

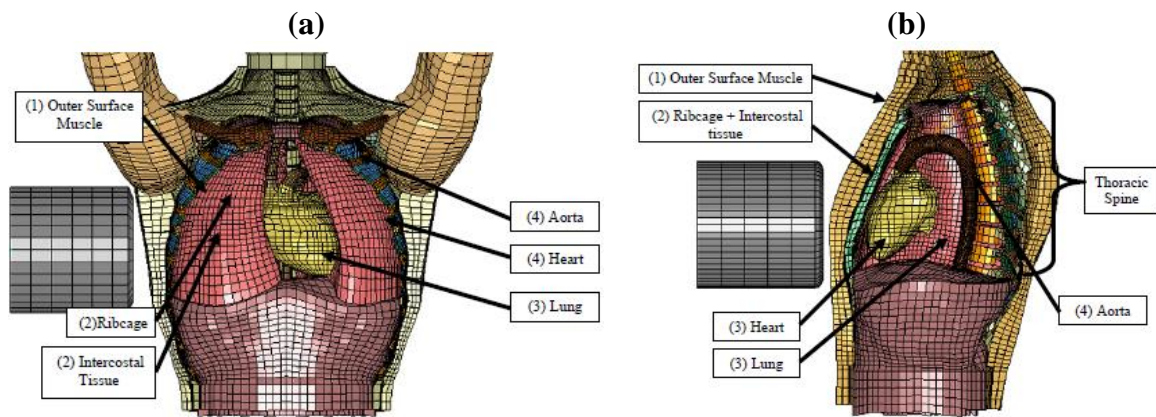


Figure 2.13: Thoracic section of the UW HBM, pendulum impact test: (a) front view, (b) lateral view (Forbes 2005).

The full-body UW-HBM was validated through free-flight 4.3 m/s and 6.7 m/s frontal pendulum impacts (Kroell 1971, 1974), free-flight oblique (4.3 m/s and 6.7 m/s) and lateral (4.3 m/s) pendulum impacts (Viano 1989) (Fig.2.14a), limited stroke 5.6 m/s lateral pendulum impacts (Chung 1999) (Fig. 2.14b), Wayne State University (WSU) rigid-wall side sled tests at 6.67 m/s and 8.89 m/s (Cavanaugh et al. 1990, 1993) (Fig.2.14c), and National Highway Transport Safety Administration (NHTSA) rigid-wall side sled tests at 6.67 m/s and 8.89 m/s (Pintar 1997) (Fig.2.14d, Fig.2.15).

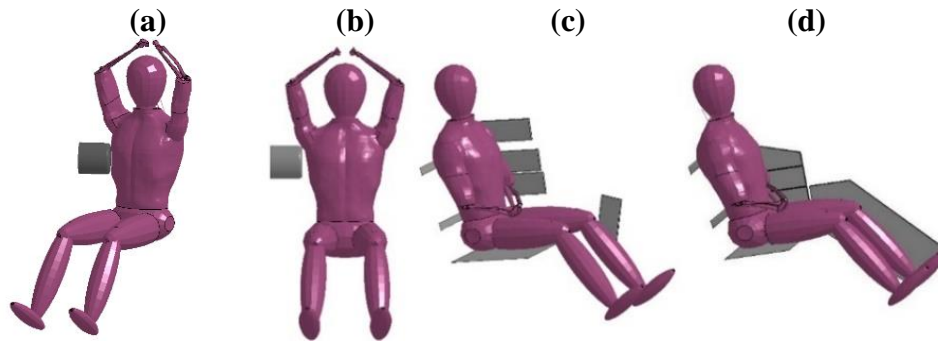


Figure 2.14: Lateral impact scenarios for the UW-HBM model assessment: (a) oblique pendulum, (b) lateral pendulum, (c) WSU-type rigid-wall sled impact, (d) NHTSA-type rigid-wall sled impact

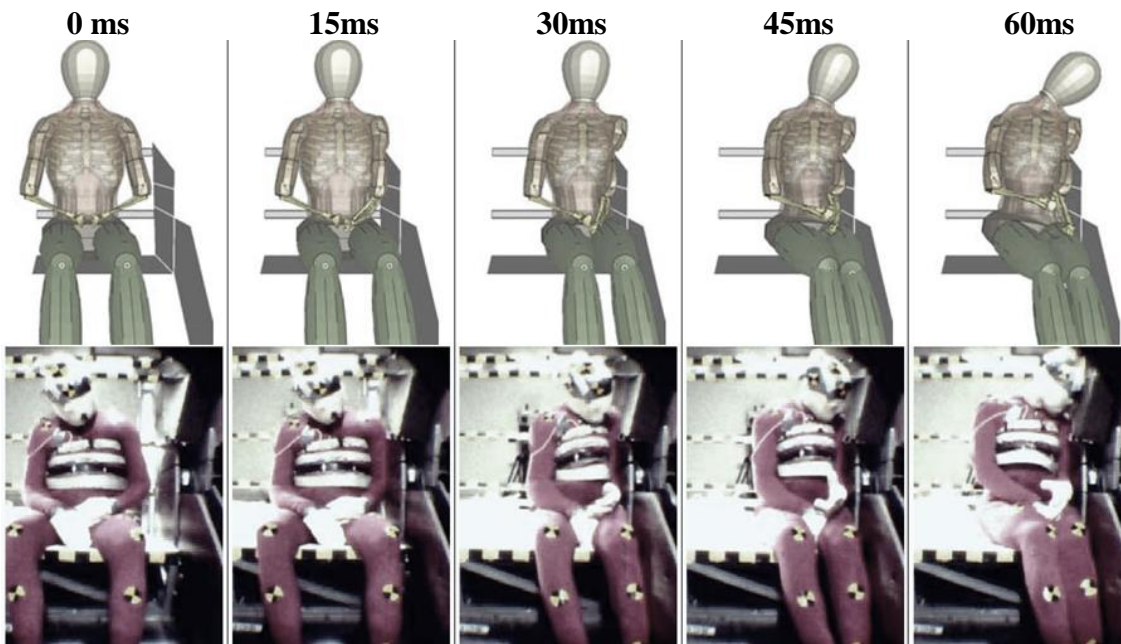


Figure 2.15: Comparison of the UW-HBM and PMHS kinematics in a 6.67 m/s NHTSA rigid sled impact (Forbes 2005, adapted from Gierczycka et al. 2015).

UW-HBM Response Assessment

Three chest deflection measurement locations in the UW-HBM model corresponded to the three rib levels in the physical ATD to enable interpretation of the results obtained with the two occupant surrogates. The ATD upper rib corresponded to rib 4 in the UW-HBM model (Samaha 2001), and the distances between the rib levels for measuring chest deflection in the UW-HBM (Fig.2.16a) were the same as between the ribs of the physical ATD (Fig.2.16b). Measurements at rib 6 in the UW-HBM corresponded to the location of the middle rib in the ATD, and measurements at the level of rib 8, to the location of the lower rib in the ATD.

In the PMHS laboratory tests the measurement of the upper thorax deflection is typically collected through a chestband located approximately at the level of the 4th rib, the middle rib corresponds to the level of the xyphoid process (approximately 7th rib) and the lower band is located approximately at the level of 10th rib (Pintar et al. 1997) (Fig.2.15). Where a direct comparison between PMHS and UW-HBM results was necessary, the chest deflection measurements were taken at ribs 4, 7 and 10 (Yuen 2010). All the results involving a direct comparison between the ATD and the UW-HBM involve a comparison of measurements at the level of ribs 4, 6, and 8.

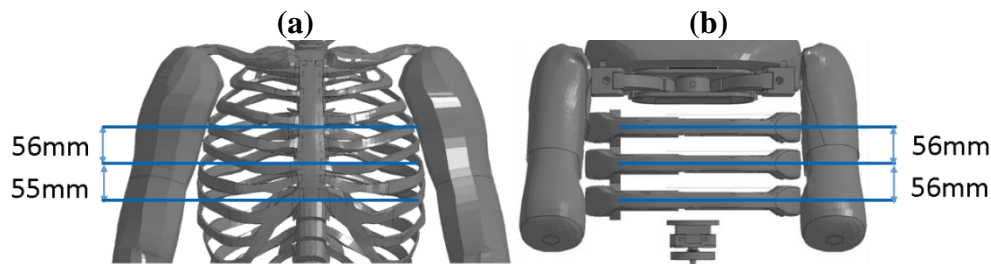


Figure 2.16: Comparison of distances between upper, middle, and lower rib levels of the: (a) UW-HBM, (b) ATD model. Outer layers removed for clarity.

In addition to the chest deflection, the Viscous Criterion was calculated to capture a potential for injury to internal organs and soft tissues, as described by Lau and Viano (1986). To evaluate the model performance, Forbes (2005) and Yuen (2010) applied an ISO biofidelity ranking based qualitative classification (ISO 1999) (Table 2.5). Experimental corridors were developed based on physical studies reported in the NHTSA database (2009) and expanded to

capture experimental range at each time according to the ISO approach (ISO 1999). For experimental responses where the corridors were not provided, the corridor was calculated based on a standard deviation projected off the experimental average (Forbes 2005, Yuen 2010).

Table 2.5: UW-HBM model biofidelity assessment method (from Yuen 2010).

Response quality	description
good	Falling within the corridor of the experimental data
reasonable	Falling outside the experimental data corridor, but within one corridor width
poor	Falling outside the experimental corridor by more than one corridor width

The UW-HBM response agreement with PMHS data in lateral impacts was between reasonable and good for all loading cases considered. An example of the assessment is shown for 6.7 m/s NHTSA-type rigid-wall impact, classified by Yuen (2010) as *reasonable* to *good* (Table 2.6), measured as chest compression at three rib levels (Fig.2.17).

Table 2.6: Assessment of the UW-HBM chest compression response in a NHTSA 6.67 m/s rigid sled impact, by loading phase (from Yuen 2010).

rib level	loading	peak	unloading
upper	good	good	reasonable
middle	reasonable	reasonable	reasonable
lower	good	good	good

Campbell (2009) integrated the UW-HBM with the vehicle, seat, and restraints model, and subjected to NHTSA Federal Motor Vehicles Safety Standard No. 214 (FMVSS 214) MDB test. The UW-HBM chest compression and VC responses at three rib levels exhibited good agreement with physical ATD response measured in FMVSS 214 NHTSA test No. 3522 for Ford Taurus MY 1996 (NHTSA 2000) (Fig.2.18).

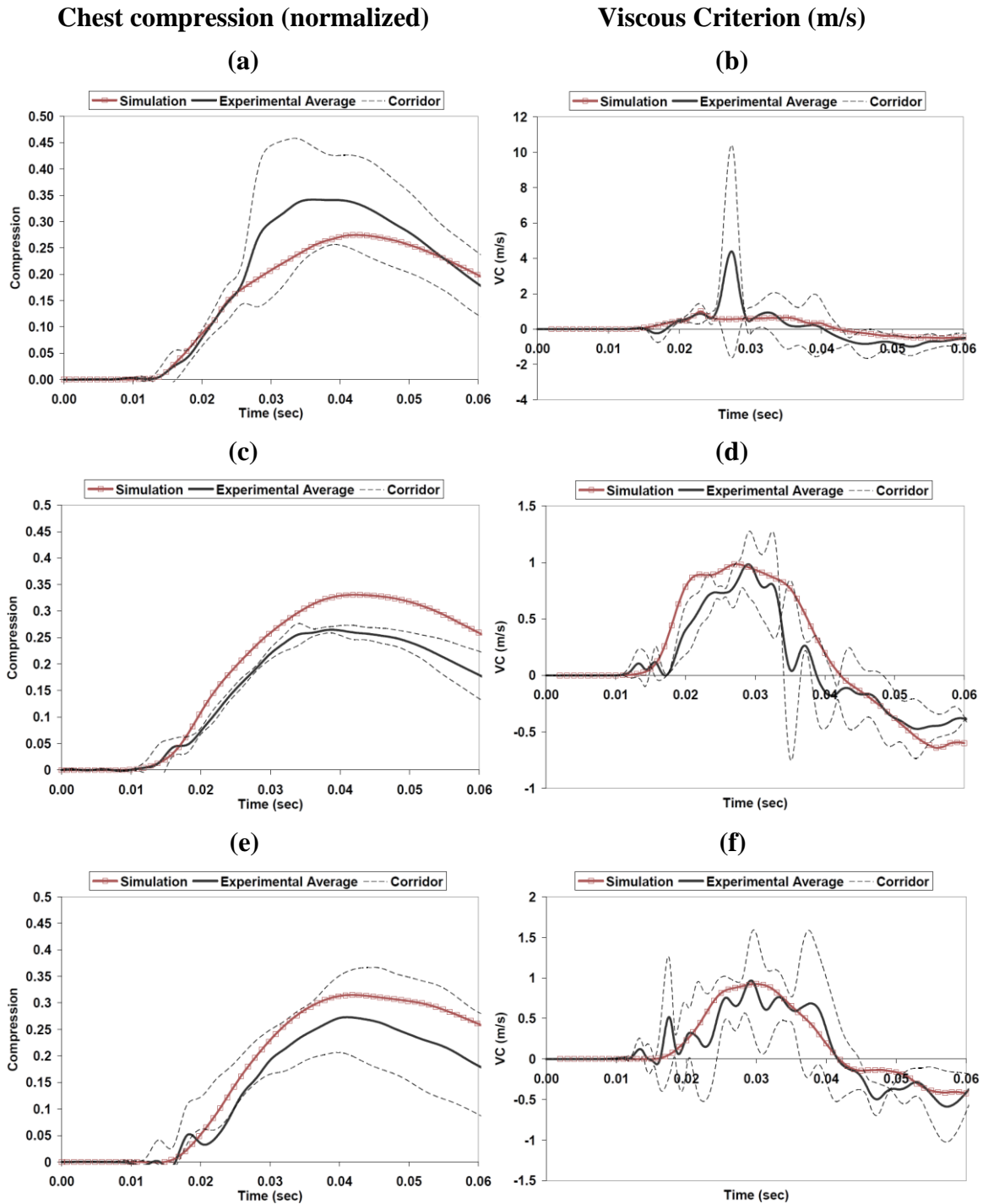


Figure 2.17: UW-HBM chest compression and VC response in 6.7 m/s NTHSA-type rigid-wall sled impact measured at: (a)(b) upper chest band, (c)(d) middle chest band, (e)(f) lower chest band (Yuen 2010, Gierczycka et al. 2015).

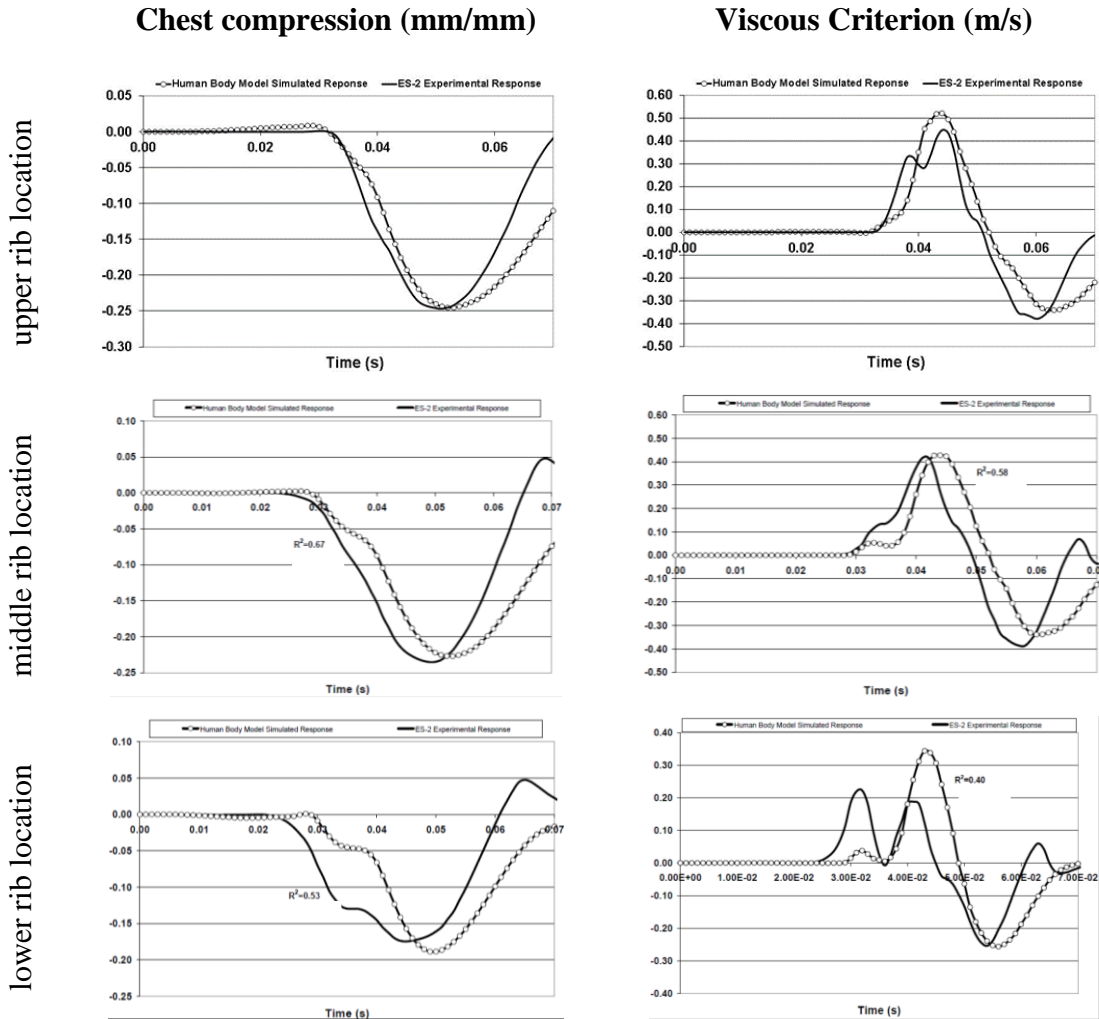


Figure 2.18: Comparison of the UW-HBM numerical and ATD experimental response at three rib levels in a FMVSS 214 MDB impact (Campbell 2009, 2014).

Rib Fracture Prediction with the UW-HBM

Rib fracture locations were predicted when elements that exceeded the failure strain were deleted from the simulation, and full rib fracture was associated with element deletion across rib thickness. The number of rib fractures predicted by the UW-HBM in rigid-wall scenarios fell within the range of fractures sustained by the PMHS in physical experiments (Cavanaugh 1990a,b, 1993; Pintar 1997, 2001) (Table 2.7). The model predicted a substantial number of

rib fractures in loading scenarios in which some PMHS also experienced multiple rib fractures. However, these comparisons are difficult to interpret in terms of predicting threshold for injury, due to large differences in anthropometry amongst the specimens, and between the specimens and the model.

Table 2.7: Number of rib fractures observed in PMHS rigid sled experiments compared to UW-HBM simulations (adapted from Yuen 2010).

	PMHS 3120	PMHS 3122	PMHS 3155	UW-HBM
NHTSA-type rigid-wall 6.7 m/s	16	0	11	15
	PMHS 2585	PMHS 2587	PMHS 4933	UW-HBM
WSU-type rigid-wall 6.7 m/s	20	16	11	18

2.2.5 Summary of the GHMBC-HBM Development

The Global Human Body Models Consortium family of HBMs (GHMBC-HBM) has been developed by a consortium of eight vehicle manufacturers and six universities over 12 years (GHMBC 2014). The Global Human Body Models Consortium (GHMBC) Human Body Model (HBM) of a mid-sized male seated vehicle occupant (M50-O), Version 4.3 (GHMBC 2014) represents the whole human body anatomy in detail. The GHMBC-HBM thorax includes the rib cage, sternum, cartilage, spine, heart, lungs, aorta, muscles, subcutaneous fat and skin. The model development was based on occupant geometry measured through Computer Tomography (CT), post-processed to surfaces and volumes, and then discretized to 2.19 million elements and 1.26 million nodes. Biological materials represented in the model have been mechanically tested, utilizing samples harvested from the Post-Mortem Human Surrogates (PMHS), or were based on the existing literature data on the biological material properties (GHMBC 2014). After a successful replication of mechanical responses at a single

element, isolated bone or internal organs level, and subsequently at the body region level such as head-neck or thorax (181 validation responses in total) (Table 2.8), the model was assembled.

Table 2.8: Number of test configurations to verify body region level response (GHBMC 2014).

Body region	#	Evaluation criteria
Head	9	Force-displacement characteristics, intracranial pressure, accelerations
Neck	39	Moment-flexion/extension angle characteristics, force-displacement characteristics, axial and shear strain, accelerations
Thorax	5	Force-displacement characteristics
Abdomen	11	Force-displacement characteristics, strain energy density, chest band deformation
Pelvis	4	Force-displacement and force-time characteristics
Lower extremity	35	Force-displacement and force-time characteristics, moment-angular displacement

The full body model validation involved comparison to a wide range of impacts representative for automotive accidents in terms of impact direction and severity, and included lateral shoulder impact, thorax and abdominal hub impact, abdominal bar impact, block impact to pelvis, lateral impact to the thorax, frontal and lateral NCAP tests, rear seat impacts, and a frontal sled impact (GHBMC 2014) (Fig.2.19) (Table 2.9). Model biofidelity was evaluated by body region (Arun et al. 2015) and achieved cross-correlation ratings (CORA) between 0.56-0.86 depending on compared signal and impact severity, indicating a reasonable match.

Table 2.9: Test configurations to verify full body model response (GHBMC 2014).

Test scenario	Evaluated response
Lateral shoulder impact	Force-time, displacement-time impactor characteristics
Thorax pendulum impact	Force-displacement impactor characteristics
Oblique abdominal pendulum impact	Force-time, displacement-time impactor characteristics
Abdominal bar impact	Force-displacement impactor characteristics
Thorax lateral impact	Occupant kinematics, impactor force-time characteristics
Frontal sled impact	Occupant kinematics, contact force-time characteristics
Frontal NCAP impact – driver side	Stability (energy balance)
Lateral NCAP impact - driver side	Stability (energy balance)
Rear seat impact	Occupant kinematics, impactor force-time characteristics

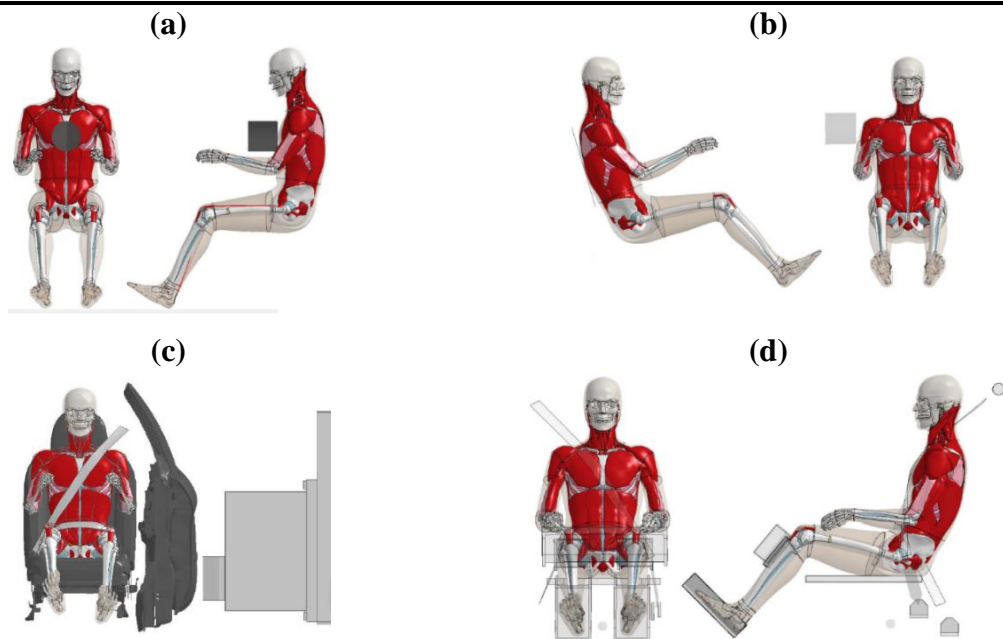


Figure 2.19: Examples of full body model validation setups of the GHBMC-HBM: (a) frontal pendulum, (b) lateral pendulum, (c) full vehicle MDB impact, (d) frontal sled-test (Wang 2014).

GHBMC-HBM Thoracic Response Assessment

Occupant kinematics was predicted based on pre-defined outputs corresponding to PMHS anatomical landmarks and locations of ATD response measurements. For the thorax, deformations of three chest bands (CB): upper, middle, and lower were available in addition to anteroposterior (sternum to vertebrae) and lateral compression outputs. Lateral compression was defined as change of length measured at the level of one chest band between two opposing markers on the outer tissue, normalized by initial thoracic breadth at the same chest band level (Fig.2.20). Thoracic acceleration was measured at the level of 8th thoracic vertebra.

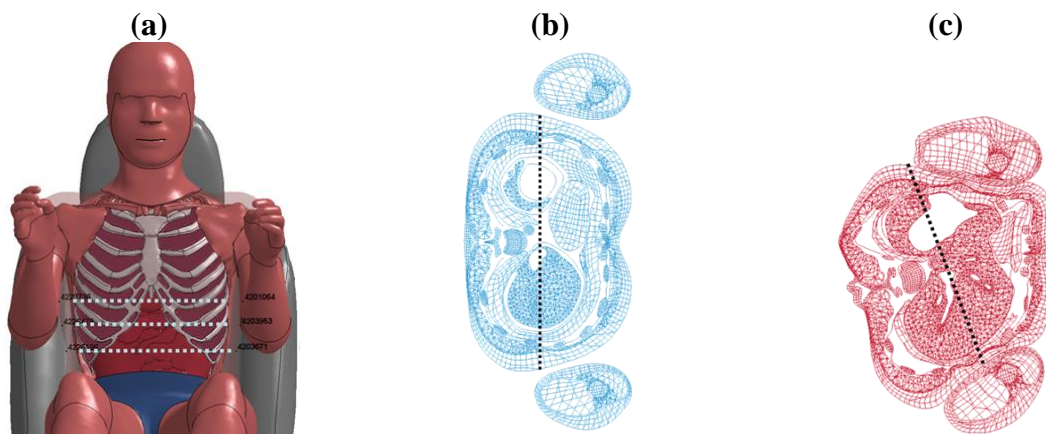


Figure 2.20: (a) Location of the pre-defined chest bands in the GHBMC-HBM, (b) lateral breadth of the thorax at one chest band level prior to the crash, (c) change in length due to crash.

2.3 Side Impact Safety Assessment

Full-vehicle lateral impacts are performed in laboratory conditions to assess vehicle performance and occupant safety (Kahane 2004). Federal regulations for side impact testing in North America include the Federal Motor Vehicle Safety Standard No. 214 (FMVSS 214) and Canada Motor Vehicle Safety Standard No. 214 (CMVSS 214). Both regulations include a Moving Deformable Barrier (MDB) test, where a standardized rigid cart known as an MDB (weighing $1,361 \pm 4.5$ kg, $3,000 \pm 10$ lbs) with a deformable bumper impacts the side of a stationary vehicle at a 27 degrees angle at 54 kph (33.54 mph) (Fig.2.21a), to model a vehicle-

to-vehicle impact in a repeatable manner. The US New Car Assessment Programme (NCAP, NHTSA 2012) and Insurance Institute for Highway Safety (IIHS 2017) side impact scenarios are consumer tests rating vehicle performance. The NCAP impact angle is 27 degrees, and initial barrier speed equals 61 kph (37.9 mph). The IIHS standard was developed to account for SUV to sedan impacts. Therefore, the barrier bumper is elevated by 100 mm compared to FMVSS and NCAP, and the MDB weight is increased to 1,500 kg (IIHS 2017). The MDB is accelerated to 50 kph and impacts the target vehicle at a 90-degree angle.

More recently, a pole impact (NHTSA 2012b) had been introduced, which includes a non-deforming pole impactor striking a stationary vehicle in the vicinity of the B-pillar (Fig. 2.21b). The pole impactor tests were developed to encourage greater side-structure strength and force the side head protection down to the small female head height. For both certification impact types, the occupant surrogate is seated in a standardized position, with arms rotated 40 degrees upwards from the torso midline, to mimic a driving posture (NHTSA 2012a). In the FMVSS and NCAP MDB impacts, an ES-2re ATD representing a 50th-percentile male (average height and weight for the male population) is seated in the driver seat, and a SID-IIs ATD representing a small, 5th-percentile female is seated the back seat, on the struck side of the vehicle. In the IIHS impacts, two SID-IIs small female ATDs are seated in the driver and rear seat, on the struck side. In the FMVSS and NCAP pole impacts, a 5th percentile SID-IIs ATD is seated in the driver seat.

Although the pole impacts are associated with severe injuries (Pintar et al. 2007), their occurrence is infrequent, compared to vehicle-to-vehicle impacts. For 13,200 passenger vehicle accidents analyzed by Otte et al. (2009) in Germany and UK, only 148 were classified as side vehicle to pole impacts, constituting less than 7% of single side impacts. Since vehicle fleet in North America is still dominated by passenger cars (over 60% in 2014) (Environmental Protection Agency, EPA 2014), for the purpose of this thesis the FMVSS and NCAP MDB standard has been adopted as a representation of the most frequent side impact crash scenario in developed countries.

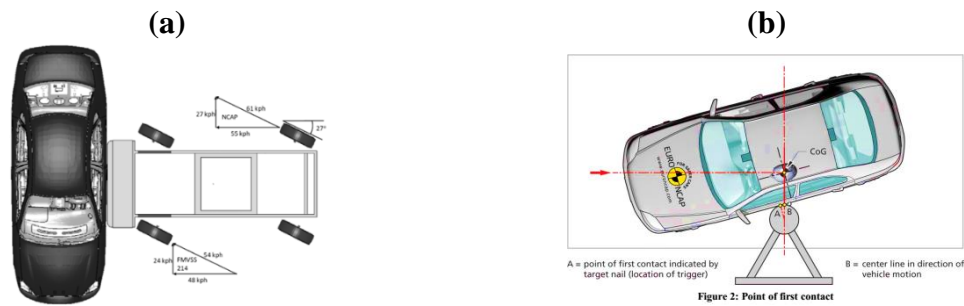


Figure 2.21: Configuration of the standardized lateral impact tests: (a) Moving Deformable Barrier (adapted from NCAP 2016), (b) pole impact (adapted from EuroNCAP 2018).

2.3.1 Occupant Kinematics and Sources of Injury in Side Impacts

In a lateral vehicle-to-vehicle impact (Fig. 2.22a), the striking car decelerates, deforming the outer door skin of the struck vehicle. Further engagement of the door structure and of the B-pillar leads to a deformation and intrusion into the occupant compartment. Relative to the struck vehicle, the occupant in the target car initially moves and rotates towards intruding door, and when no side curtains are present in the vehicle, the occupant head contacts the side window. When no thoracic side airbags are present, the shoulder, upper torso, pelvis and lower extremities contact the intruding door (Fig. 2.22b). As the door consolidates due to increasing impact velocity, the thorax is subjected to lateral compression. The rate of intrusion and loading on the occupant thorax decreases as the target car accelerates, and the occupant eventually rebounds from the door. While the entire event duration is on the order of 200 ms (NHTSA 2018), peak loading occurs during the first 100 ms (NHTSA 2018, Watson 2010). Contact with the intruding vehicle door has been identified as the main source of thoracic injuries in side crashes (Morris 1997), where the door panel was the primary interface between the occupant and the striking car (Tencer et al. 2005).

A typical vehicle door structure comprises: outer door skin (sheet metal), inner door skin (sheet metal) including window mechanisms and possibly a side impact beam, and the inner door panel (rigid polymer with crushable foam structures) and is required to meet both

structural and non-structural requirements. Morris et al. (1997) noted that the most common source of injuries in real world crashes is contact with the door, so the interior properties remain an important consideration even with the incorporation of thorax airbags. Strother et al. (1984) demonstrated that the severity of injuries in side impact was predominantly affected by a difference in velocity between the occupant and contacted surface rather than by the vehicle intrusion itself. Recommendations for effective countermeasures included solutions that reduce the relative velocity and distribute the impact (padding, airbags), rather than expensive changes to the vehicle structure to reduce intrusion (Strother et al. 1984). Modification of the structures was later introduced in response to side impact compliance tests, predominantly the pole impact (NHTSA 2012b).

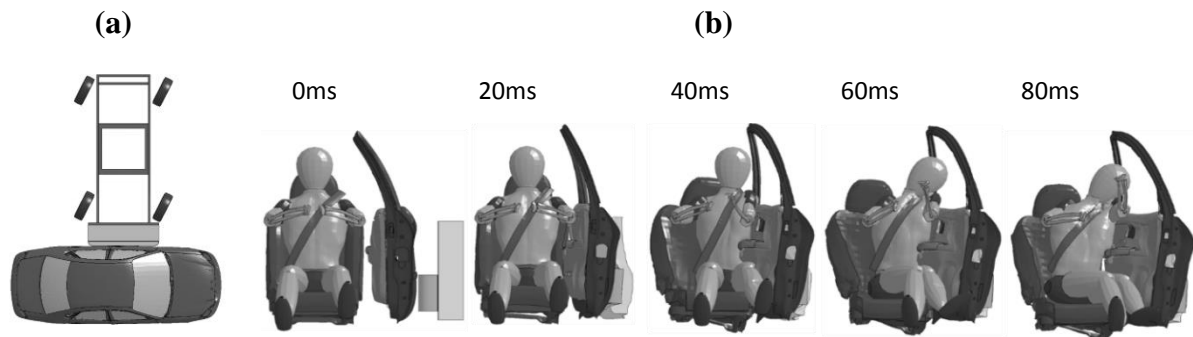


Figure 2.22: Human Body Model in a side impact scenario: (a) Moving Deformable Barrier test setup (NHTSA 1996), (b) the Human Body Model coupled with the vehicle, showing occupant motion during a side impact event.

Few full-scale experimental studies of side impact have been conducted due to the cost and challenges of large-scale impact testing. The effect of the inner door panel on occupant response was investigated by Lorenzo et al. (1996) for different potential energy absorbing materials and structures, and it was identified that different designs could be used to change the energy absorbing characteristics of the door. Deng et al. (1989) evaluated the importance of boundary conditions when determining the effects of door construction on side impact response for free-flight impact and a prescribed velocity pulse. The tested padding thickness was 6 cm and the stiffness ranged from 0.5 to 1.50 kN/cm. In case of the free flight impact, no

significant change in thorax deformation was observed, while thoracic acceleration, velocity and VC were reduced by padding. For the prescribed velocity pulse, added padding reduced thoracic acceleration and velocity but increased VC and rib deformation. Deng et al. concluded that the vehicle to vehicle side impact scenario is more accurately represented by an applied velocity pulse. However, the studies were based on responses of mid-sized male side impact ATD models and did not consider the distribution of occupant characteristics, including body mass, contour, and the height of various structures above the seat (Carter et al. 2014, Reed and Ebert 2016).

Campbell (2014) performed a series of simulations using an HBM and various modifications of a Ford Taurus door model in two FMVSS 214 impact scenarios. Amongst other parameters, the influence of door shape and door compliance on the injury prediction was investigated. The presence of a deformable door compared to a rigid door reduced VC_{max} up to 16%, showing that the shape of the door intrusion velocity profile highly influences thoracic response. Two arm positions were considered: standard driving and vertical (arms aligned with the torso). For the vertical arm position, the predicted VC_{max} value increased 42% with respect to the driving position for the same impact scenario. Campbell also noted that stiffer seat foam reduced thorax compression and VC. However, this study was limited to a simplified human/door interaction due to computational limitations, and it was recommended that future analysis should consider full vehicle models. More recent studies on side impacts focus on interaction of the occupant with side impact restraints, namely side airbags.

2.3.2 Side Impact Restraint Systems

Restraint systems for automotive use were first patented in early 1900 (Leveau 1903) in the form of seatbelt harness, and three-point seatbelts became mandatory in vehicles sold in the United States in 1969 (Snyder 1969). Side airbags (SABs) have been first introduced in vehicles in the 1990's (Haland 1994), following the success of frontal airbags that reduced occupant injury (Dischinger 1996, Fitzharris 2004). The initial assessment of SABs effectiveness by McCartt and Kyrychenko (2007) and Yoganandan et al. (2007) was based on evaluation of mid-sized sedans from 1997-2004 model years. Injury reduction in side impacts

turned out to be predominantly related to an increasing stiffness of vehicles rather than to the presence of SABs. In the following years, researchers divided SABs into categories to investigate benefits of specific designs: side curtain airbags, head-and-torso airbags, thoracic airbags, and pelvic airbags (Griffin et al. 2012, D'Elia et al. 2013, Kahane 2014, Viano and Parenteau 2016). An evaluation of the 2000-2010 model year mid-sized sedans and controlled laboratory tests revealed a high effectiveness of side curtains in mitigating head injury, and conflicting results on the thoracic side airbags (tSABs) (Table 2.10).

The curtain and head-and-thorax SABs were found to be very effective in reducing fatalities in side impacts and also positively contributed to occupant protection in other accident scenarios (D'Elia et al. 2013, Kahane 2014). For the near-side impacts, the estimate of fatality reduction due to a combination of curtain and tSAB was 32.8%, for the curtain only it was 16.8%. For the tSAB only, the reduction of driver fatalities was 10.4%. Kahane's study (2014) demonstrated that tSAB effectiveness in far-side impacts was lower than in near-side impacts. The tSAB was estimated to have no effect or increase odds of fatal injuries for the right-front passenger in the near-side (-0.4 %), and for both driver and right-front passenger in far-side (-4.9 %) impacts. Sources of these differences included a wide range of potential impact forces and directions for the far-side impacts (Kahane 2014), and potentially the occupant pre-crash position.

Studies based on the National Automotive Sampling System - Crashworthiness Data System (NASS-CDS) (Aldaghlis et al. 2010) and German In-Depth Accident Study (GIDAS) (Gaylor and Junge 2015) crash databases did not identify a statistically significant reduction of injuries attributed to tSABs, comparing similar model year vehicles with and without tSABs. Interestingly, the results obtained in matched-pair full vehicle side impacts with ATDs (Viano and Parenteau 2016) revealed that tSABs reduced the probability of head injury only, and did not provide a benefit for the thorax (Table 2.10). In general, older studies and those with ATDs (Luzon-Narro et al. 2014, Viano and Parenteau 2016) suggest a benefit of reduced injury metrics using tSAB, while more recent epidemiological studies have identified neutral effects, or increases in injury rates (Griffin 2012, D'Elia 2013, Gaylor and Junge 2015) for side impacts.

Table 2.10: Summary of experimental studies on tSAB effectiveness (adapted from Gierczycka and Cronin 2017).

tSAB effect	reference, vehicle model years, test type	occupant surrogate
tSABs did not contribute to AIS 2+ injuries and were not observed to cause severe chest injuries	Yoganandan et al. 2007, MY 1997-2004 vehicles	
occupant with and without tSAB had a similar injury risk; injury risk increased for occupants 50-year-old and older	Griffin et al. 2012, MY 2000-2009 vehicles	
injury risk, including fatal injury, increased for vehicles with tSAB (+5.2%), results were not statistically significant	D’Elia et al. 2013, MY 2001-2010 vehicles	epidemiological studies
fatalities reduction of 7.8% due to tSABs (confidence interval 0.4-14.7%)	Kahane 2014, MY 1994-2011 vehicles	
driver fatality risk reduced by 26% for passenger cars and 30% for SUVs due to tSABs	McCartt and Kyrychenko 2007, MY 1997-2004 vehicles	
tSAB reduced head injury risk, but increased chest (+22%, SD 5%) and pelvis (+16%, SD 4%) injury risk	Viano and Parenteau 2016, SID IIs ATD in 2003-2007 MY vehicles, 50 kmh MDB test	experimental ATD tests
large volume tSAB reduced peak rib deflection by 40%, compared to commonly used designs	Luzon-Narro et al. 2014, ES2 ATD, 50kmh MDB	
rib fractures occurred despite low chest deflection values when a large volume tSAB was deployed	Shaw et al. 2014, rigid sled 4.4 m/s, 3 PMHS	experimental PMHS tests
tSAB affected load distribution, thorax deformation and rib fracture pattern	Trosseille et al. 2008, static deployment, 3 PMHS	

2.3.3 Side Impact Modeling Using a Full Vehicle Finite Element Model

The crash response of Ford Taurus MY 2001 numerical vehicle model (Opiela 2008), the most detailed vehicle model available in the public domain (Danelson 2015), was assessed for frontal impact by Lockhart et al. (2013), and for side impact by Watson (2010, 2011) (Fig.2.23a). For side impact, the stationary vehicle was struck by a Moving Deformable Barrier (MDB) weighing 1368 kg, at 54 kph (33.5 mph) (FMVSS 214, NHTSA 2012a) and 61 kph (37.9 mph) (NCAP, NHTSA 2012a).

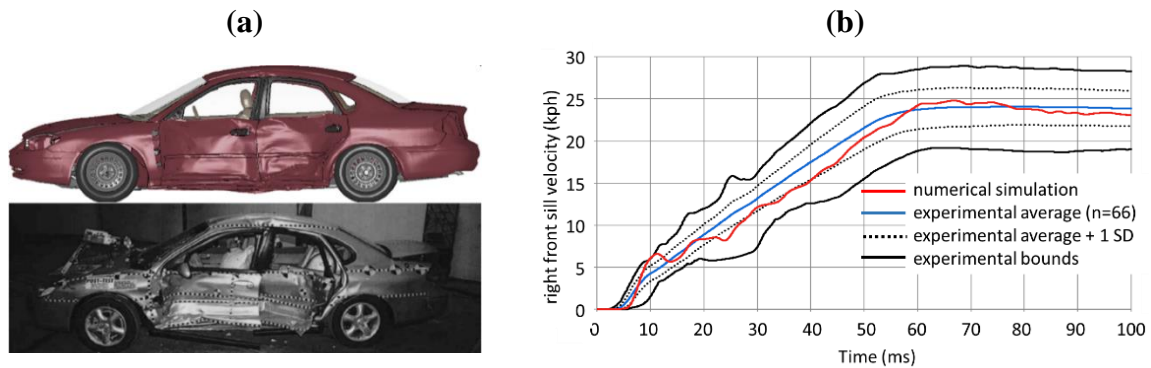
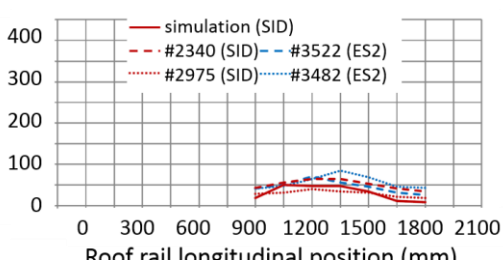
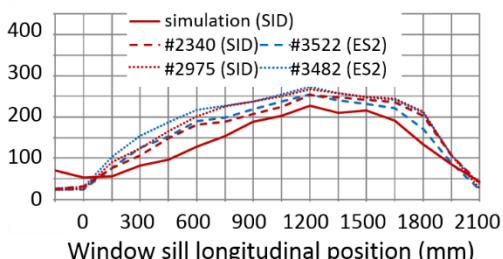
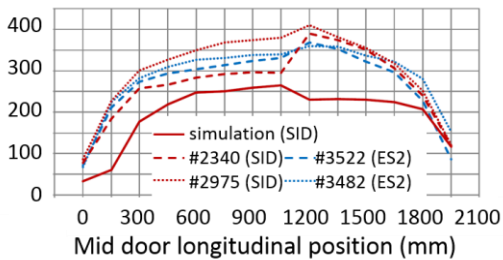
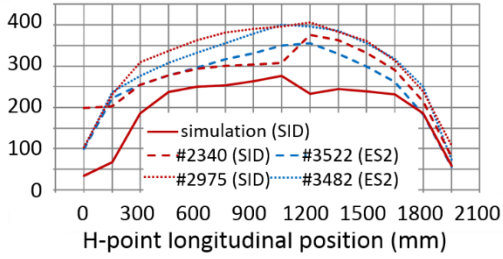
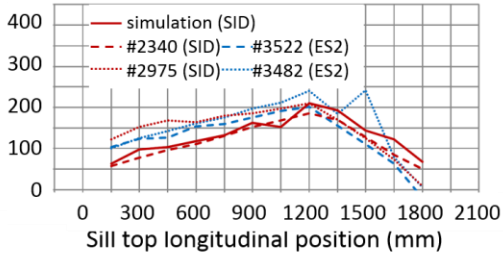


Figure 2.23: (a) Ford Taurus model and physical vehicle intrusion, (b) comparison of the vehicle model right front sill velocity to experimental results of 66 mid-sized sedan from MY 1996-1999 range (Watson 2010).

The vehicle model response to MDB impacts was compared by Watson (2010, 2011) to experimental data from a MY 2000 vehicle (NHTSA test #3263, NHTSA 2000) that represented the same generation of Ford Taurus as the computational model. The simulation and physical results compared well in terms of shape and magnitude of the intrusion (Fig.2.24). The MY 1996-1999 experimental data used for additional verification of the computational model through a comparison of intrusion measurement at seventeen locations on the vehicle, represented third generation of Ford Taurus, preceding the computational model (Fig.2.23b). Watson (2010, 2011) previously enhanced the model through improving driver side window material properties, constraining driver seat to vehicle floor, and updating the material model definitions for thoracic and pelvic foam pads in the driver side door to characterize the actual material more accurately.

FMVSS 214 vehicle crush distance (mm)



NCAP vehicle crush distance (mm)

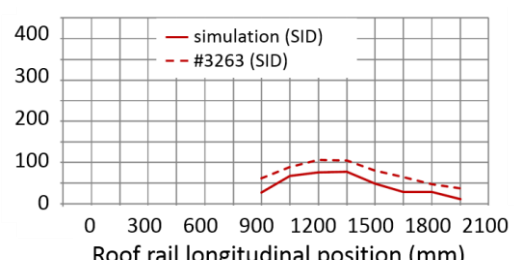
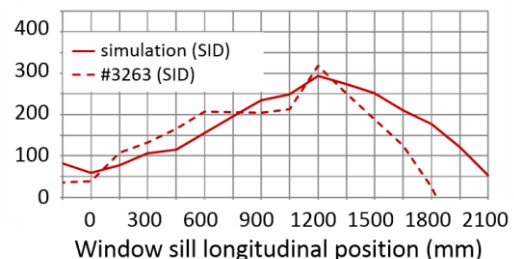
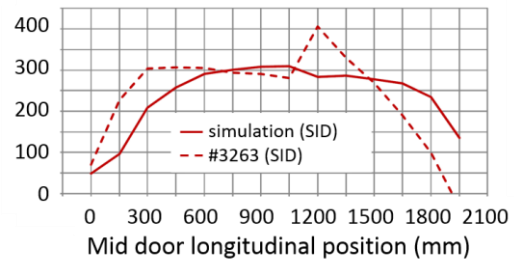
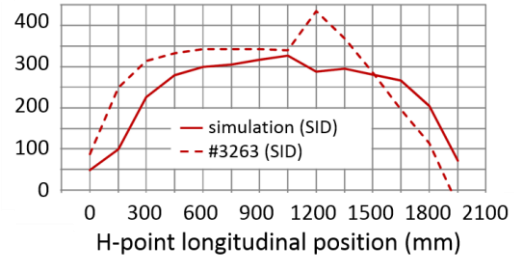
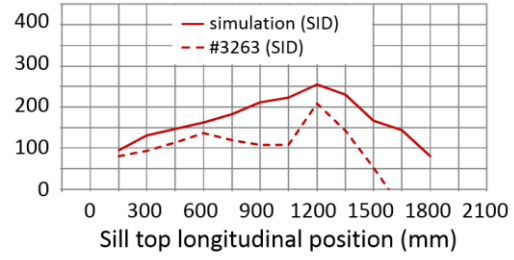


Figure 2.24: Deformation time histories of five different location of the vehicle and corresponding physical test results. Simulation results are presented with red solid line, physical test results with dashed line (Watson 2010, from Gierczycka et al 2015).

The MDB numerical model available in public domain was verified by Bhalsod and Krebs (2008), where the barrier model was impacting a 300 mm diameter rigid pole at 25 kph (15.5 mph), and a flat rigid-wall at 35 kph (21.7 mph) in a frontal impact configuration. Tests repeated by Watson (2010) demonstrated a very good agreement between the model and experimental responses for both validation test scenarios (Fig.2.25).

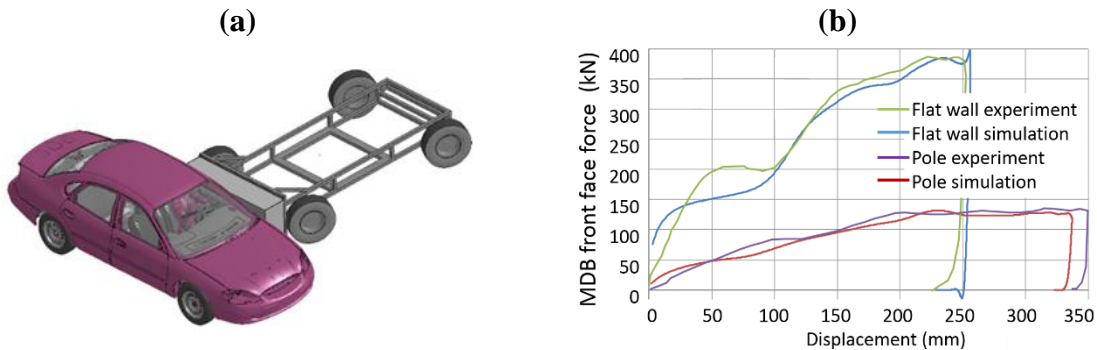


Figure 2.25: (a) Vehicle model integrated with the MDB model, (b) MDB force-displacement response in two validation scenarios, from Watson (2010).

Seat and Seatbelt Models Validation Summary

Seat geometry (Fig.2.26a) was based on the seat model integrated in the baseline vehicle model (Opiela 2008), and included a seat frame, seat and back foam cushions, and a headrest. The seat frame material properties were evaluated with tensile tests and implemented using a piecewise linear plasticity metal model (Watson 2010, 2011). The seat foam material was enhanced by Campbell and Cronin (2009, 2014) and characterized as a low-density foam. The foam material properties for low strain rates were obtained through compression tests, for intermediate strain rates through pendulum tests, and for high strain rates through a Polymeric Split Hopkinson Pressure Bar tests (Campbell and Cronin 2009, 2014).



Figure 2.26: Numerical models of the: (a) seat (gray) and a three-point seatbelt (red), (b) UW-HBM integrated with the vehicle. Side door removed for clarity.

The seatbelt model consisted of a shoulder and lap belt (Fig.2.26a) and was based on a 2000 Ford Ranger driver seat belt model (Watson and Cronin 2011). The seatbelt material characteristics followed the results of the experiments by Baudrit et al. (1999) for both the 2-D sections that contacted the occupant and 1-D sections that were not in contact with the occupant (Fig.2.26b). The pre-tensioner drew in 60 mm of the seatbelt in over 7.5 ms, and the delay after firing the pre-tensioner was 10 ms after the acceleration sensor in the lower seat frame measured a peak acceleration of 5 g. The force-limiter was set to 6 kN, based on the system developed by Baudrit et al. (1999).

2.4 Limitations of the Existing Research Methods in Predicting Occupant Response

HBMs help to bridge the gap in realism between the ATDs and PMHSs, providing a solution to certain limitations of the existing research methods. HBMs have the potential to provide additional insight into injury tolerance, patterns, and mechanisms; however, this potential has not yet been realized for side impact. Although HBMs predict occupant response at a global level through measurement of accelerations, velocities, and displacements, a primary benefit is tissue-level injury prediction and higher sensitivity to the pre-crash parameters, compared to the Anthropometric Test Devices (ATDs) (Baudrit 1999, Trosseille 2011, Gehre 2013).

2.4.1 Differences in Occupant Surrogates Sensitivity to Pre-Crash Parameters

Variability of the PMHS and volunteers test subjects due to anatomical, age, gender, or medical history differences can introduce variability to the PMHS injury responses in parametric studies (Miller and Rupp 2011). Most cadavers available for biomechanical research are over 70 years old and the causes of death include chronic diseases that affect the structural response of the thorax wall and mechanical properties of individual tissues (Rhule 2011). Installation of accelerometers, strain gauges or load cells require surgical interventions that can affect the kinematic response and soft-tissue injury prediction. The passive musculature of the PHMS also does not represent the effects of muscle tonus and voluntary or reflex responses. PHMS testing may also raise ethical concerns in some countries.

On the other hand, the durable design of ATDs and repeatability requirements prevent direct representation of injuries, such as fractures, ruptures, lacerations or contusions, through material failure (Wismans 2005, Cronin 2011). The capacity of the ATDs to reflect internal anatomy of human occupants is very limited, since the ATDs are designed to measure global kinematic response in terms of forces, accelerations, and displacements at discrete locations. Moreover, ATDs have been tailored for specific impact directions and pre-crash positions, therefore their biofidelity in off-axis impacts, which commonly occur during parametric studies on restraint effectiveness, is reduced.

Kim et al. (2016) highlighted differences between the ES-2re ATD and PMHS response for a lateral impact with a large volume tSAB, and identified challenges related to biofidelity of the ATD arm, lower back, and connection to the pelvis. Unrealistic behavior of those body regions resulted in the load transmission path being different between the ATD and the PMHS (Kim et al. 2016). Trosseille et al. (2010) reported a low sensitivity of the ES-2re ATD to test configuration, comparing rib deflection for experimental tests in rigid sled and padded sled impact, which impaired ATD application in parametric studies (Trosseille and Petitjean 2010).

2.4.2 One Standardized Pre-Crash Arm Orientation to Model Driver Position

Current vehicle certification standards include only one driving position, where the occupant is seated with arms at a 40-degree angle with respect to the torso midline (NHTSA 2012a).

However, epidemiological studies reported that the occupant position changes during the driving process (Viano et al. 1989, Reed and Ebert 2016, Reed et al. 2018), especially when approaching an intersection, negotiating a curve, or performing parking maneuvers. The ongoing efforts on the development of self-driving cars also open a possibility of occupant seating positions that are not common among drivers, though some may already be observed for passengers. Multiple studies have reported an effect of arm position on the predicted occupant response, but the conclusions are conflicting. Viano conducted ATD side-impact sled tests at 8.7 m/s, using a padded wall with different armrest designs mounted on the fixture. Changing the ATD arm position from horizontal (Viano 1991) to vertical, Viano (1994) demonstrated that the effect of the arm on the predicted ATD chest deflection and rib acceleration was strongly dependent on the location and type of armrest (Viano 1994).

The influence of arm position on the deflection of the thorax was tested by Stalnaker et al. (1979) using fresh unembalmed PMHS in free-fall tests, taking into account two arm positions: driving position and arms above the head. The cadavers were hung supported at shoulders, hips and legs with ropes and dropped from a height of 1m on a rigid or padded surface. Stalnaker et al. found that having the arm located in the loading path (driving position) reduced the number of rib fractures for the rigid impact condition and recommended further research on the influence of arm position.

Cesari et al. (1981) performed free-flight pendulum tests using unembalmed cadavers. Results suggested that arm position along the impacted side of the thorax could distribute the load and prevented impactor intrusion; an increase of the impact speed necessary to produce rib fracture was also discussed. The authors noted that arm position did not affect the type of injuries observed in the testing.

Kemper et al. (2008) undertook a series of non-injurious impacts (16 kg rigid impactor at 3 m/s, low energy) and injurious impacts (23.4 kg rigid impactor at 12 m/s, high energy). The non-injurious tests were performed on cadavers with arms in horizontal, vertical and in the driving position (lifted 45 degrees with respect to the thorax in the sagittal plane). In the low energy impacts, involvement of the arm and shoulder reduced impactor force, rib deflection and rib strain compared to the values obtained during direct rib impacts. During the

injurious high-energy impacts, the arms were located in the driving (45 degrees) or vertical positions. The position of the arm had a considerable effect both on the total number and distribution of rib fractures, reducing the injury metrics when positioned in the impactor loading path (vertical arm position) (Kemper 2008).

A more recent numerical study (Watson 2011) investigated occupant position (fore, aft, lateral) using the ES-2re, SID and WorldSID ATD models, and compared the maximum rib deflection and VCmax for different load cases. The viscous criterion was more sensitive to changes in position than the thorax deflection, and small changes in occupant position could result in significant changes in predicted response. The maximum response values were predicted to occur at the top or middle chest band levels of the ATDs. However, the effect of the pre-crash arm position on the occupant response and interaction with passive restraints has not yet been demonstrated in a full-vehicle side impact.

2.4.3 Lateral Impact Type to Represent Side Crash

Due to high costs associated with full-vehicle impacts, side impact crash scenarios have often been represented with simplified setups, such as pendulum and rigid- or padded-wall sled impacts at the development stage (Jordan 1974, Deng 1989). The impact velocities and acceleration profiles of the component tests were adjusted to replicate the amount of energy transferred to the occupant body during the full-vehicle side crash. Due to a risk of serious injury, volunteers do not participate in these experimental tests, and the occupant response is assessed with PMHSs and ATDs.

Although the component-level tests such as pendulum or rigid-sled impacts are cost-effective and accelerate the design process, Deng et al. (1989) demonstrated that free-flight impacts were not suitable for capturing the effects of velocity-pulse vehicle to vehicle side impacts. Deng's observation was based on a parametric numerical study that utilized multibody models and force-deflection characteristics to define contact between the occupant body and a pendulum impactor with changing padding thickness. Deng also theorized that rigid wall sled designs may not be capable of capturing the load transfer to the occupant body under a full

vehicle impact, which was further demonstrated by Rupp et al. (2011) in experiments comparing rigid-wall and padded dual-sled designs.

Researchers have shown that direct comparison of the side-impact ATD and PMHS responses in impact positions other than purely lateral impacts is challenging due to the complex kinematics and have suggested that additional studies to quantify the effect of these differences (Ratingen 2001, Yoganandan 2011, Wismans 2005, Cronin 2011, Kim 2016). However, the effect of the impact type on sensitivity of occupant response in a side impact has not yet been demonstrated, due to challenges in maintaining repeatability between PMHS occupant surrogates in parametric experiments.

2.4.4 Occupant Response Measurement Method

The kinematic responses measured with use of PMHSs and ATDs are not directly transferable between the two surrogate types (Baudrit 1999, Pyttel et al. 2007). The biofidelity of side-impact ATD responses has been verified through comparison to impactor displacements and accelerations measured in PMHS pendulum impact tests. Comparison of plate forces in rigid-wall sled impact scenarios and accelerations of two thoracic vertebrae measured in PMHS (Ratingen 2001, Wismans et al., 2005) further contrasted ATD to PMHS response. Therefore, comparison between the ATD and PMHS responses for the ATD development has been based on external kinematic metrics (Pintar 1997, Kuppaa 2004, Kim 2016). In order to compare internal, chest-deflection measurements between ATDs and PMHSs, Kuppaa et al. (2004) performed 38 PMHS and side-impact ATD rigid-wall sled tests. PMHS half-thorax deflection was measured using chest-bands, while ATD half-thorax deflection was measured using RD potentiometers. Chest-deflection values predicted by the ATD were significantly lower than the PMHS responses, indicating underestimation of the probability of injury to human body with the ATD in Kuppaa's experiment (2004).

Yoganandan et al. (2011) compared the side-impact ATD rib deflection (RD) potentiometer measurements to chest band (CB) deflection measurements made on the same ATD. The upper CB was located at the level of rib 4 on the ATD, and the lower CB was located at the superior half of the ATD abdomen. While purely lateral impact responses between the

RD and CB methods were comparable within a 5% margin, for oblique impacts the differences between the two were in the order of 300%, which was attributed to padding on the ATD rib modules and jacket (Yoganandan 2011).

Several studies have compared responses of ATD and HBM models. Park et al. (2014) compared the WorldSID, ES-2re and GHBMC model responses (forces, accelerations, rib deflections) to those of two PMHSs in a rigid sled side impact. The forearms of the GHBMC model were removed to match the amputated arms of the PMHS subjects. Of all the models considered, the computational human body model showed the best agreement with the experimental results; however, the authors identified a significant influence of the shoulder kinematics on the whole-body kinematics during the impact and suggested further research in this area. The authors also identified issues related to biofidelity of the ATD models.

Several researchers have highlighted the scaling method and indirect comparisons between the surrogates as a potential source of discrepancies between the laboratory prediction and epidemiologically observed effectiveness of the passive restraints (Agnew 2017, Donnelly 2017). While the assessment method based on the injury criteria provides a prediction of probability of injury of certain severity, namely an AIS score, assessments using global (whole-body) injury criteria do not enable a prediction or estimate of the specific injury type and its exact location (Baudrit 1999, Pyttel et al. 2007).

Chapter 3

Verification of Vehicle and Occupant Surrogate Models

The University of Waterloo Human Body Model (UW-HBM) has been previously validated under a wide range of impact scenarios by Forbes (2005), Campbell (2009), and Yuen (2010), and the ES-2re Anthropometric Test Device (ATD) finite element (FE) model response was evaluated by Watson (2009). For the purpose of this thesis, the UW-HBM and ATD responses were re-assessed with respect to selected existing experimental pendulum, rigid-wall sled, and full-vehicle impact data. The Global Human Body Models Consortium Human Body Model (GHBMC-HBM, version 4.3) has been further verified in this study using an accident reconstruction and a comparison of predicted injury locations and severity to physical occupant injury reported in a documented side crash (Crash Injury Research, CIREN 2018).

3.1 Methodology

3.1.1 UW-HBM and ATD Model Thoracic Response

For the purpose of this thesis, the UW-HBM thoracic response to lateral impacts was re-assessed, and the repeated experiments are marked in bold in Table 3.1.

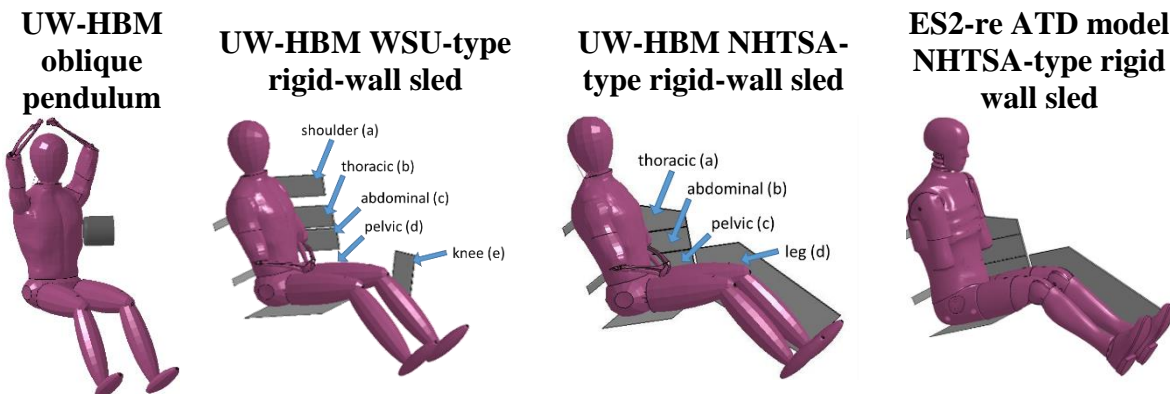


Figure 3.1: Validation scenarios of the occupant surrogate models re-assessed in this thesis.

The UW-HBM response to the pendulum impacts (Fig.3.1) was measured as impactor force and maximum predicted chest deflection. In the rigid wall sled impacts (Fig.3.1), UW-HBM response was assessed through a comparison of forces predicted at all contact plates as a result of contact with the occupant body to experimental values measured in PMHS experiments.

Table 3.1: The UW-HBM response verification and verification scenarios simulated in previous studies (Forbes 2005, Campbell 2009, Yuen 2010), and repeated for the purpose of this thesis (bold font).

Body region	Direction	Impactor	Velocity	Reference
Pelvis	Lateral	Pendulum	4.83 and 9.65 m/s	Viano et al. 1989
Abdomen	Oblique	Pendulum	4.5, 6.7, 9.4 m/s	Viano et al. 1989
Shoulder	Lateral, 3 angles	Pendulum	3, 4, 9 m/s	Compigne et al. 2004
Thorax	Frontal	Pendulum	4.3, 6.7 m/s	Kroell et al. 1971, 1974
	Oblique	Pendulum	4.3, 6.7 m/s	Viano et al. 1989
	Lateral	Pendulum	4.3, 6.7 m/s	Viano et al. 1989, Chung et al 1999
Full body	Lateral	Sled (NHTSA)	6.67 , 8.89 m/s	Pintar et al. 1997, 2001
	Lateral	Sled (WSU)	6.67 , 8.89 m/s	Cavanaugh et al. 1990, 1993
	Lateral (FMVSS 214)	Full vehicle	15 m/s	NHTSA tests #3522, #3668, NHTSA 2001

For the rigid wall sled impacts, responses of both UW-HBM and ATD occupant surrogates have been compared to biomechanical corridors (Yuen 2010) established based on the experimental data from PMHS tests, and the occupants were seated with upper arm aligned with the torso, following the experimental procedure (Cavanaugh 1990, 1993; Pintar 1997). The re-assessed ES-2re ATD NHTSA-type rigid wall lateral sled and full-vehicle impacts are marked in bold in Table 3.2.

For the full vehicle impacts, the UW-HBM and ATD responses at the three rib levels were compared to existing experimental data from the physical ES-2re ATD response in a Ford Taurus model year (MY) 1996 FMVSS 214 MDB impact at 54 kph (tests #3522 and #3482, NHTSA 2000). The occupants were seated in a standard *driving* position, with the angle between the upper arm and the torso set to 40 degrees, following the FMVSS 214 MDB protocol (NHTSA 2012). The seat cushion angle with respect to vehicle floor was 5 degrees, and the angle between seat back and vehicle floor was 70 degrees (NHTSA 2012). The seat centerline in the coronal plane was in the middle position, 310 mm from the armrest. The vehicle received good safety ratings in NCAP test (NHTSA 2000); however, MY 1996 and 2001 did not include thoracic airbags.

Table 3.2: The ES2-re ATD model response verification and verification scenarios simulated during previous studies and repeated for the purpose of this thesis (bold font).

Body region	Direction	Impactor	Velocity	Reference
Rib module	Lateral	Pendulum	1, 2, 3, 4 m/s	US Federal Code Title 49 Part 572, 2008 ECE 95
Thorax, no jacket	Lateral	Pendulum	5.5 m/s	US Federal Code Title 49 Part 572, 2008
Shoulder	Lateral	Pendulum	4.3 m/s	US Federal Code Title 49 Part 572, 2008
Full body	Lateral	Rigid wall (NHTSA)	6.7 m/s	Pintar et al. 1997, 2001
	Lateral (FMVSS 214)	Full vehicle	15 m/s	NHTSA tests #3522, #3482, #2340, # 2975, NHTSA 2001
	Lateral (NCAP)	Full vehicle	17 m/s	NHTSA test #3264, NHTSA 2001

3.1.2 GHBMCM-HBM Response Assessment

For the purpose of this thesis, the GHBMCM-HBM full body model response was assessed in a full vehicle side impact scenario replicating a physical side crash. Accident reconstruction using HBM presents challenges due to uncertainty in the input information and differences between the HBM and the case occupant. However, simulation of physical crash that resulted in known injuries can improve confidence in the FE model if the numerical predictions show similarity to the reported outcome. The interaction of the HBM with the vehicle and the capability of the HBM to predict the occupant injury patterns in a full vehicle impact was examined through a comparison to existing side impact crash data of the same vehicle (CIREN 2018). The reported crash was classified as a side impact involving a Ford Taurus MY 1999 vehicle struck by a 2003 Navistar delivery truck at an estimated speed of 48 km/h (30mph) (CIREN 2018) (Fig.3.2a). This scenario was identified in the CIREN database as being the closest to the baseline case for this study in terms of vehicle, occupant, and impact type and severity.

The occupant was an 18-year old male, 183 cm (6 ft) height and a mass of 80 kg (176 lbs). This mass is similar to the value for the 50th percentile male GHBMCM-HBM, but 8 cm taller (for comparison, the standard deviation of stature for all adult men in the US is approximately 8 cm; the occupant's stature was approximately the 85th percentile for US men). In the simulation, the driver was seated in a nominal driving position with the arms rotated 40 degrees upwards from the torso midline; however, information on pre-crash arm orientation during the physical crash was not available. The driver was wearing a three-point seatbelt, and no side airbag was present in the vehicle. All these pre-crash conditions were replicated in the simulation (Fig.3.2b). The occupant response was assessed through identifying locations of predicted rib fractures and assessing potential for soft tissue injury according to criteria embedded in the GHBMCM-HBM, described in Chapter 2, section 2.1.3 and 2.2.5.

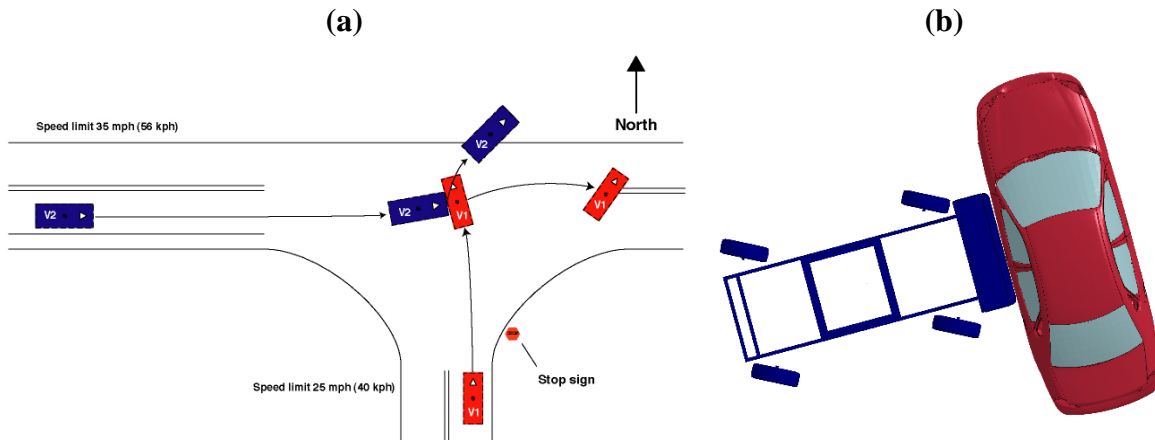


Figure 3.2: (a) The CIREN side crash scenario schematic (CIREN 2018), (b) reconstruction of the crash with the vehicle and Moving Deformable Barrier models.

Integration of the Occupant with the Vehicle and Restraint Models

The GHBMC-HBM was coupled with the vehicle, seat, and restraint systems (as described in section 2.3.3, section 4.1) during a series of pre-simulations (Fig.3.3a). To couple the occupant with the seat, the HBM was positioned above the seat avoiding any initial contact or penetration, and then gravity was applied to the HBM until a standard driving position was reached and the occupant was equilibrated with the seat (Fig.3.3b). The occupant was assumed to be equilibrated with the seat when the seat foam deformation followed the occupant pelvis contour, and the oscillation of the z-acceleration (vertical) response of the pelvis centre of gravity remained below 1 mm/s (Watson and Cronin 2011). The equilibrated assembly was subjected to a Moving Deformable Barrier (MDB) impact at the National Car Assessment Program (NCAP) impact velocity of 61 km/h (NHTSA 2012). The coupled vehicle-occupant side impact models were solved using a commercial explicit finite element code (LS-Dyna, version 6.1.1) (LSTC 2018).

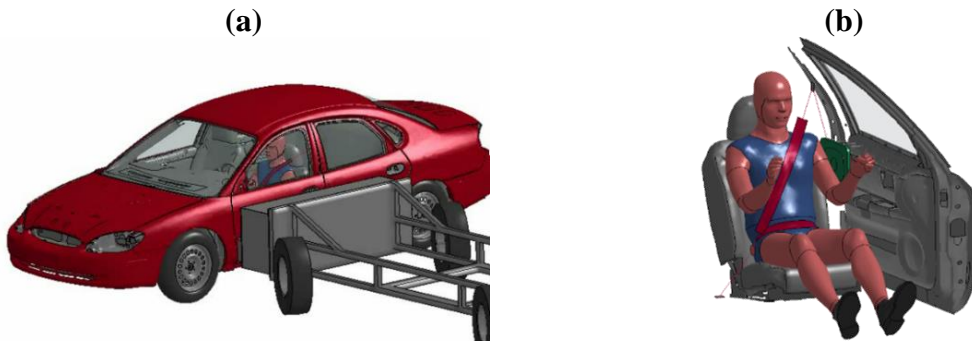


Figure 3.3: (a) Moving Deformable Barrier test configuration, (b) GHBM Human Body Model integrated with the vehicle, seat and the restraints.

3.2 Results

3.2.1 UW-HBM Response to Pendulum and Sled Impacts

The oblique impactor scenario at 6.7 m/s was used for verification of the UW-HBM response to concentrated load (Fig.3.1a). The predicted impactor force followed the lower boundary of the experimental corridor (Fig.3.4a) in agreement with previous studies. The maximum chest compression time history initially followed the lower boundary of the experimental corridor (Chung 1999), and matched the peak value of average experimental response, but 10 ms later in time (Fig.3.4b).

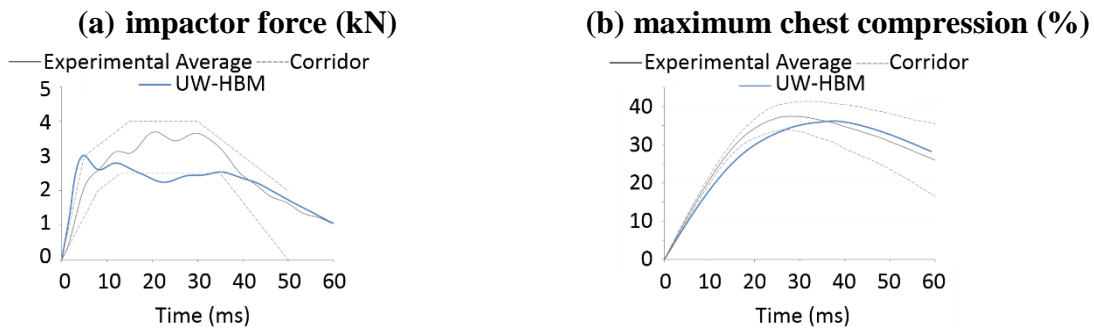


Figure 3.4: UW-HBM response (blue) for an oblique pendulum impact at 6.7 m/s, PMHS results in gray.

In the WSU-type rigid-wall sled test, shoulder (Fig.3.5a) and thoracic plate (Fig.3.5b) forces were in good agreement with the experimental data in terms of shape and magnitude. The thoracic plate response followed the experimental average for the loading phase (0-15 ms), and upper experimental bound for peak (15-30 ms) and unloading phase (30-60 ms). The total force predicted at all plates (Fig.3.5f) matched the shape of the experimental curves, following the upper experimental bound for the loading and unloading phases, and remaining within one corridor width for the peak phase (15-30 ms). An increase in maximum force was driven by the pelvic (Fig.3.5d) and knee plate (Fig.3.5e) responses that both over predicted the experimental response (but remaining within one corridor width), due to simplified geometry of the lower body of the UW-HBM.

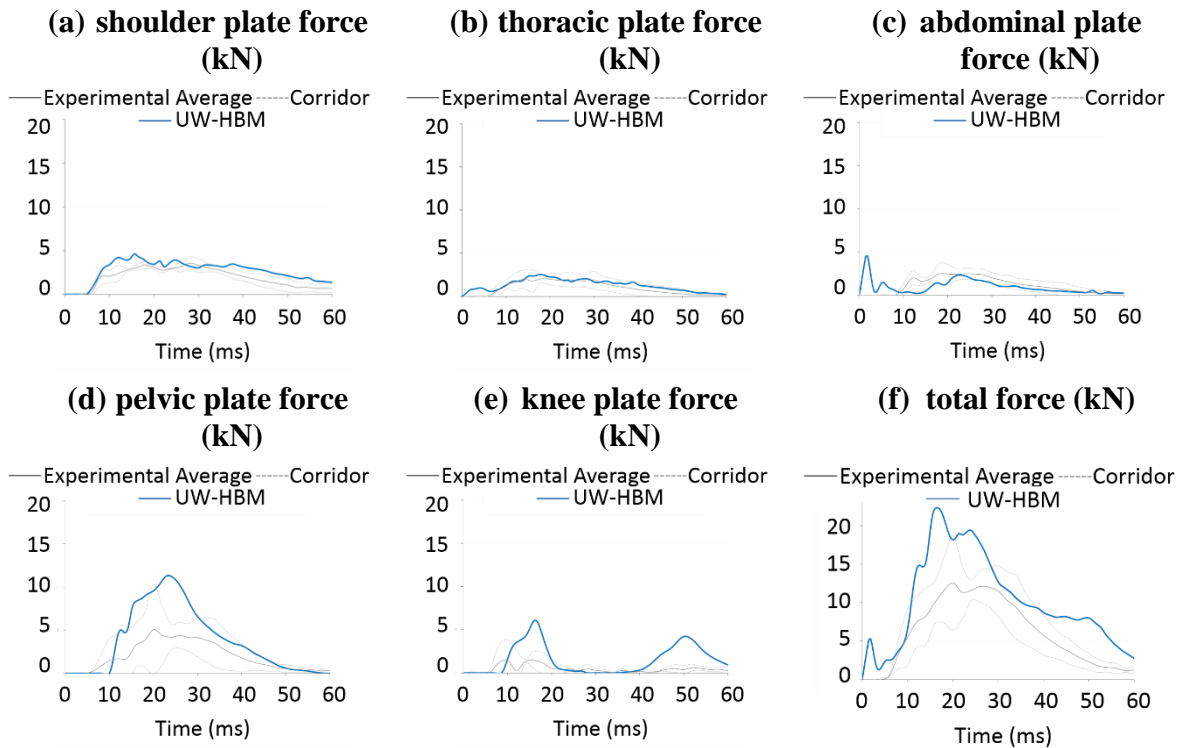


Figure 3.5: UW-HBM response (blue) in a WSU-type rigid-wall sled at 6.7 m/s, compared to PMHS data (gray).

In the NHTSA-type rigid wall sled test, the predicted thoracic force in the simulation followed the experimental average for the loading and peak phase and exceeded the upper experimental bound for the unloading phase (30-60ms) (Fig.3.6a). The UW-HBM response remained within the lower experimental bound for the abdominal plate (Fig.3.6b). The model over predicted pelvic (one corridor width) (Fig.3.6c), and leg plate force (more than one corridor width) (Fig.3.6d), due to simplified representation of the lower extremities. Total force response (Fig.3.6e) was in a good agreement with the experimental upper bound for the peak phase (15-30ms) in terms of amplitude; however, the rise time for the UW-HBM was shorter that for the experiment, mainly due to a contribution from the leg plate force component.

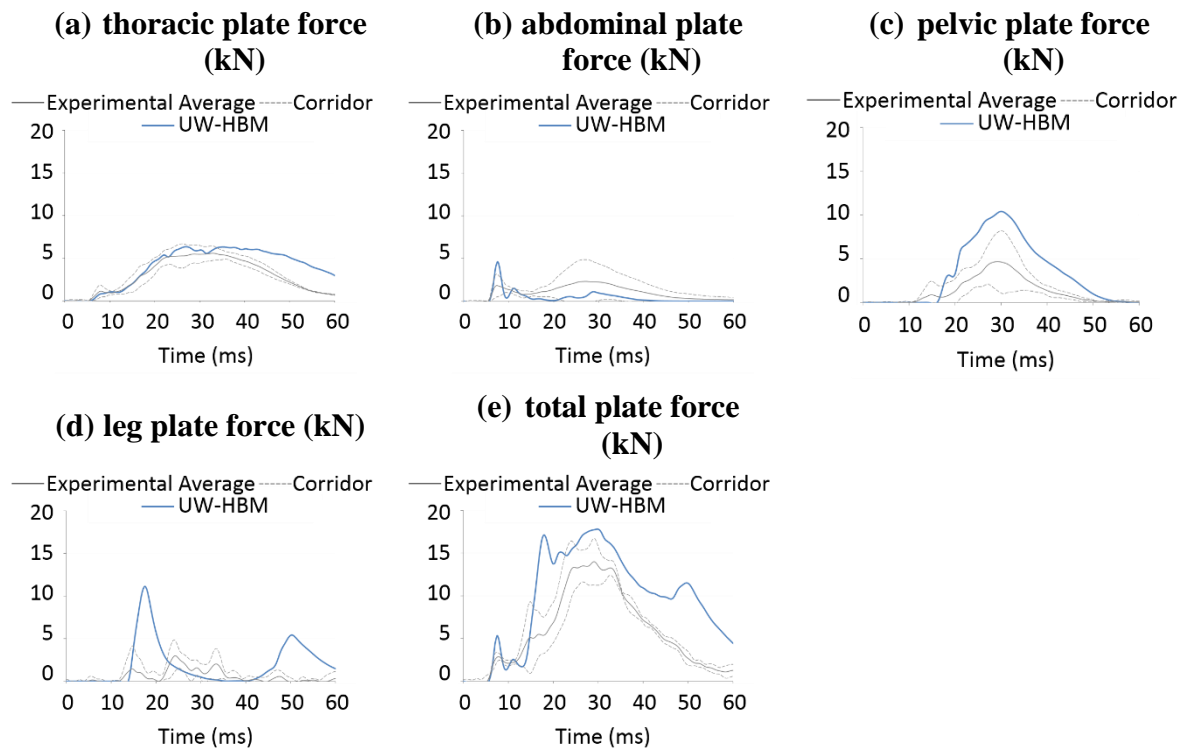


Figure 3.6: UW-HBM response (blue) in a NHTSA-type rigid-wall sled test at 6.7 m/s, compared to PMHS data (gray).

3.2.2 ATD and UW-HBM Chest Compression Response in a Rigid-Wall Sled Test

During the NHTSA-type rigid-wall sled impact, the UW-HBM chest compression and VC time histories compared well with the PMHS response and remained within the biomechanical corridors at the three rib levels (Fig.3.7). The ATD predicted no chest compression at the upper rib level, since the upper rib remained above the edge of the rigid wall (Fig.3.7) throughout the entire impact event. The ATD predicted higher chest compression at the middle rib level compared to the UW-HBM and the biomechanical corridors, since all the impact energy was transferred to the two ribs: middle and lower. At the lower rib level, the peak ATD compression was comparable to the upper range of the biomechanical corridor. The rise time of the ATD responses at the middle and lower rib level was shorter than of the UW-HBM, since the soft tissues modeled in the UW-HBM attenuated the rigid-wall impact energy, in contrast to steel ATD ribs. The cross-correlation (CORA) rating, calculated based on equally weighed progression, size, and phase shift rating between the ATD and UW-HBM chest deflection responses was equal to 0.12 for the upper rib, because the ATD upper rib did not engage with the thoracic plate. For the middle rib, the CORA rating was 0.87, and 0.89 for the lower rib. CORA rating values range from 0 (no correlation between the compared signals) to 1 (overlapping curves).

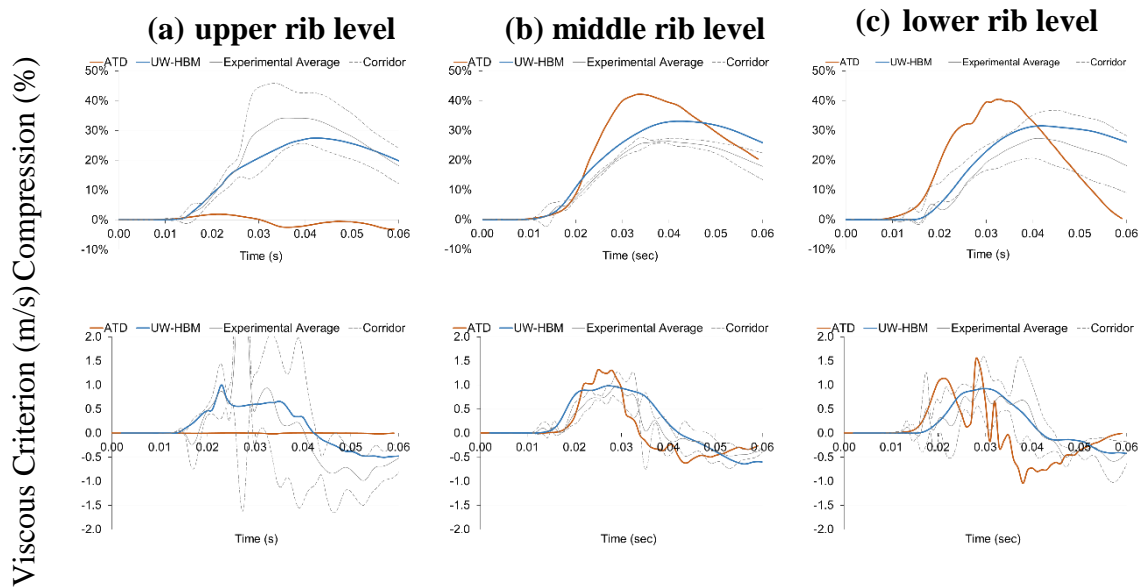


Figure 3.7: Comparison of the ATD and UW-HBM chest compression and VC responses in a NHTSA-type rigid sled impact at 6.67 m/s at the three rib levels. Experimental corridors and averages are based on PMHS experiments (Pintar et al. 1997).

3.2.3 Comparison of the UW-HBM and ATD Models Responses to Full-Vehicle Experimental Data

Chest deflection values predicted by both computational occupant surrogates (Fig.3.8) were similar to the experimental data at the three rib levels (Table 3.3).

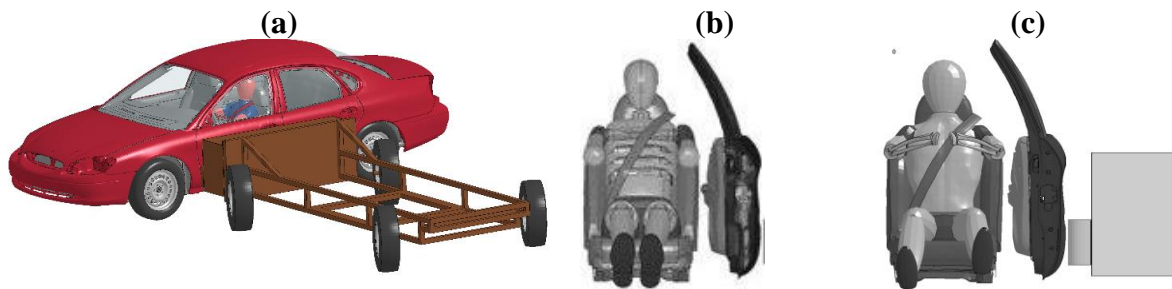


Figure 3.8: Computational model of the (a) Moving Deformable Barrier impact scenario, (b) ES-2re ATD model integrated with vehicle and restraints, (c) UW-HBM integrated with vehicle and restraints (Gierczycka et al. 2015).

Table 3.3: Comparison of rib deflection values (mm) at three rib levels for the physical and computational test surrogates (NHTSA 2000) subjected to a FMVSS 214 MDB impact in a Ford Taurus vehicle.

	Upper	Middle	Lower
NHTSA test #3522	34	32	25
NHTSA test #3482	39	40	37
ATD model	41	33	36
UW-HBM	42	30	40

3.2.4 Examination of GHBMCM-HBM Occupant and Vehicle Response for a Reconstructed Side Crash Event

Injury locations and severity predicted by the GHBMCM-HBM in a reconstructed CIREN accident were in agreement with the reported occupant injury. Since the focus of the comparison was the occupant injury prediction and the vehicle response has been validated in prior studies (Watson 2009), the comparison of the vehicle deformation pattern was not examined in detail (Fig. 3.9). However, it was noted that the model predicted less roof crush, possibly due to low impact height of the MDB.



Figure 3.9: Deformation pattern (a) of the physical vehicle (CIREN 2018), (b) predicted by the computational model.

A complete list of injuries sustained by the physical occupant, with corresponding AIS codes, is presented in Table 3.4. For the purpose of the GHBMCM-HBM response assessment, only the thoracic and abdominal injury was assessed. Injuries are listed from the most to the least severe.

Table 3.4: Injuries sustained by the physical occupant in a side crash (CIREN 2018).

AIS Code	Injury type	Aspect	Injury source
4	Diaphragm rupture with herniation	Inferior/ lower	Left side hardware or armrest
4	Major spleen laceration	Left	Left side hardware or armrest
3	Rib cage fracture 2-3 ribs any side with hemo-/ pneumothorax	L rib 11, L rib 12	Left side hardware or armrest
3	Thoracic cavity injury with pneumomediastinum (air in chest cavity)	Bilateral	Left side hardware or armrest
3	Femur fracture shaft	Left	Left side interior surface, excluding hardware or armrest
3	Pelvis fracture open/ displaced/comminuted	Left	Left side interior surface, excluding hardware or armrest
3	Tibia fracture shaft open/ displaced/comminuted	Left	Floor (including toe pan)
2	Mandible fracture open / displaced/comminuted body/angle with or without ramus involvement	Bilateral	Hood
2	Colon laceration no perforation	Inferior/lower	Left side hardware or armrest
2	Pelvis fracture closed	Right; left; anterior/ front/ ventral	Left side interior surface, excluding hardware or armrest
2	Kidney contusion minor	Left	Left side hardware or armrest
1	Teeth fracture	Inferior/ lower	Hood
1	Facial skin laceration minor	Left	Hood
1	Upper extremity skin abrasion	Left; upper arm	Hood edge

The most severe injuries to the thoracic region sustained by the physical occupant were the laceration of the left aspect of the spleen (AIS 4), diaphragm rupture in the lower inferior aspect (AIS 4), and two rib fractures: of left rib 11 and left rib 12 leading to pneumothorax (AIS 3) (CIREN 2018). The GHBMC-HBM predicted three rib fractures at left ribs 9-11, matching the location and severity of the physical hard tissue injury (Fig. 3.10a). The model also indicated an increased maximum effective stress location in the lower inferior aspect of the diaphragm, suggesting the potential for injury to this tissue (Fig.3.10b). The GHBMC-HBM also predicted maximum effective stress of 180 kPa in the left aspect of the spleen (Fig.3.10c), that exceeded the failure stress of 35 kPa (Kemper 2012), indicating a probability of major spleen laceration, as observed in the physical crash.

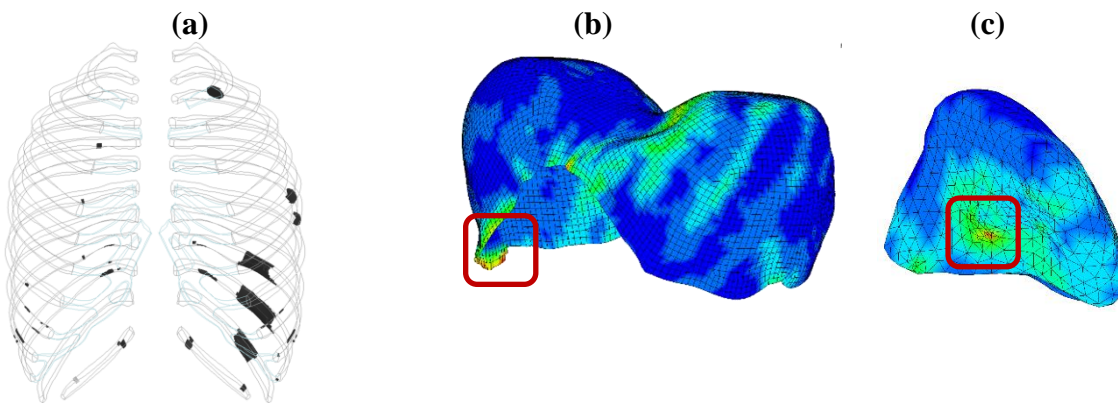


Figure 3.10: Locations of severe thoracic injuries predicted by the GHBMC-HBM, in agreement with the physical data: (a) rib fractures, (b) diaphragm rupture, (c) spleen laceration.

3.3 Discussion

The UW-HBM demonstrated the capability to predict PMHS response in a NHTSA-type rigid-wall impact scenario (Pintar 1997). Responses of the ATD predicted in the simulations matched the physical ATD measurements in the full vehicle crash scenarios and over-predicted PMHS response in the NHTSA-type rigid wall sled. These differences were attributed to a more upright seating position of the ATD in the sled impact, compared to PMHS and UW-

HBM, and to higher stiffness of the ATD thorax, compared to the UW-HBM which included soft internal organs and deformable outer tissues. Although some of the injury measures proposed in the GHBMC-HBM are still preliminary, the model generally predicted higher tissue response (e.g. strain) at the location of injuries reported for the physical occupant at impact conditions resembling the real crash scenario.

Limitations

The ATD model response was re-assessed at the full body level only, rib module and thorax pendulum impacts were not repeated. While the UW-HBM arms could be positioned similarly to the PMHS pre-crash arm orientation in the rigid wall sled impact (aligned with the thorax and rotated anteriorly), the ATD upper arms could only be aligned with the torso due to the ATD shoulder design constraints. Although distances between rib deflection measurement locations were uniform in the coronal plane between the ATD and UW-HBM, consistent rib width at the three levels in the ATD and, in contrast, anatomically variable in the UW-HBM, could lead to different chest compression values despite having similar rib deflection measurements. Chest compression is defined as change in chest breadth at a given rib level normalized by initial chest breadth at this level, and same chest deflection. Same value of chest deflection would result in higher chest compression at upper rib levels, and lower at the lower rib levels for the UW-HBM and human occupants, which could directly affect injuries of underlying soft tissues.

Verification of the integrated vehicle, restraint system and GHBMC-HBM was limited to one crash reconstruction impact scenario. While in the physical crash the vehicle was in motion and was struck by a truck, in the simulation the stationary vehicle was impacted by a Moving Deformable Barrier. Since no information on physical occupant pre-crash position was available, the driver's position was approximated with a standard driving position (FMVSS 214, NHTSA 2012). The human driver was 80 mm taller than the GHBMC-HBM, which could potentially affect the seating height and longitudinal location of the seat in the physical vehicle. The injury criteria embedded in the GHBMC-HBM were used as-delivered with the original version of the model (M50-O v.4.3).

Chapter 4

Occupant Surrogate Sensitivity to Door Compliance and Pre-Crash Position²

Several authors have identified the importance of occupant interaction with interior components and occupant position (Viano 1991, 1994; Watson and Cronin 2011) on the occupant response in side impact crash scenarios. As lead-in work to the larger study on restraint systems, the University of Waterloo Human Body Model (UW-HBM) and ES-2re Anthropometric Test Device (ATD) models were used to investigate the importance of these parameters on occupant response and to identify differences between the HBM and ATD response. The UW-HBM was utilized as the occupant surrogate in addition to the ATD model since the kinematic responses of PMHS have been found to differ from those of ATDs in full vehicle crash tests (Klaus and Kallieris 1983).

Previous studies (Watson and Cronin 2011) demonstrated an increase of thoracic injury risk when occupants, modeled using three different side impact ATDs (USSID, ES-2re, and WorldSID), were seated close to the door (271 mm between the armrest and seat centerline) and in the vicinity of B-pillar. Variation of the occupant response due to longitudinal and lateral position in the vehicle was found to be affected by interaction with the arm. Watson and Cronin (2011) recommended integrating HBMs into the vehicle crash environment to further investigate the effect of the arm on thorax response. Recent experimental research on interaction between the ES-2re and PMHS with a large-volume thoracic side airbag (tSAB) in a side impact highlighted lack of biofidelity of the ATD arm (Kim et al. 2016). Since the ATD models demonstrated sensitivity to position in the vehicle (Watson and Cronin 2011), this section of the study focused on assessing the ATD and UW-HBM models sensitivity to door

² Figures 4.2, 4.3, 4.4, 4.7, tables and section 4.3 (Discussion) were previously published in the International Journal of Crashworthiness © 19 Jan 2015 – <https://www.tandfonline.com/10.1080/13588265.2014.998000>, used with Publisher's permission.

compliance and pre-crash arm position prior to further parametric studies on interaction between the arm and side restraints. Door compliance was studied because the intruding door panel was found to be the most frequent source of injuries (Morris 1997). The pre-crash arm position effect was investigated since the effectiveness of side impact restraints is tested for one driving position, (NHTSA 2012), despite a wide range of driving positions reported in epidemiological studies (Viano 1989b). The purpose of this investigation was to identify an occupant surrogate capable of capturing the effect of modifications of pre-crash parameters to establish a foundation for further studies.

4.1 Methodology

Two occupant surrogates, an ES-2re ATD finite element (FE) model (DYNAmore GmbH, 2014) and the UW-HBM FE model were coupled with seat and restraints models within a vehicle. The integration of the occupant and vehicle models required a pre-simulation to position the occupant model in the seat and to allow the occupant models to achieve an equilibrium position through compression of the seat foam. Seat belt fitting was performed using pre-processing software with a belt fitting option (LS-PrePost, LSTC). At this stage of research, side airbags were not incorporated since the physical vehicle considered did not incorporate side restraints. A parametric study on the effect door trim material properties and arm position on predicted occupant thorax response was performed using an explicit FE solver commonly used by the automotive industry for crash analysis (LS-Dyna, version 5.1.1).

The computationally intensive process of integrating the GHBM-C-HBM with the vehicle included multiple pre-simulations, namely calculations performed prior to the experiment to apply appropriate initial conditions, performed in parallel to studies on occupant response assessed with the UW-HBM. The Global Human Body Models Consortium HBM (GHBM-C-HBM) was evaluated in a later study to assess trends predicted with the UW-HBM with use of an HBM more widely used in the automotive industry. A frontal steering-wheel airbag was included in the vehicle model and enabled (Lockhart et al. 2013); however, as expected, it did not deploy during the side crash simulation since it was only triggered by forward deceleration.

Although the FMVSS and CMVSS standards for side impact testing impact velocity is 54 kph (33.5 mph) (NHTSA 2012), this investigation uses the higher NCAP target impact velocity of 61 kph (37.9 mph). The 7 kph (4.3 mph) velocity increase has a significant effect on crash severity. Analysis of 118 passenger vehicle crashes (Richards 2010) demonstrated that while for the 54 kph impact speed fatal injury risk for the driver was on the order of 40%, the 61 kph impact velocity was associated with 80% risk of driver fatality. Previous studies (Watson and Cronin 2011) also demonstrated higher sensitivity of occupant response to a variation pre-crash parameters at higher impact velocities.

The occupant response was measured as a full-thorax deflection, between markers located directly on ribs on both sides of the thorax at three rib levels to facilitate direct comparison between the ATD and UW-HBM (Fig.4.1). The maximum chest deflection and VCmax, described as global response, and the deflection at each of the three rib levels, described as local response, were compared to evaluate sensitivity to impact conditions. The thorax impact velocity considered in the study was comparable with the impact velocity boundaries for VC suggested by Lau and Viano (1986).

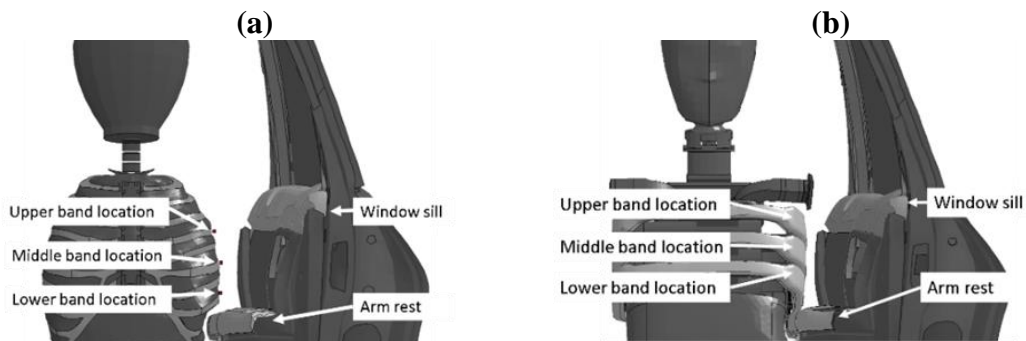


Figure 4.1: Location of the three rib levels in the: (a) UW-HBM model, (b) ATD model, with respect to the vehicle door.

4.1.1 Variation of the Door Trim Material Properties

In the as-delivered vehicle finite element model (Opiela 2008), the interior trim components were modeled with a piecewise linear-plasticity material formulation, where the material properties fell within the reported range for acrylonitrile butadiene styrene (ABS). ABS was a

common material used in interior door trim in 2000 MY vehicles (Watson 2010) and was therefore used as a reference for defining upper and lower bounds used in this parametric study (MatWeb 2010). This was a simplified representation, since the inner door panel may consist of multiple materials (Fig.4.2).

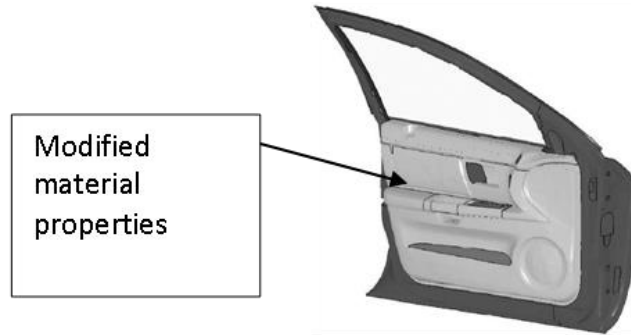


Figure 4.2: Vehicle side door, the highlighted door trim section indicates location of the modified elements.

The Young’s modulus, density and yield strength of the ABS material were varied according to upper and lower bounds for ABS identified in the literature (MatWeb 2010) (Table 4.1). The door trim material stress-strain curves were scaled in accordance with the yield strength, with a 1.44 scaling for the *high* strength and 0.61 for the *low* strength material, relative to the average ABS material properties (MatWeb 2010).

Table 4.1: Baseline and extreme values for the door trim ABS material properties.

	Density (g/cm ³)	Young’s modulus (MPa)	Yield strength (MPa)
high	1.3	6100	65.0
baseline	1.2	2800	45.0
low	0.3	1520	27.6

A screening study of main effects and interactions between the door trim material properties was designed as a 2³ full-factorial experiment (Table 4.2) (Montgomery 2012) for

Young’s modulus, yield strength and density examined at two levels (Table 4.3). Occupants were seated in a standard driving position (Fig.4.3b), with the arm rotated 40 degrees upwards with respect to torso midline, according to side impact test protocol (NHTSA 2012).

Table 4.2: Coded (Table 4.3) experimental design for the eight runs of the factorial design.

run	E	r	Er	s	Es	Rs	Ers
1	-	-	+	-	+	+	-
2	-	-	+	+	-	-	+
3	-	+	-	-	+	-	+
4	-	+	-	+	-	+	-
5	+	-	-	-	-	+	+
6	+	-	-	+	+	-	-
7	+	+	+	-	-	-	-
8	+	+	+	+	+	+	+

Table 4.3: Description of the experimental factors and variable codes.

		-	+
factor	E	Young’s modulus (MPa)	1,520 4,500
	r	Density (g/cm ³)	0.3 1.2
	s	Yield strength (MPa)	27.6 65.0

Following the factorial experiment, a one-variable-at-the-time study was performed to investigate the main effects in detail. One material property was modified in each run, and the other two remained at a *baseline* level (Table 4.1). Occupant response was assessed for both ATD and UW-HBM models at three rib levels in a standard driving position. The magnitude of the effect, namely change of the chest deflection and VC due to change of parameter value, were assessed with use of half-normal probability plots and marginal means plots. The potential for interactions between the factors was assessed with use of marginal means plots. Since replicates of the experiments, namely repeated numerical runs, yielded identical responses, the analysis of variance (ANOVA) and further tests to assess significance of the observed effect were not feasible.

4.1.2 Arm Position and Door Compliance Interactions

To study interactions between varying door trim material properties and pre-crash arm position, a 2^3 full-factorial experiment (Montgomery 2012) was conducted (Table 4.4). The UW-HBM response to arm position (A) was varied between horizontal and vertical, and Young's modulus (E) and yield strength (s) of the door trim material were varied between *high* and *low* levels (Table 4.5). The UW-HBM was the only occupant model used in this experiment, since the ATD model exhibited very small sensitivity (<5% change in chest deflection) to varying door trim material properties.

Table 4.4: Coded experimental design for the eight runs of the factorial design.

run	A	E	AE	s	As	Es	AEs
1	-	-	+	-	+	+	-
2	-	-	+	+	-	-	+
3	-	+	-	-	+	-	+
4	-	+	-	+	-	+	-
5	+	-	-	-	-	+	+
6	+	-	-	+	+	-	-
7	+	+	+	-	-	-	-
8	+	+	+	+	+	+	+

Table 4.5: Description of the experimental factors and variable codes.

		-	+
factor	A	arm position	horizontal vertical
	E	Young's modulus (MPa)	1,520 6,100
	s	Yield strength (MPa)	27.6 65.0

4.1.3 Arm Position Effect for ATD and UW-HBM Responses

Since the preliminary results revealed a strong domination of the arm position effect over other factors, a one-variable-at-a-time examination was run for three arm positions to study the magnitude of the arm effect for ATD and UW-HBM response. The ATD shoulder response was previously verified by Watson (2009), and the UW-HBM arm and shoulder response was previously assessed by Forbes (2005, 2006).

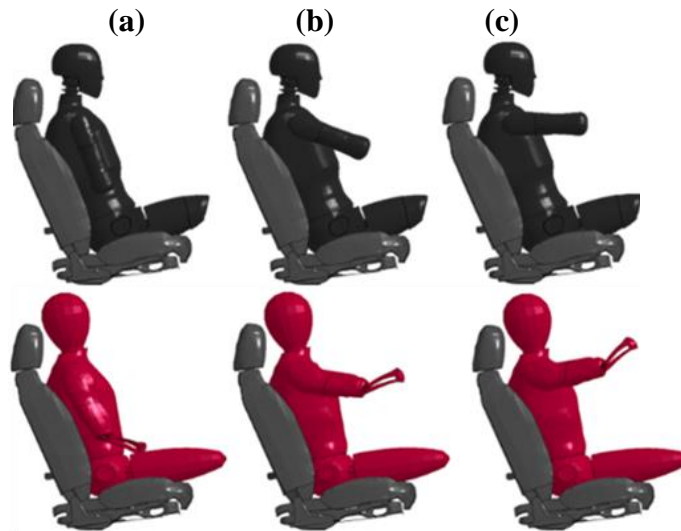


Figure 4.3: Three pre-crash arm positions: (a) vertical, (b) driving, (c) horizontal for the ATD (upper row) and the UW-HBM (bottom row).

Three occupant arm positions were investigated: *vertical* (upper arms parallel to the torso) (Fig.4.3a), *driving* (40 degrees angle between the upper arm and the torso, NHTSA 2012) (Fig.4.3b), and *horizontal* (upper arms parallel to the ground) (Fig.4.3c), to simplify the possible range of pre-crash occupant positions reported in the epidemiological data (Viano 1989b). The occupant arm orientation was changed during a pre-simulation, and the occupant was equilibrated with the seat for each vehicle impact simulation.

4.1.4 UW-HBM and GHBMC Sensitivity to Arm Position

The UW-HBM (Fig.4.4a) and GHBMC-HBM (Fig.4.4b) were integrated with the vehicle and compared in an unbelted, standard driving position, to minimize the effects of interaction with the restraint system in this lead-in study. The control points for positioning the HBMs in the vehicle were locations of the hip and head centre of gravity measured with respect to vehicle chassis, and an ability to reach pedals and steering wheel while maintaining a 40-degree angle between the upper arm and torso, following the side impact test protocols (NHTSA 2012).

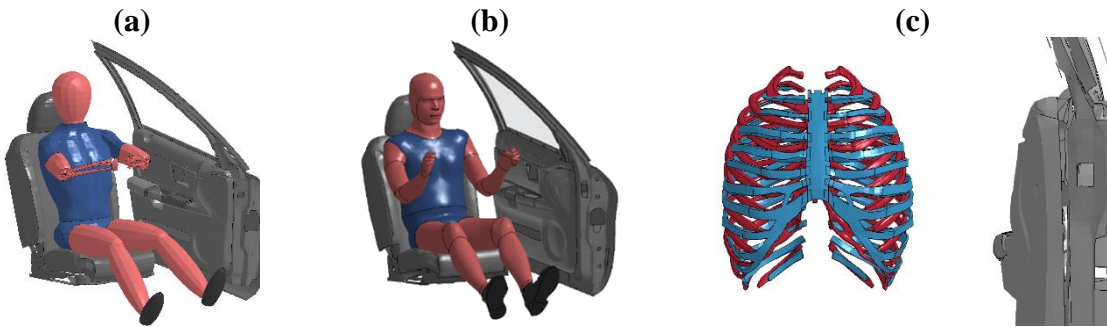


Figure 4.4: Two Human Body Models integrated with the vehicle in a driving position, unbelted: (a) UW-HBM, (b) GHBMHC-HBM, (c) comparison of the ribcage position with respect to the door, oblique view: UW-HBM (blue), GHBMHC-HBM (red).

Although both the UW-HBM and GHBMHC-HBM represented a nominal “50th percentile male” occupant with reference stature of 175 cm (5’9”), weight of 78 kg (172 lbs) and comparable erect sitting height (92 cm, 36”), differences in chest depth and extremities lengths between the models led to different upper torso orientations when seated in the vehicle. The position and orientation of control points, namely hip, head, feet and hands was the same between the two models (Fig. 4.4c, 4.5a). Difference in the lateral distance between the models and vehicle door was below 5mm at the head centre of gravity, below 5mm at the left glenohumeral joint, 13mm at the left humeroradial joint, and below 14mm at the hip level (Fig. 4.5b). The UW-HBM was leaning backward more than the GHBMHC-HBM (Fig.4.5c).

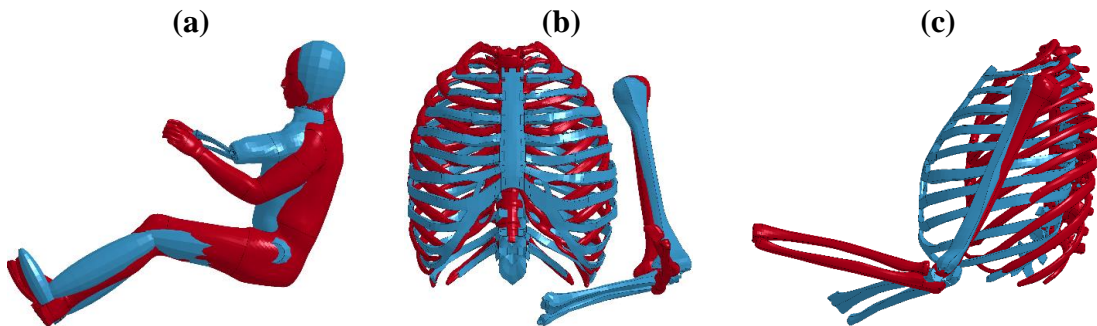


Figure 4.5: Two Human Body Models integrated with the vehicle: (a) driving position, lateral view, (b) vertical arm position, front view, (c) vertical arm position, lateral view, UW-HBM (blue), GHBMHC-HBM (red).

Responses of the UW-HBM and GHBMC-HBM were also compared for a vertical arm position, with the upper arm aligned with the torso (Fig.4.5c). The *vertical* arm position of both models was achieved through applying a gravitational load on the forearm while maintaining an upright position of the head and torso. Owing to differences in the upper torso orientation, where the UW-HBM was leaning backwards more than the GHBMC-HBM, the *vertical* arm position led to a direct alignment of the upper arm with rib compression measurement locations in the UW-HBM, contributing to higher sensitivity of the UW-HBM to arm position.

4.2 Results

For the 61-kph NCAP MDB standard impact (NHTSA 2012) the UW-HBM and ES2-re occupant kinematics were comparable throughout the impact sequence (Fig.4.6). The upward rotation of the shoulder and upper arm was more pronounced in the UW-HBM compared to the ATD model, which resulted in a lower rotation of the upper body of the UW-HBM towards the intruding door, compared to the ATD.

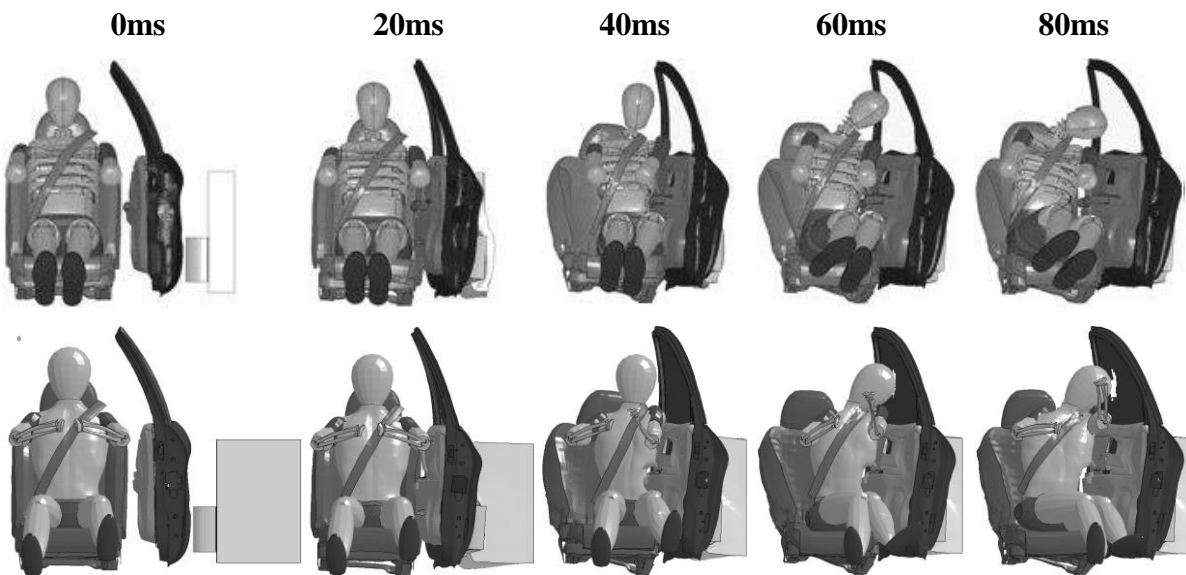


Figure 4.6: Comparison of the HBM and ATD kinematics in the full vehicle MDB impact.

Reduced upper body rotation of the UW-HBM, compared to the ATD, led to a shift in the point of contact with the door at the level of rib 4 between the UW-HBM and ATD, which contributed to higher value of chest deflection (66 mm) predicted by the UW-HBM compared to the ATD (50 mm). CORA rating of the two responses, based on equally weighed progression, shape, and size metrics compared for the two chest deflection time histories, was 0.75, indicating a reasonable correlation. At the other two rib levels, peak chest deflection responses predicted by the two occupant surrogates differed by less than 15% (Table 4.6). At the middle rib level, CORA rating of the two responses was 0.89, and at the upper rib level, 0.96 indicating good correlation.

Table 4.6: Comparison of rib deflection values for the computational occupant surrogates subjected to a NCAP (61 kph) impact.

	Upper	Middle	Lower
ES2-re ATD model	50	43	42
UW-HBM	66	38	49

4.2.1 Change of Occupant Response Due to Door Compliance Variation

Two-level interactions between the factors were assessed through marginal means plots (Montgomery 2012) at three rib levels (Fig. 4.7). Marginal means are calculated as mean response for one factor across levels of the other factor. Parallel lines indicate no interaction, crossing lines indicate strong interaction, and lines at an angle with respect to one other indicate moderate or possible interaction.

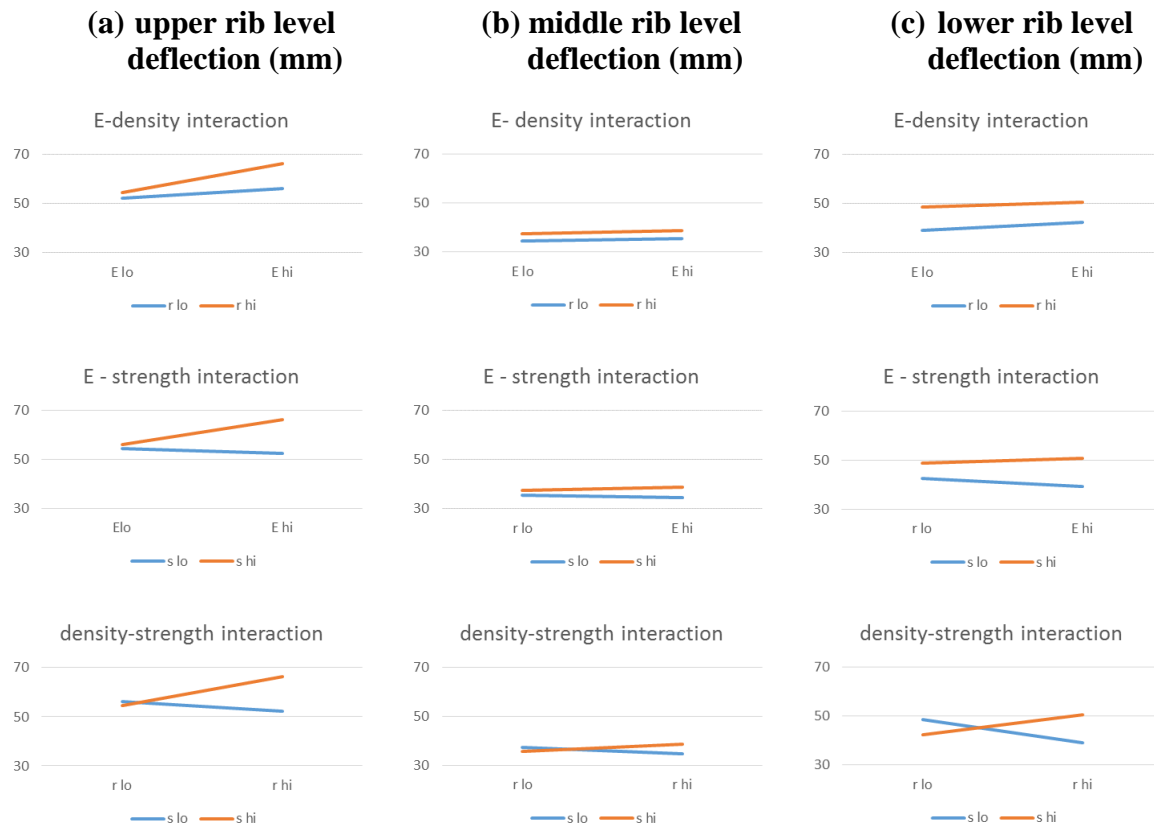


Figure 4.7: Marginal means plots visualizing mean factor effects of and two-factor interactions between the Young's modulus, density, and yield strength for rib deflection, predicted by the UW-HBM at the (a) upper, (b) middle, and (c) lower rib level.

The sensitivity of the ATD model to the parametric changes was very low, and responses predicted for different combinations of the door material properties provided similar responses (Appendix 1). For the UW-HBM, potential interactions were predicted at the upper rib level, between Young's modulus and density, Young's modulus and yield strength, and density and yield strength (Fig.4.7a). The most noticeable evidence for interactions between factors was predicted for density-yield strength at the lower rib level (Fig.4.7c).

The importance of the main effects and of the potential interactions was assessed through half-normal probability plots (Fig.4.8, Montgomery 2012) at the three rib levels. If a

factor did not contribute to changes in occupant response, it would follow a linear trend line. Outliers indicated a potentially important effect of the factor for the occupant chest deflection.

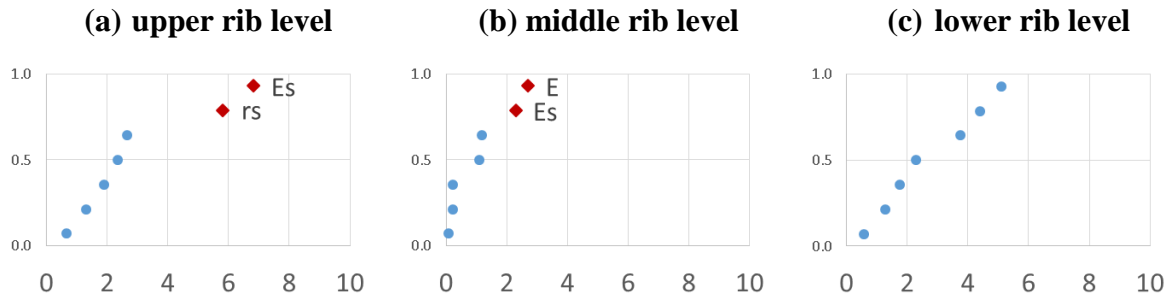


Figure 4.8: Half-normal probability plots of the effects at each rib level, for the chest deflection response (mm). E – Young’s modulus, rs – interaction between the Young’s modulus and density, Es – interaction between the Young’s modulus and yield strength. Distinguishable effects marked in red.

The magnitude of the effects associated with variation of the door trim material properties for the UW-HBM chest deflection was rather small (0-7 mm change, Fig.4.9). Interaction between Young’s modulus and yield strength had the highest effect for chest deflection predicted at the upper rib level, and the change in chest deflection due to Young’s modulus variation was the most pronounced at the middle and lower rib levels.

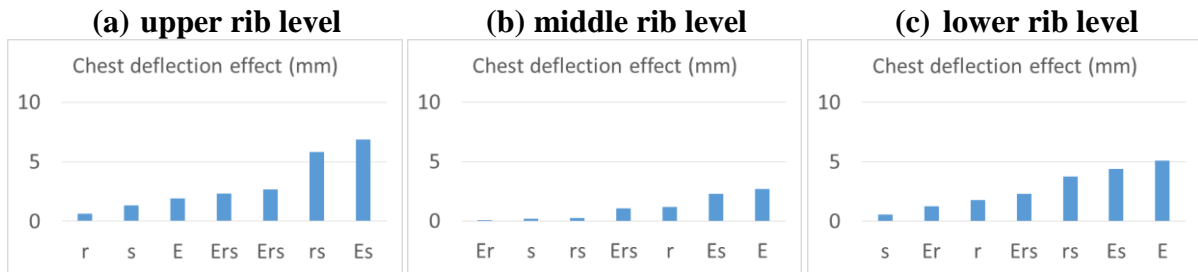


Figure 4.9: Pareto charts of effects, for the three rib levels. E – Young’s modulus, s – yield strength, r – density. Er – interaction between the Young’s modulus and density, Es – interaction between the Young’s modulus and yield strength, Ers – interaction between the three factors.

For single factor variations of the door trim material properties, the ATD and UW-HBM responses differed both in terms of global response (maximum thorax deflection and VCmax) and local response (response measured at three rib levels). The highest values of thoracic deflection were controlled by the upper rib location for both the UW-HBM and the ATD. The ATD rib deflection response changed by less than 5%, indicating low sensitivity to modifications of the door trim material properties (average correlation between the responses was 0.97-0.99, Table 4.7). The VCmax values measured with the ATD model were higher than the UW-HBM responses (Table 4.8), where the highest values of VCmax were controlled by the middle chest band location for the ATD. The ATD model was the most sensitive in terms of VCmax to low (relative VCmax reduction of -16.5%, with respect to baseline material properties) and high (-13%) values of door trim material Young's modulus. The average correlation between the ATD VC responses was still high, between 0.95-0.96 (Table 4.7). Detailed analysis of response correlation ratings is provided in Appendix 1.

Table 4.7: Average CORA rating for the occupant responses compared at three rib levels between baseline-low, and baseline-high material properties setting.

	ATD	UW-HBM	ATD	UW-HBM
	Chest deflection		Viscous Criterion	
density	0.99	0.95	0.98	0.83
Young's modulus	0.98	0.96	0.95	0.92
yield strength	0.97	0.95	0.97	0.86

The UW-HBM predicted a decrease in the maximum chest deflection from 66 mm to 52-56 mm (-18 to -27%) when the door trim material properties were assigned the upper boundary properties, captioned as *high* in Table 4.8. The most significant rib deflection change was predicted by the HBM for the *high* yield strength. The average correlation between the chest deflection responses was 0.95-0.98 (Table 4.7). The UW-HBM demonstrated an expected trend of decreasing VCmax with increasing yield strength of the door trim material,

decreasing from 0.79 m/s (*low strength*) to 0.59 m/s (*high strength*), where the highest values of VCmax were controlled by the upper chest band location. The average correlation between the UW-HBM VC responses indicated a moderate effect of varying material properties (0.83-0.92), more pronounced than in the ATD (Table 4.7). Detailed analysis of response correlation ratings is provided in Appendix 1.

Table 4.8: Percentage change of the maximum global response with respect to the baseline case for both occupant surrogates and all modified material properties.

	ATD		UW-HBM	
	Max deflection	Max VC	Max deflection	Max VC
Density				
Low (% change)	+2%	-2%	-6%	-5%
Baseline	50 mm	1.56	66 mm	0.67
High (% change)	+2%	-5%	-20%	0%
Young's modulus				
Low (% change)	+1%	-16%	-6%	+4%
Baseline	50 mm	1.56	66 mm	0.67
High (% change)	0%	-13%	-18%	+3%
Yield strength				
Low (% change)	4%	-3%	0%	+13%
Baseline	50 mm	1.56	66 mm	0.67
High (% change)	0%	-6%	-27%	-13%

4.2.2 Interaction between the Arm Position and Door Compliance

The arm position had a noticeable effect for chest deflection response of the UW-HBM at all three rib levels, with the highest magnitude of the effect at the lower rib level (85 mm increase with arm in vertical position). Interaction between the arm position and yield strength of the

door trim material was the second highest effect, but with a magnitude considerably lower (5 mm change) compared to the effect of arm position (85 mm change for vertical arm position) (Fig.4.10).

To evaluate interactions between the arm position and door compliance, marginal means were plotted for each interaction (Montgomery 2012) at three rib levels. Potential interaction between the arm position and the door trim material yield strength was predicted at the middle rib level (Fig.4.11b). However, the actual effects of these interactions on the occupant response were negligible, compared to the magnitude of the effect of the arm position itself (Fig.4.10).

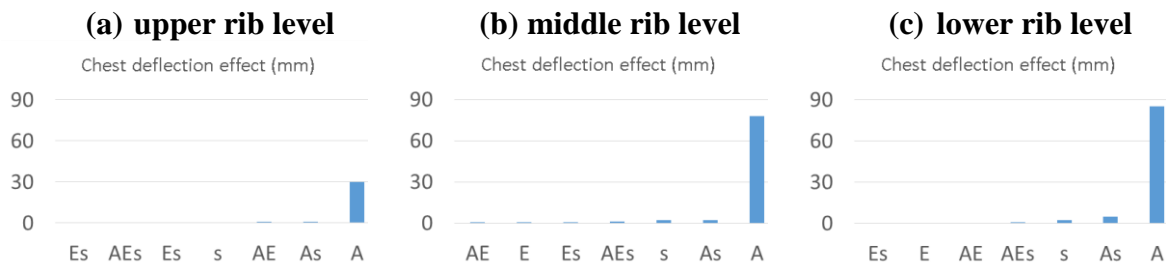


Figure 4.10: Pareto charts of effects at three rib levels. A – arm, E – Young’s modulus, s – yield strength, AE – interaction between the arm position and Young’s modulus, As – interaction between the arm position and yield strength, AEs – interaction between the three factors.

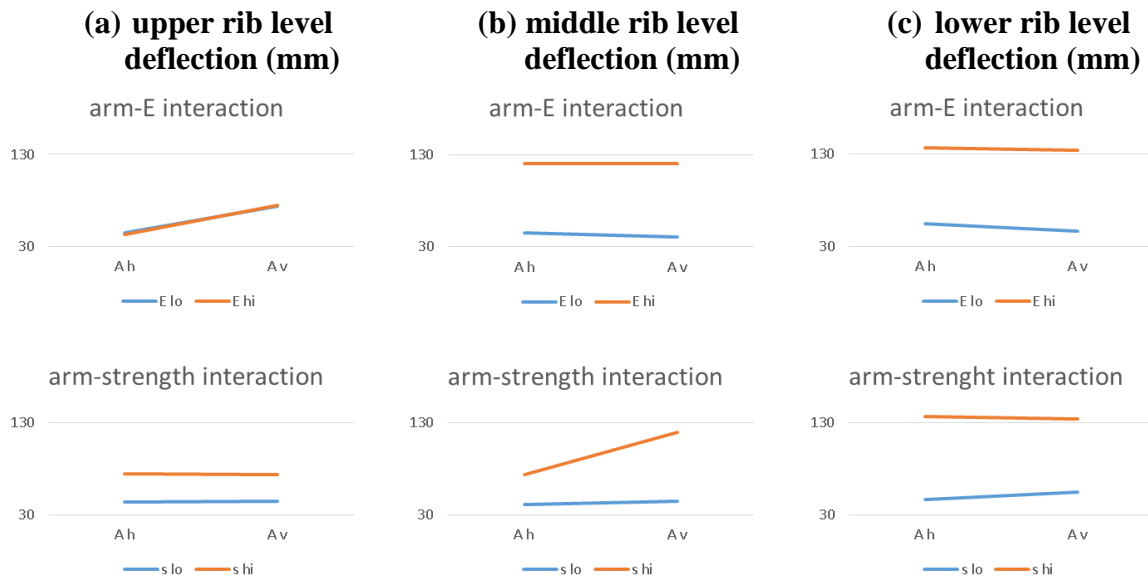


Figure 4.11: Marginal means plots visualizing mean factors effects and two-factor interactions between the arm position, Young’s modulus and yield strength, predicted by the UW-HBM at the three rib levels.

4.2.3 Arm Position Effect on Occupant Thorax Response

For variation of the arm position only, chest deflection values were comparable between the ATD and the HBM for *horizontal* and *driving* positions at the middle and lower chest band level. The ATD chest deflection values remained within the 40-52 mm range for all the rib levels and all arm positions. The cross-correlation rating calculated at three rib levels for three arm positions remained between 0.93-0.95, indicating low sensitivity of the ATD chest deflection response to the arm position. In contrast, the HBM deflection response was significantly different for the *vertical* arm position at all rib levels, compared to *driving* and *horizontal* positions (Table 4.9). The most significant increase in the rib deflection predicted by the UW-HBM was observed for the *vertical* arm position at the middle and lower rib locations. The cross-correlation rating for the UW-HBM chest deflection ranged from 0.70 at the middle rib level to 0.82 at the upper rib level, indicating rib-level specific sensitivity to arm

position. Detailed analysis of correlation ratings and time histories of chest deflection responses are available in Appendix 1.

Table 4.9: Chest deflection responses predicted by the ATD and UW-HBM at all three rib levels for three pre-crash arm positions (maximum values shown in bold).

	ATD			UW-HBM		
	vertical	driving	horizontal	vertical	driving	horizontal
Upper	49	50	52	79	66	47
Middle	40	43	43	123	38	46
Lower	48	42	43	134	49	51

While for the *horizontal* and *driving* arm positions the difference between maximum rib deflection values of the ATD and UW-HBM remained within a 25% margin, for the *vertical* arm position the UW-HBM maximum chest deflection value increased by 200% (0.70-0.76 correlation rating, Table 4.10), while the ATD model predicted no change (Fig.4.12a) (0.89-0.93 correlation rating). The VCmax values were generally higher for the ATD than for the HBM for the driving and horizontal arm positions; however, the HBM VCmax value (1.7 m/s) exceeded the ATD response (1.0 m/s) for the vertical arm position at the lower chest band location (Table 4.11).

Table 4.10: Average cross-correlation rating for the occupant responses compared at three rib levels between driving-horizontal, driving-vertical, and vertical-horizontal arm positions.

	ATD	UW-HBM	ATD	UW-HBM
	Chest deflection		Viscous Criterion	
Upper rib	0.94	0.82	0.93	0.76
Middle rib	0.93	0.70	0.89	0.70
Lower rib	0.95	0.76	0.90	0.75

The ATD predicted the highest values of VC for the driving position, and the VC response was the lowest for ATD with the vertical arm position (Fig.4.12b). Maximum ATD VC values were predicted by the middle chest band location for all arm positions. For the HBM, the highest VC response was found for the vertical arm position and the lowest VC values were predicted for the horizontal arm position. Maximum UW-HBM VC values were predicted by the lower chest band location for the vertical arm position and by the upper rib location for the driving and horizontal arm position (Table 4.11). VC response sensitivity assessment with cross-correlation rating was reported in detail in Appendix 1.

Table 4.11: Viscous Criterion responses predicted by the ATD and UW-HBM at all three rib levels for three pre-crash arm positions (maximum values shown in bold).

	ATD			UW-HBM		
	vertical	driving	horizontal	vertical	driving	horizontal
Upper	0.9	1.1	1.1	0.9	0.7	0.3
Middle	1.0	1.6	1.4	1.6	0.3	0.3
Lower	0.8	0.8	0.8	1.7	0.3	0.3

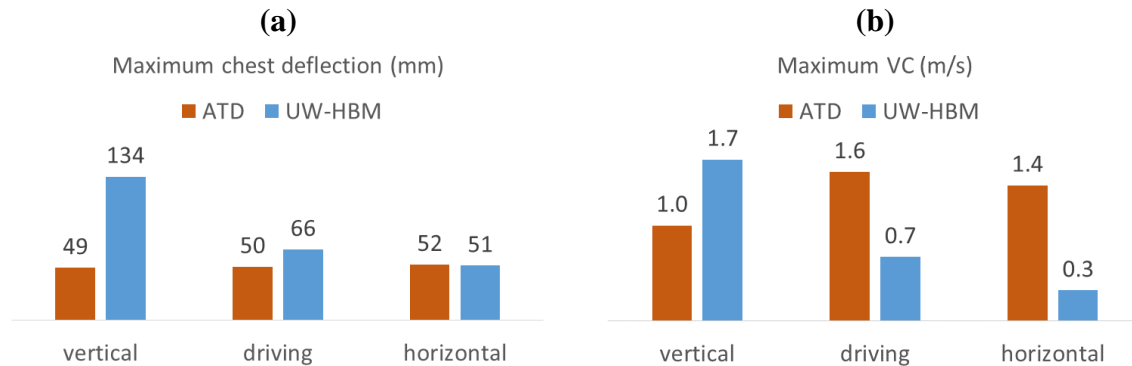


Figure 4.12: (a) maximum chest deflection, (b) VCmax, predicted by the ATD and UW-HBM models for the three arm positions.

4.2.4 GHBM and UW-HBM Thorax Response to Varying Arm Position

The UW-HBM and the GHBM-HBM predicted comparable values of chest compression for an unbelted mid-sized occupant at the level of rib 6 (17%) and rib 8 (17-20%) in a full vehicle lateral MDB impact at 61 kph. However, the chest compression values varied at the level of rib 4 (30% for the UW-HBM and 8% for the GHBM-HBM, Fig.4.13a). Due to higher pre-crash backward leaning of the upper torso, maintaining a standard driving arm position of 40 degrees angle between the torso and upper arm (NHTSA 2012) resulted in a relatively higher rotation of the upper arm of the UW-HBM compared to the GHBM-HBM, with respect to vehicle door. Therefore, the UW-HBM thorax was exposed directly to contact the intruding sharp edge between the window sill and the door trim, at the level of rib 4, while in the GHBM-HBM the soft tissue of the upper arm got compressed between the upper door trim and the ribcage and reduced the direct deformation to the ribs. The UW-HBM therefore predicted significantly higher chest compression at the level of rib 4 (Fig.4.13a).

Chest compression values for the vertical arm position increased at all three rib levels for both HBMs. However, the magnitude of the increase was more pronounced for the UW-HBM. While at the rib 4 level both HBMs predicted a 20% relative increase of the chest compression values due to the arm position, at the level of rib 6 the UW-HBM predicted a +162% relative increase, while the GHBM-HBM only measured a relative +16% increase of the chest compression. The highest relative increase of the chest compression was predicted at the level of rib 8 by both HBMs, +157% for the UW-HBM, and +61% for the GHBM-HBM respectively (Fig.4.13b).

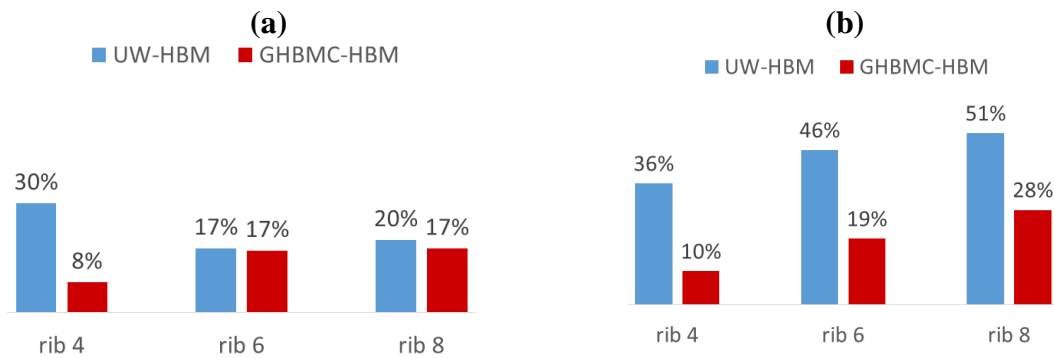


Figure 4.13: Comparison of the UW-HBM (blue) and GHBMHC-HBM (red) chest compression at three rib levels in a full vehicle side impact in a: (a) standard driving position, (b) vertical arm position.

4.3 Discussion

For the standard driving position, the UW-HBM and ATD rib deflection responses were comparable between the models at the middle and lower rib levels, and the difference for the upper rib response between the HBM and ATD remained within a 25% corridor (Table 4.6). This is one of the standard measures used in vehicle compliance and performance testing and constitutes an important baseline for the present work.

4.3.1 Influence of the Door Trim Material Properties

For the door trim material properties modifications, the ATD responses indicated low sensitivity of the ATD, which was also observed by Trosseille (2010), by comparing a physical ES-2re rib deflection in a padded and rigid sled impact conditions. The maximum rib deflection values were identified at the upper rib level for both the ATD and UW-HBM. The ATD did not show sensitivity to change of door trim material properties in terms of rib deflection response. These findings were only apparent through the use of local response (e.g. considering the response at each rib level) and were not apparent at the global level (e.g. the usual global measurement of deflection or VCmax). A reduction of maximum rib deflection response was observed for the UW-HBM when the door trim material was stiffer.

In terms of the VCmax response, the ATD response changed by -13 to -16.5% for both stiffer and more compliant door trim material. The VCmax values were controlled by the middle rib level. For the UW-HBM, the VCmax decreased by -13.5% for higher yield strength of the door trim material and were controlled by the upper rib level. Although the VCmax values for the UW-HBM were recorded at the upper rib level, both the upper and lower rib level showed similar moderate sensitivity to the material modifications. The ATD thorax deflection and VC values were lower for all modifications considered compared to the UW-HBM.

4.3.2 Influence of Arm Position in Side Impact

Arm position influenced shoulder kinematics and arm motion (Fig.4.6) and subsequently the loading of the thorax. During the impact, the UW-HBM arm typically rotated upward for the initial driving and horizontal positions. In contrast, the ATD arm moved in the sagittal plane only, and the GHBMC-HBM arm moved in coronal plane only, without a noticeable rotation (Fig.4.6). For the *vertical* arm position, the UW-HBM arm provided a load transmission path to the thorax, increasing the thoracic deflection; whereas the ATD model arm did not transmit the loading and instead protected the chest. For the GHBMC-HBM, the *vertical* arm position placed the upper arm more anteriorly to the rib compression measurement locations. Upper arm soft tissue was compressed between the intruding door and rib compression measurement locations, providing additional padding. Therefore, the predicted chest compression increase due to the *vertical* arm position was lower for the GHBMC-HBM than for the UW-HBM. The results of this study agree with previous observations (Watson 2010) regarding low sensitivity of the ATD to changes in pre-crash arm position.

The highest values of rib deflection typically occurred at the upper rib location for both the ATD and the UW-HBM due to contact with the window sill (Table 4.9) and load transferred to the thorax by interaction with the upper arm, before the arm rotation or movement occurred. For the GHBMC-HBM, the highest values of rib deflection were predicted at the lower rib location, due to concentrated load transferred through the distal end of the humerus, when compressed between the intruding door and GHBMC-HBM torso.

While the literature on the effect of the arm suggested a potential protective effect when located in the load path, it is important to note that the proposed protective effect of the arm was observed in a free-flight distributed load impact (dropping the PMHS on the floor) or in a velocity-pulse concentrated load impact (limited stroke pendulum). However, the limitations of both of these scenarios in representing the vehicle-to-vehicle side impact (Deng 1989) will be further discussed in Chapter 5. The potential protective effect of the arm, reported by some authors (Cesari 1981, Stalnaker 1979, Kemper 2008) is also further discussed in Chapter 5.

For non-standard arm positions, the primary response differences between the HBM and ATD were attributed to shoulder kinematics and arm compliance. The ATD shoulder allowed for sagittal plane arm movement only and was isolated from the thoracic cage through the connection to the spine box in the ATD. The UW-HBM shoulder was connected to the thorax through the scapula, clavicle and musculature providing a physiological range of motion of the arm in all directions and coupling to the thorax. The UW-HBM kinematics were comparable to the PMHS tests for the same NHTSA-type sled side-impact scenario in terms of arm rotation and displacement (Forbes 2005). Biofidelity of the GHBMC-HBM shoulder was recently investigated by Park et al. (2016); however, the proposed improvements altered the predicted side impact response by only 5%.

Movement of the elbow anterior to the thorax in the driving and horizontal positions reduced the load transferred to the thorax through the UW-HBM arm, while the GHBMC-HBM arm was rotating predominantly in the coronal plane during the entire impact sequence. The vertical arm position resulted in higher values of maximum thoracic deflection and VC, compared with other arm positions for the UW-HBM in side impact. The ATD arm model was softer compared to the UW-HBM arm model, which resulted in lower loading to the thorax for the vertical arm position. The models demonstrated that the plate mimicking the humerus located inside the ATD arm deformed around the metal rib bands and the arm foam acted as additional padding to the ATD ribs. This difference can explain a reduced value of global thoracic deflection for the vertical arm position for the ATD compared to the UW-HBM.

For the *driving* and horizontal arm positions, the global VCmax values were higher for the ATD owing to higher rib deformation velocity. The initial contact between the ATD

ribcage and the intruding door resulted in a high initial rib peak velocity that did not occur in the UW-HBM. For most of the cases the ATD rib deformation velocities were higher than the UW-HBM rib deformation velocities at all rib levels, with the peak value occurring during the loading phase, after contact with the door. This observation confirms findings of Watson and Cronin (2011) who demonstrated that the ATD model was more sensitive to change of arm position in terms of VCmax than in case of rib deflection, since the VCmax was mainly influenced by rib deformation velocity. The time of the deformation velocity peak in the ATD corresponded to the time of the VCmax response. For the UW-HBM, the maximum VC occurred between the peak values of the rib deformation velocity and chest compression during the loading phase.

Both UW-HBM and GHBMC-HBM predicted an increase of injury metrics for the *vertical* arm position; however, individual anthropometric differences between the two “average male” models yielded distinctive, occupant-specific results in terms of sensitivity to the pre-crash position. The occupant responses demonstrated a sensitivity to the location where the response was measured. The response rating based on global metric (maximum thoracic deflection, VCmax) did not match the sensitivity of individual chest bands to door trim material modifications for the VCmax-based rating. The analysis of responses measured at three chest band levels provided an opportunity to identify local effects that were not noticeable using global thoracic response and to assess the responses in an objective manner. The local evaluation identified potential areas for improvement in side impact safety through modifying door contact area or restraint systems.

Contacts defined between the occupant models and the vehicle interior, seat, and the restraints could have contributed to the predicted arm kinematics. However, the coefficient of static friction of 0.3 used in this study was comparable to coefficient of friction of 0.294 measured between the PMHS and seat in a lateral impact (Lessley et al. 2010), and representative for typical skin-to-fabric or fabric-to-fabric contact (Vilhena and Ramalho 2016). Experimentally measured dynamic coefficients of friction between occupant clothes and automotive seats ranged between 0.344-0.906 (Cummings et al. 2009), and a dynamic coefficient of friction 0.35 used in this study represented the lower range of this range. Of

course, real occupants would be expected to have a wide range of clothing and initial positions that could affect arm kinematics.

The UW-HBM demonstrated a capacity to capture the effect of modification of pre-crash parameters, and was subsequently applied in the parametric study on the occupant response sensitivity to lateral impact type (Chapter 5), owing to its applicability in predicting pulmonary contusion (PC) (Yuen 2010). Although the GHBMC-HBM was a more detailed model recognized in automotive industry, the potential of the GHBMC-HBM to predict PC has not been previously demonstrated, and no Crash Induced Injury criteria were associated with the lungs constitutive model (GHBMC 2014). The calculation times for the UW-HBM were also significantly reduced compared to the GHBMC-HBM, which was an advantage for a parametric study involving 10 load cases. The computation runtime for 100 ms of the impact sequence was over 60 hours on 32 computing cores for the GHBMC-HBM, and for the UW-HBM it took 24 hours with 6 computing cores.

- Change of the ATD response to varying door trim material properties was more pronounced for the VC than for the chest deflection.
- The UW-HBM demonstrated significantly higher sensitivity to pre-crash parameters than the ATD in terms of chest deflection and VC responses.
- Change of the chest deflection and VC responses of the UW-HBM was higher for varying arm positions than for different door trim material properties.
- The thesis should focus on the effect of the arm position, and evaluate its effect for different lateral loading scenarios and interaction with the restraints.
- UW-HBM has a potential to capture the effects of parametric changes and should be used as the occupant surrogate for the purpose of this thesis.

Limitations

The model year of the vehicle used in this study was 2001 and originally tested at 61 kph with the US SID ATD. The vehicle received good safety ratings in NCAP test (NHTSA 1996). Elevated values of predicted rib deflection and VC response in this study are due to the NCAP

impact velocity (61 kph) and use of a different ATD (ES-2re, instead of the USSID). Validation with the ES-2re ATD was carried out at 54 kph to address FMVSS 214 requirements.

The UW-HBM lower arm was simplified; however, this was not expected to affect the results since the tissue mass was accounted for, and lower arm was not in contact with the occupant body. Only one vehicle, seat location, and crash scenario were used at this stage of the study. The occupant size was representative for a mid-sized male, yet demonstrated differences related to individual anthropometry of the UW-HBM and GHBMC-HBM. Although the shoulder is acknowledged to be an important load transmission path in side impact crash scenarios, changes in the load path due to arm orientation were not investigated in the thesis due to limited capacity of the ATD model to predict shoulder response in off-axis impacts. The shoulder model of each occupant surrogate was previously validated using concentrated pendulum impacts, while the full vehicle crash was similar to a distributed load impact.

Chapter 5

Human Body Model Sensitivity to Lateral Impact Type

In Chapter 4, a significant effect of arm position for occupant responses related to thoracic injury was predicted by two Human Body Models in a full-vehicle side-impact scenario. The results showed that the local geometry of the impacting surface, as well as intervening structures such as the arm, can have large effects on thoracic injury measures. However, in research studies, side impacts are commonly simplified to pendulum and sled impacts due to the high cost associated with full vehicle crashes. Consequently, more study is needed of the differential responses associated with the nature of the lateral loading scenario.

This chapter presents a numerical parametric study to examine differences in occupant response sensitivity to lateral impact type. The UW-HBM was selected due to its capacity to predict potential for lung injury and high computational efficiency. Four standardized side impact test scenarios were considered, namely pendulum impacts (Viano et al. 1989, Chung et al. 1999) and rigid-wall impacts (Pinter et al. 1997, Cavanaugh et al. 1990), and the results of those scenarios were compared to occupant response in a full-vehicle MDB impact (NHTSA 2012). The arm position prior to impact was varied from a position aligned with the torso to above the head.

5.1 Methods

5.1.1 Lateral Impact Scenarios

The UW-HBM injury response sensitivity to parametric changes was investigated to quantify the effect of the arm position for different lateral impact scenarios. The geometries and boundary conditions for the pendulum and rigid-wall impacts were based on biomechanical test standards and component level tests (Fig.5.1). Impact velocities, geometry of the impactors, and corresponding literature references are summarized in Table 5.1. Pendulum impactors were 152 mm in diameter and weighed 23.4 kg (Viano et al. 1989, Chung et al. 1999). Rigid-sled geometries were based on two standards: National Highway Transport

Safety Administration (NHTSA) (Pintar et al. 1997), and Wayne State University (WSU) (Cavanaugh et al. 1990) designs.

Table 5.1: Summary of standard lateral impact conditions.

Impact type	Free-flight		Velocity-pulse	
	Pendulum	Rigid sled	Pendulum	Full vehicle
Impactor type	Pendulum	Rigid sled	Pendulum	Full vehicle
Initial velocity	4.3 m/s	6.7 m/s	5.6 m/s, 51 mm displacement	17 m/s (NCAP)
Impactor weight / dimensions	23.4 kg, $\phi 152\text{mm}$	NHTSA/ WSU	23.4 kg, $\phi 152\text{ mm}$	vehicle door
Code	P-F	NHTSA-F, WSU-F	P-V	NCAP-V
Reference	Viano et al, 1989	Pintar et al.1997 Cavanaugh et al.1990	Chung et al.1999	NHTSA, 2012

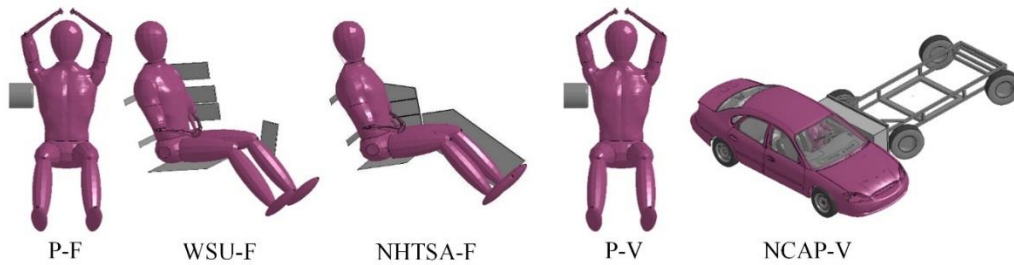


Figure 5.1: Lateral impact scenarios: (P-F) free-flight pendulum, (WSU-F) free-flight WSU rigid sled, (NHTSA-F) free-flight NHTSA rigid sled, (P-V) velocity-pulse pendulum, (NCAP-V) velocity-pulse full vehicle NCAP (Gierczycka and Cronin 2015a).

The literature data discussed in Chapter 2 suggest that the arm may act as a load transmission path to the thorax for vehicle impacts that are primarily displacement-controlled impacts (compared to free flight impacts where the pendulum is decelerated by the body). In the case of low-energy impacts, the arm serves to attenuate and distribute the load and assist

in decelerating the impactor resulting in lower thorax response. Therefore, impact scenarios were grouped in two categories: free-flight, and velocity-pulse. For the free-flight impacts, the impactor initial energy was pre-determined through an initial velocity and the pendulum was slowed down by the mass of the occupant after impacting the occupant body. For the velocity-pulse categories, a velocity profile was assigned to the impactor as a function of time or displacement, similarly to the velocity profile of the intruding door in the physical vehicle crash.

5.1.2 Occupant Pre-Crash Position

The goal of the study was to compare thoracic response when impacted directly to impacts with arm in the load path, to investigate response sensitivity to arm for different loading types. Two pre-impact positions of the HBM were considered: with upper arms aligned with torso (*arm down*), and with arms moved above the head or in a horizontal position, exposing the thorax to impact (*arm up*) (Fig.5.2). For the full vehicle scenario, a horizontal arm position was sufficient to expose the thorax to intruding door panel. A fully vertical arm position, similar to occupant position in pendulum and rigid wall impacts, was not pursued due to contact between lower arms and vehicle roof.

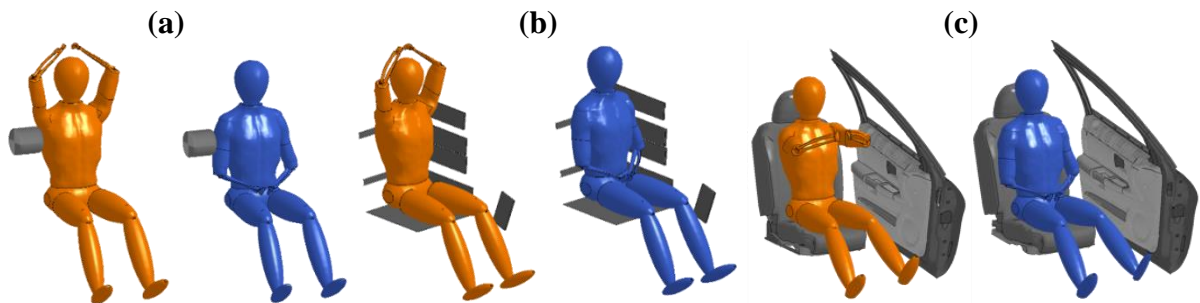


Figure 5.2: Examples of the two arm positions for the lateral impact conditions: *arm up* in orange, *arm down* in blue, (a) pendulum impacts, (b) rigid-wall sled impacts, (c) full vehicle impacts.

5.1.3 Occupant Response Assessment

To predict occupant response in accordance with automotive standards (NHTSA 2012), and understand compression pattern along the ribcage, the occupant response was evaluated as chest compression measured at three rib levels, rib 4, 6, and 8, corresponding to three locations of the ATD ribs at a standard driving position in the vehicle, as explained in Chapter 2, section 2.2.4. In addition to local deflection response, the maximum of three rib-level chest compressions and VC values were included in the assessment and referred to as maximum chest compression and VCmax.

The UW-HBM has been also previously used to predict pulmonary contusion through determination of the volume of elements exceeding certain pulmonary injury criteria (Yuen 2010). This advantageous capacity of the UW-HBM enabled a comparison of occupant response prediction with use of standard injury metrics (maximum chest compression, VCmax) with local injury response (chest compression and VC measured at three rib levels), and with the tissue level injury prediction (lung contusion). For the purpose of this study, the pulmonary contusion criterion adopted by Yuen, namely dynamic compressive pressure exceeding 52.4 kPa measured at an individual element level, has been adopted. To ensure adequate temporal resolution, the lung response was monitored at 40,000 Hz (Yuen 2010), and volumes of all the elements that exceeded the threshold pressure at any phase of the simulation, loading and unloading, were summed. The volume of elements exceeding the pressure criterion threshold were divided by the original lung volume to obtain percentage of the contused lung volume.

5.2 Results

5.2.1 Concentrated Versus Distributed Load

The UW-HBM with a vertical arm position, *arm down*, predicted an increase of the chest compression for all the load cases, except for the velocity-pulse pendulum impact. The magnitude of the effect was dependent on the impact scenario, where the highest increases of the chest compression (+140%) were predicted in the full vehicle scenario, a relative increase between +56 to +69% was predicted for both rigid-wall sled impacts, and the chest

compression remained relatively insensitive to the arm position in the pendulum impacts (-13 to +10%). The effect of the arm was even more pronounced for the VC metric, where the full vehicle scenario resulted in a +428% increase of VCmax with *arm down*, the two rigid-wall sled impacts change remained within the +56 to +76% range, and the free-flight pendulum (P-F) predicted a negligible change (-11%). However, the *arm down* position led to a decrease of VCmax (-36%) for the velocity-pulse pendulum (P-V) scenario (Table 5.2).

Table 5.2: Relative changes in occupant metrics due to *arm down* pre-crash position.

Impact type	P-F	WSU-F	NHTSA-F	P-V	NCAP-V
compression	+10%	+69%	+56%	-13%	+140%
VC max	-11%	+76%	+56%	-36%	+428%

Changing the arm position for concentrated load impacts, namely pendulum impacts, resulted in a lower relative change of the occupant response compared to distributed load impacts, namely rigid-wall sled and full vehicle scenarios. Although the relative change of chest compression did not exceed +/-13% in the pendulum impacts, the chest compression pattern, determined as a measurement of a peak compression at each rib level, indicated that the maximum chest compression location moved from rib 4 to rib 8 with *arm down* position for both pendulum impacts (Fig.5.3a,d). For the distributed load scenarios, the change due to *arm down* position ranged between +56 to +140%. While the maximum chest compression location was maintained for both the WSU-F and NHTSA-F scenarios, for the full-vehicle impact the maximum chest compression location moved from rib 4 to rib 8 with the *arm down* position.

Chest deformation pattern between the WSU-F and full-vehicle impacts demonstrated the same trend, where the *arm up* position led to chest compression values approximately equally distributed over the three ribs. For the *arm down* position, the highest values of chest compression were predicted at the level of rib 8 for both the WSU-F and NCAP-V scenario (Fig. 5.3b,e). For the NCAP-F scenario, the *arm down* position led to an increase of the chest

compression, while the thoracic deformation pattern remained the same, with the lowest chest compression at the level of rib 4, and the highest at the level of rib 8 (Fig.5.3c). Despite similarities in the chest compression patterns, the relative increase of the chest compression due to arm position was larger for the NCAP-V scenario than for both rigid-wall sled impacts (+140% versus +69% in WSU-F, and +56% in NHTSA-F), which was even more pronounced in the predicted VCmax (+428 versus +76 in WSU-F, and +56% in NHTSA-F).

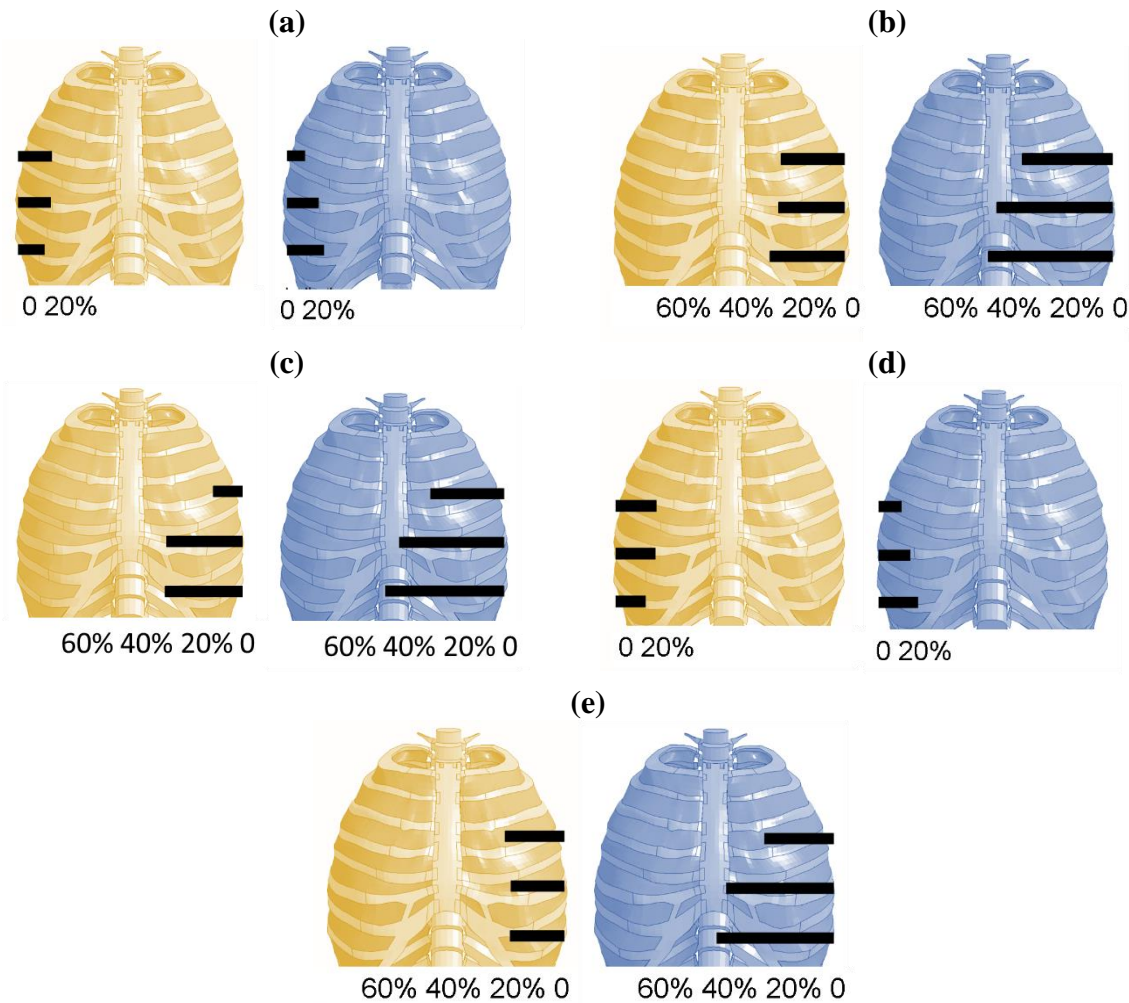


Figure 5.3: Patterns of the peak values of chest compression at three rib levels, two arm positions: arm up (orange) and arm down (blue); (a) free-flight pendulum (P-F), (b) WSU-type rigid-wall sled (WSU-F), (c) NHTSA-type rigid-wall sled (NHTSA-F), (d) velocity-pulse pendulum (P-V), (e) full-vehicle impact. Chest compression patterns

reflect the lateral impact direction, according to experimental standards (left for rigid-wall sled and vehicle, right for pendulum).

5.2.2 Free-Flight versus Velocity-Pulse

The relative change in the occupant metrics predicted by the UW-HBM was higher in the velocity-pulse impacts (-V) than in the free-flight impacts (-F) (Fig.5.4). The sensitivity of the chest compression and VCmax to the *arms down* position was comparable between the free-flight rigid sled impacts (WSU-F and NHTSA-F), increasing by 56-76% for both chest compression and VCmax metrics.

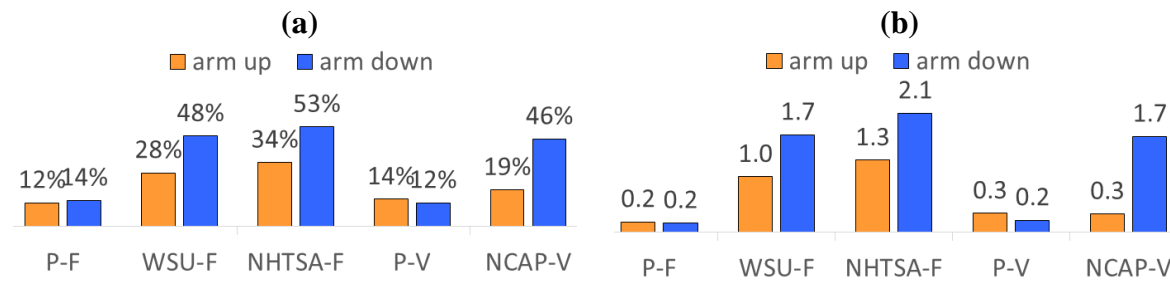


Figure 5.4: Maximum (a) chest compression, (b) VC (m/s) for free-flight and velocity-pulse impacts.

In the case with the arm in the load path (*arm down*) chest compression was lower for the velocity-pulse pendulum impact (relative reduction of -13%) and increased for other impact types. The VCmax response followed the same trend, where the *arm down* position reduced the VCmax by -36% in the velocity-pulse pendulum impact. Both rigid sled configurations predicted an increase of chest compression between 56-69% (Table 5.2), while the highest relative increase of chest compression was observed for the full vehicle impact (+140%). With arm in the load path (*arm down*), time between maximum compression and maximum velocity was shorter, therefore the VCmax response increase was even more pronounced and reached 1.7 (+428%) for the full vehicle impact.

5.2.3 Prediction of Lung Contusion Severity and Pattern

Predicted volumes of contused lung tissue were in agreement with chest compression and VC criteria (Fig.5.5). The *arm down* position had a negligible effect on contused lung volume in the free-flight pendulum scenario (3% to 2% decrease, P-F). For the velocity pulse pendulum, the injured lung volume was reduced from 7% to 4% with the *arm down* position, confirming the protective effect of the arm for this impact scenario. For the WSU-F rigid sled, the *arm down* led to an increase of predicted contused lung volume from 38% to 48%, and a similar 10% increase was found for the *arm down* position in the full vehicle scenario (50% to 60%, NCAP-V). For the NHTSA-F, although the chest compression and VC values increased for the *arm down* position, the lung contusion response remained relatively unchanged (38% to 36% reduction, NHTSA-F). Shoulder soft tissues in the *arm down* position provided additional padding in the area above rib 4 that contacted a rigid edge of the NHTSA-F sled wall in the *arm up* position.

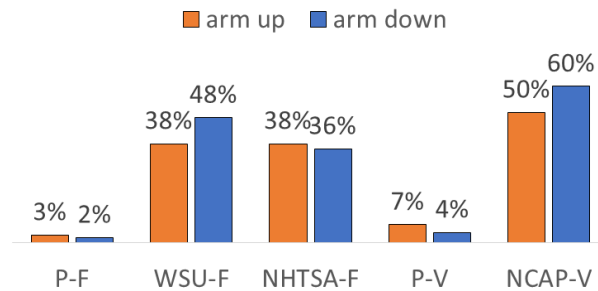


Figure 5.5: Predicted total contused lung volumes for two arm positions, for all loading types.

Lung contusion patterns for the WSU-F and NCAP-V scenarios that yielded comparable chest compression patterns at three rib levels for both *arm up* and *arm down* positions, demonstrated higher predicted volume of contused lungs in the full-vehicle scenario (NCAP-V) (Fig.5.5). Although the maximum chest compression for the *arm up* position was higher in the WSU-F scenario (28%) than in the NCAP-V scenario (19%), the full vehicle impact resulted in higher predicted total contused lung volume (50%) than the rigid sled (38%)

(Fig.5.6). Similarly, for the *arm down* position the predicted contused lung volume was higher in the full vehicle scenario (60%) than in the rigid sled (48%), although the WSU-F scenario yielded a higher maximum chest compression (48s%) than the NCAP-V (46%).

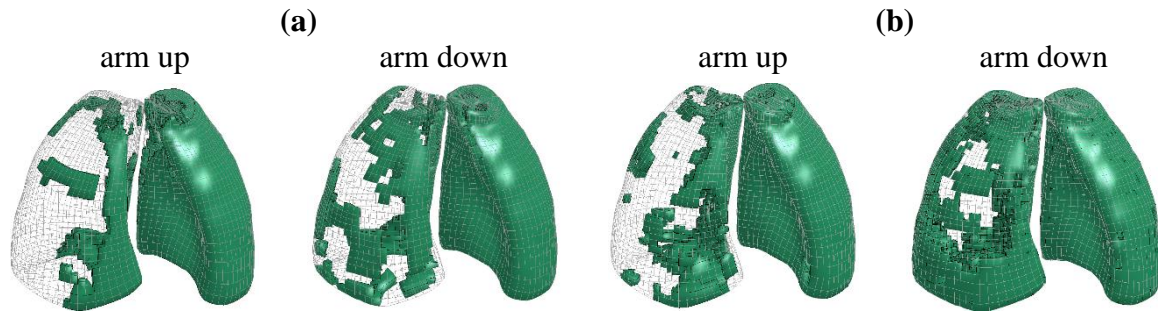


Figure 5.6: Predicted contused lung volumes for (a) WSU-F scenario, (b) NCAP-V scenario, for the two arm positions.

5.3 Discussion

The UW-HBM enabled a direct comparison of three occupant injury assessment methods: global, expressed in terms of maximum chest compression and VCmax employed by safety standards; local, namely chest compression and VC measured at three rib levels; and tissue-level, measured as the contused lung volume.

The UW-HBM confirmed previous observations on the protective effect of the arm in a low-severity velocity-pulse pendulum impact (Kemper 2008). The increase of the predicted occupant response, both in terms of kinematic and tissue-level criteria, was the most pronounced in the full vehicle impact, indicating an increased sensitivity of the UW-HBM to the arm position in velocity-pulse impacts, such as vehicle crashes.

Changes in occupant kinematic response due to modifications of the pre-crash position (lateral, fore, aft) has been previously demonstrated by Watson and Cronin (2011) with use of three side-impact ATD numerical models. Campbell also observed an increased susceptibility of the occupant VCmax response due to a vertical arm position in a component-level occupant to door impacts (Campbell and Cronin 2014). The VCmax response exhibited higher sensitivity to changes of occupant position than chest compression, attributed to a short

duration between the maximum chest compression and maximum chest compression velocity of the ATD ribcage, which amplified the effect of the pre-crash parameter change (Watson and Cronin 2011), explained also in Chapter 2. This study expanded previous findings investigating a variety of side impact scenarios and application of the HBM in a full-vehicle impact.

For the P-F, WSU-F, P-V, and NCAP-V scenarios, all three response measurement methods: global, local, and tissue-level, predicted the same trends in change of the occupant injury response due to arm. Interestingly, for the NHTSA-F, although the VCmax increased from 1.3 to 2.1 with *arm down* position, which indicated an increase of serious injury risk to soft organs according the current standards (Lau and Viano 1986), the lung-specific contusion metric sensitivity to the arm position was negligible in the NHTSA-F scenario. While the VC response was based entirely on deformation of hard tissues, namely rib compression and rib compression velocity, the lung contusion response was affected by deformation and load transfer between hard and soft tissues throughout the entire occupant body. The *arm down* position, although resulting in increased the chest compression values, provided a uniform load distribution over the upper thorax above the discrete location of chest compression measurement at the level of rib 4, which protected the top of the lungs from loads transferred from the edge of the rigid wall.

Although the impact energy absorbed by the occupant body was comparable between the rigid-sled impacts and the full vehicle impacts, the UW-HBM sensitivity to the arm position was 3 times higher in the full vehicle impact compared to rigid sled impacts. The UW-HBM predicted probability of severe injury when the arm was located in the load path for both the rigid sled impacts and full vehicle impact, exceeding the threshold value of 33.9% for chest compression and 1.0 for VCmax. However, these loading conditions were used as an example of an extreme pre-crash condition that is not incorporated in the current safety standards or testing procedures. Despite lower chest compression and VCmax values in the NCAP-V scenario, compared to the WSU-F and NHTSA-F, the predicted contused lung volume was the highest for the full-vehicle impacts. These findings confirm Deng's et al. (1989) suggestion that free-flight impacts, such as pendulum or rigid-wall sled as representations of real impact conditions, do not capture all the effects of full vehicle crashes. A clear demonstration of the

occupant response changes due to pre-crash position, and a comparison of kinematic and tissue-level responses, were enabled by the application of a numerical HBM. UW-HBM provided additional insights into injury mechanisms in side impacts, highlighting advantages and limitations of lateral impact scenarios used to model side impacts.

Chapter 6

Occupant Thorax Response Variations Due to Arm Position and Restraint Systems in Side Impact Crash Scenarios³

Thoracic SAB (tSAB) effectiveness in reducing thoracic injury severity in side impacts has not been consistently demonstrated (D'Elia 2013, Gaylor and Junge 2015, Kahane 2014, Shaw 2014, Viano and Parenteau 2016, Yoganandan 2007). To investigate sources of variability in vehicle side impact restraint effectiveness, it would be beneficial to study both global and tissue-level injury metrics in interaction with a tSAB (Shaw 2014). Confounding factors, such as the anthropometric differences between the occupants and occupant pre-crash position have impeded parametric studies on contribution of various factors to differences in predicted occupant response in interaction with tSAB. In Chapter 4 the occupant arm position was demonstrated to affect the Human Body Model (HBM) thorax response measured using chest deflection (+140%) and the Viscous Criterion (VC) (+428%). In contrast, a wide range of side door compliance changed chest deflection and VC by only 18% and 16%, respectively. In Chapter 5, the importance of utilizing a full vehicle scenario to model occupant response in side crashes was demonstrated. Compared with a rigid-wall impact, the effects of arm position on chest compression and VC in the HBM thorax were up to 2.5 and 7.6 times higher, respectively, in a simulated full-vehicle impact. That is, rigid-wall tests underestimate the importance of arm position.

In this final study, the kinematic response of the occupant and potential for thorax injury in side impact were assessed for interaction with a tSAB. Importantly, response was assessed using kinematics for two different HBMs, to reinforce the importance of this effect through consistent outcomes, and at the tissue level on HBM where this was possible. The UW-HBM was used due to its capacity to predict lung injury, and GHBMC-HBM was used as

³ This Chapter contains figures, tables, and excerpts from articles previously published in the Journal of Accident Analysis and Prevention © 14 Jun 2017 - <https://doi.org/10.1016/j.aap.2017.05.017>, and Journal of Biomechanics © 26 Jun 2018 - <https://doi.org/10.1016/j.jbiomech.2018.04.044> - used with Publisher's permission,

it is the most recent and widely validated HBM for automotive crash simulations. Importantly, the effect of the thorax deformation measurement location and method on predicted performance of seatbelts and tSABs in a side crash could be investigated using the GHBMCHBM. Occupant response was assessed through chest band (CB) deformation, and as a change in distance between markers on the ribs (rib deflection). Multiple measurement locations in the GHBMCHBM enabled direct comparison between the two methods to demonstrate that different outcomes may be predicted with use of a HBM for the same impact scenario depending on the measurement method. Four restraint configurations: belted and unbelted, with and without a tSAB, were considered in a full vehicle MDB impact at 61 kph.

6.1 Methods

The thoracic side airbag (tSAB) was modeled as a generic rectangular thoracic airbag, 7 liter in volume and 130 mm in thickness to match criteria established by Haland and Pipkorn (1996) when fully inflated (Fig.6.1a). Pipkorn and Haland (1996) stated that side airbag thickness has to be greater than 120 mm when fully inflated, to fill the available clearance between the occupant chest and door surface and engage occupant arm and shoulder. The highest reduction of chest deflection and VC metrics was obtained with a 40 kPa airbag (Pipkorn and Haland, 1996). The airbag inflation properties were based on an existing airbag model (Opiela 2008), where the mass flow rate was scaled down volumetrically to achieve a peak pressure of 40 kPa recommended by Haland and Pipkorn (1996) as an operating range for tSABs. The tSAB was integrated with the vehicle side door and deployed over the shoulder and upper thorax region (Griffin 2012, Kahane 2014), in contrast to older seatback mounted small volume tSABs (Loftis et al. 2011). Development of the seat and three-point seatbelt model (Fig.6.1b) was described in section 2.2. While the modeled restraint systems are typical, only this configuration was considered. The goal was to evaluate the interaction with arm position for typical restraint systems, and future work should consider an optimization of the side restraints.



Figure 6.1: Restraint models: (a) inflated tSAB, (b) seat with a three-point seatbelt.

6.1.1 Arm Position, tSAB Location and Pressure Effect for UW-HBM Response

The University of Waterloo Human Body Model (UW-HBM) with a detailed thoracic section was integrated with seat, seatbelts, and vehicle model representing a mid-sized sedan in a Moving Deformable Barrier (MDB) side impact at 61 kph. The tSAB model was attached at the typical location between the seat and the door (McCartt and Kyrychenko 2007, Loftis et al. 2011), and four positions were investigated (Fig.6.2) to cover the shoulder and upper thorax area and to fill the initial gap between the occupant and door during impact (Morris 2005).

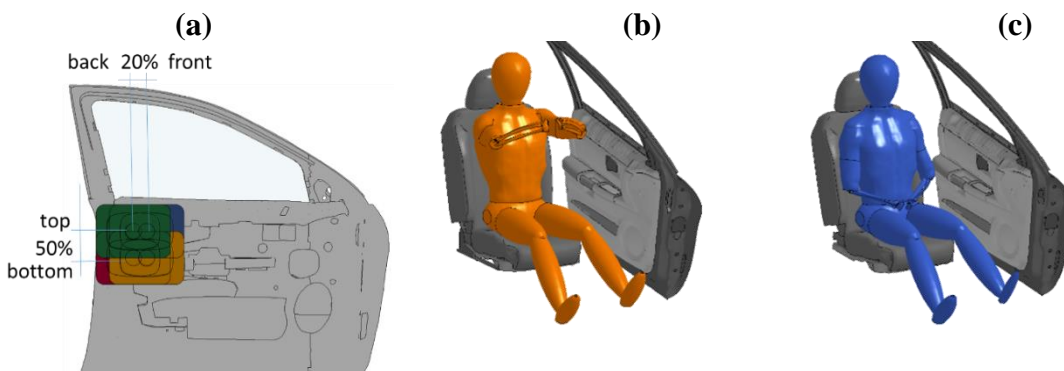


Figure 6.2: (a) four considered tSAB locations; UW-HBM with varying arm positions: (b) horizontal, (c) vertical.

Simulations were run with and without the tSAB. For the simulations involving the tSAB, a screening fractional factorial 2^{4-1} experiment (D=ABC) has been designed to study

main effects of the: (A) arm position (Fig.6.2b,c), (B) fore-aft location of the tSAB, (C) vertical location of the tSAB, and (D) the peak pressure of the tSAB inflator (20 or 40 kPa, Haland and Pipkorn 1996) (Table 6.1), in eight runs (Table 6.2).

Table 6.1: Description of the experimental factors and variable codes.

		-	+
factor	A	Arm position	horizontal vertical
	B	Longitudinal tSAB position	back front
	C	Vertical tSAB position	bottom top
	D	Peak tSAB pressure	20 kPa 40 kPa

Table 6.2: Coded experimental design for the eight runs of the fractional factorial design

run	A	B	C	D	AB	AC	AD	BC	BD	CD	ABC	ABD	ACD	BCD	ABCD
1	-	-	-	-	+	+	+	+	+	+	-	-	-	-	+
2	+	-	-	+	-	-	+	+	-	-	+	-	-	+	+
3	-	+	-	+	-	+	-	-	+	-	+	-	+	-	+
4	+	+	-	-	+	-	-	-	-	+	-	-	+	+	+
5	-	-	+	+	+	-	-	-	-	+	+	+	-	-	+
6	+	-	+	-	-	+	-	-	+	-	-	+	-	+	+
7	-	+	+	-	-	-	+	+	-	-	-	+	+	-	+
8	+	+	+	+	+	+	+	+	+	+	+	+	+	+	+

A factorial 2^3 experiment was then run to study magnitude of the effect of interactions between the arm and tSAB location (factors A, B, C, Table 6.1) for the peak tSAB pressure of 40 kPa, following recommendations of Haland and Pipkorn (1996) for tSAB settings. For all the experiments, the HBM pre-crash arm position was varied between a horizontal (Fig.6.2b), and vertical arm position (Fig.6.2c).

UW-HBM Response Assessment

The effect of the factors on the occupant response was assessed in terms of maximum chest deflection (Viano 1989) and VCmax (Lau 1986) assessed at the three rib levels corresponding to locations of the ATD ribs (explained in Chapter 2). Global injury response was expanded through evaluation of tissue level response, namely number of fracture locations in the left half of the thorax and predicted contused volume of the lungs (Yuen 2008, 2010). A cluster of eroded elements was referred to as a rib fracture, when the elements eroded throughout the entire cross-section of the rib bone at a given location.

6.1.2 GHBM-C-HBM Response to Varying Arm Position and Restraint Combinations

The GHBM-C-HBM was previously equilibrated with the seat and vehicle models (Chapter 3, section 3.3.2). Four restraint combinations were modeled (Fig. 6.3) to account for different combinations of restraints implemented in vehicles, and provide a spectrum of loading. Contribution of the presence or removal of each aspect of the restraint system was assessed (Table 6.3). The coupled vehicle-restraint-occupant model was subjected to MDB impact at 61 kph (16.9 m/s) (NHTSA 2012), representative for high-severity side impact crash scenarios.





	-B-tSAB	-B+tSAB	+B-tSAB	+B+tSAB
				
Seatbelt	-	-	+	+
tSAB	-	+	-	+

Figure 6.3: Restraint system configurations for vehicle side-impact scenario (Gierczycka et al. 2018).

Two pre-crash arm positions were considered: with arms in the driving position (arm 40 degrees with respect to torso; Figure 6.4a), and with arms in the vertical position (arm aligned with the torso; Figure 6.4b), pre-positioned as described in Chapter 3. While the UW-HBM arm position ranged from a vertical alignment with the torso to arm parallel with the ground, the GHBMC-HBM arm positions ranged from a vertical to standard driving position, to ensure consistent orientation of the upper torso between the two positions. The effect of vertical arm position for both HBMs was previously compared in Chapter 4, section 4.1.4.



Figure 6.4: GHBMC-HBM pre-crash position: (a) arms in driving position, (b) arms in vertical position.

Table 6.3: Simulation configurations (aD = arms in driving position, aV = arms in vertical position, -B = unbelted, +B = belted, -tSAB = without tSAB, +tSAB = with tSAB deployed).

scenario code	aD-B	aD-B	aD+B	aD+B	aV-B	aV-B
	-tSAB	+tSAB	-tSAB	+tSAB	-tSAB	+tSAB
seatbelt	no	no	yes	yes	no	no
tSAB	no	yes	no	yes	no	yes
arm position	drive	drive	drive	drive	vertical	vertical

GHBMC-HBM Response Assessment

The occupant response was assessed by tracking spinal curvature and measuring chest compression using two methods: the rib-deflection (RD) method, characteristic for the ATD measurements, and the chest-band (CB) method that is specific for the PMHS experiments. In the CB method, chest compression was measured as a change in distance between markers located on the outside of the thorax, at three locations. The upper (rib 8) and lower (rib 10) CB locations corresponded to PMHS CB locations (Pintar et al. 1997), and a middle CB location (rib 9) was also included in order to provide additional information on the deformation profile of the thorax (Fig. 6.5a). Chest compression measurement for the CB was based on the central thorax deflection methodology described by Kuppa et al. (2003) and Shaw et al. (2014) and defined as a change in length between the opposing measurement points due to impact deformation, divided by the pre-crash thorax width (Fig. 6.5b).

The RD method assessed chest compression through measurement of change of distance between measurement points directly on the ribs, at the location of maximum rib curvature, and symmetric with respect to the coronal plane (Fig. 6.5c). Measurements were taken on the GHBMC-HBM ribs 4, 6, 8 – which are comparable to locations of the ribs in the ATDs – and ribs 9 and 10, to match the CB locations (Fig.6.5a).

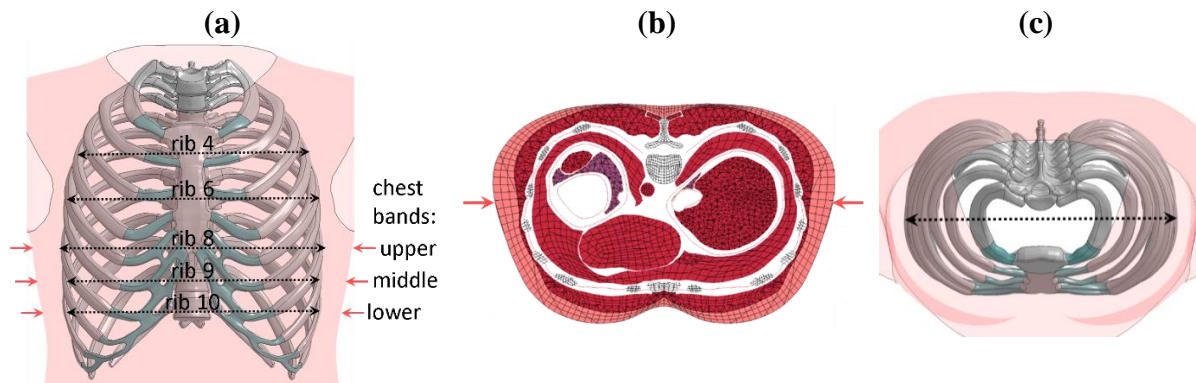


Figure 6.5: Chest compression measurement location: (a) tissue outer contour with chest-band locations marked with respect to the ribcage, (b) chest-band (CB) method, (c) rib-deflection (RD) method (Gierczycka et al. 2018).

Chest deflection was divided by initial breadth of the thorax at a given chest band level, measured externally for the CB methods or directly on the ribs for the RD method, to express it as a chest compression. The predicted locations of rib fractures were also assessed with the model. The GHBMC-HBM predicted locations of rib fractures based on a plastic strain failure criterion embedded in the cortical bone material model definition. Element erosion occurred during the simulation when the plastic strain criterion was exceeded, and elements were virtually removed, leading to discontinuity of the rib. For the purpose of this study, the failed elements were identified using a post-processing software (LS-PrePost software (LSTC, 2018)) was used to locate the eroded elements, which indicated potential rib fractures predicted by the GHBMC-HBM.

Displacements of the GHBMC-HBM vertebral bodies (thoracic vertebrae T1, T6, T11, and the lumbar vertebra L3), and of the pelvis center of gravity were tracked in the coronal plane to capture the occupant whole-body kinematics, similarly to methodology described by Shaw et al. (2014). A consistent spine curvature, namely a consistent relative lateral distance between the vertebrae, was described by Kaneko et al. (2007) as a potential metric that correlates with chest compression in a lateral impact. For the purpose of this thesis, the GHBMC-HBM spine curvature measurements focused on the time of the maximum chest compression, which occurred between 40 and 50 ms. Chest compression and VC responses were compared to measured trends of displacements of the spine and pelvis to verify the observations from Kaneko et al. (2007) on the decrease of chest compression values when consistent spine curvature was maintained during the crash (Kaneko et al. 2007).

6.2 Results

6.2.1 Interaction with tSAB Depending on Arm Position Predicted by the UW-HBM

As previously demonstrated in Chapters 4 and 5, for belted occupants without the tSAB the chest compression and VC increased for the vertical arm position (+140% relative increase for maximum chest compression, and +428% for VCmax) compared to the driving position.

Predicted rib fracture locations followed the arm alignment with the torso. For the horizontal arm position, the HBM predicted the potential for rib fractures at the costovertebral joints. Three rib fracture locations were predicted at the rib angles for the horizontal arm position, for ribs 2 and 5 (Fig.6.6a). For the vertical arm position, fracture locations at the rib angles were predicted at nine locations (Fig. 6.6b). The predicted contused lung volume also increased with the arm in the vertical position (Fig.6.6). When the arm was aligned with the torso, contused volume of the right lung increased by as much as 90% (from 13-18% to nearly 30% volume). Contused left lung volumes exceeded 70% for both arm positions, indicating risk of onset of the acute respiratory distress syndrome. However, it is acknowledged that for such high impact severity, based on level of thorax deformation, the lung contusion criterion sensitivity may be compromised.

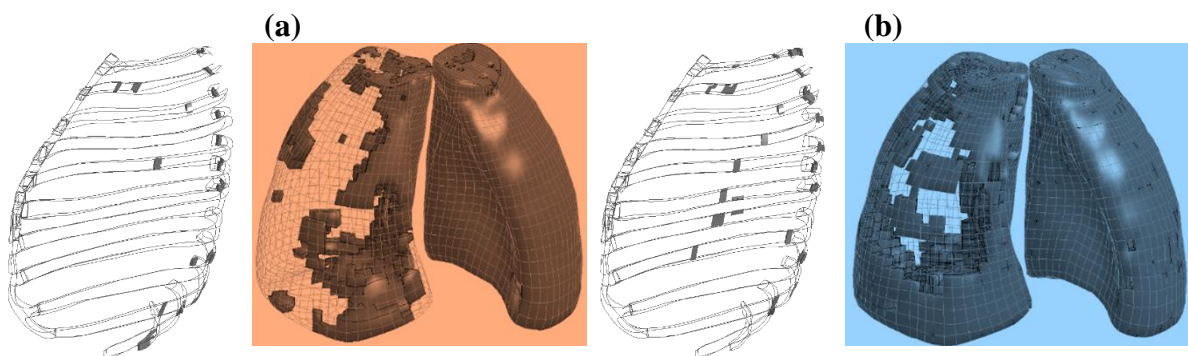


Figure 6.6: Predicted locations of rib fractures, left view, and contused lung pattern: (a) horizontal, and (b) vertical arm position.

After adding the tSAB to the analysis, the arm position was identified as a dominant effect for chest deflection measured at all three rib levels, and for the maximum overall chest deflection and VCmax (Fig.6.7). The effect of the tSAB pressure on the predicted occupant response (D in Fig. 6.7) was less evident than the effect of arm position (A in Fig.6.7). With the higher SAB pressure, the maximum chest deflection increased by approximately 9% and the VCmax by 15%, for the considered SAB locations and occupant pre-crash positions. Due to the aggressive nature of the impact, total volume of contused lungs remained above 40% for all load cases, indicating an elevated risk of onset of acute respiratory distress syndrome

regardless of the tSAB configuration. With the tSAB located in the shoulder and upper thoracic region, contused lung volume increased by 30% compared to tSAB location in the lower thoracic and abdominal region.

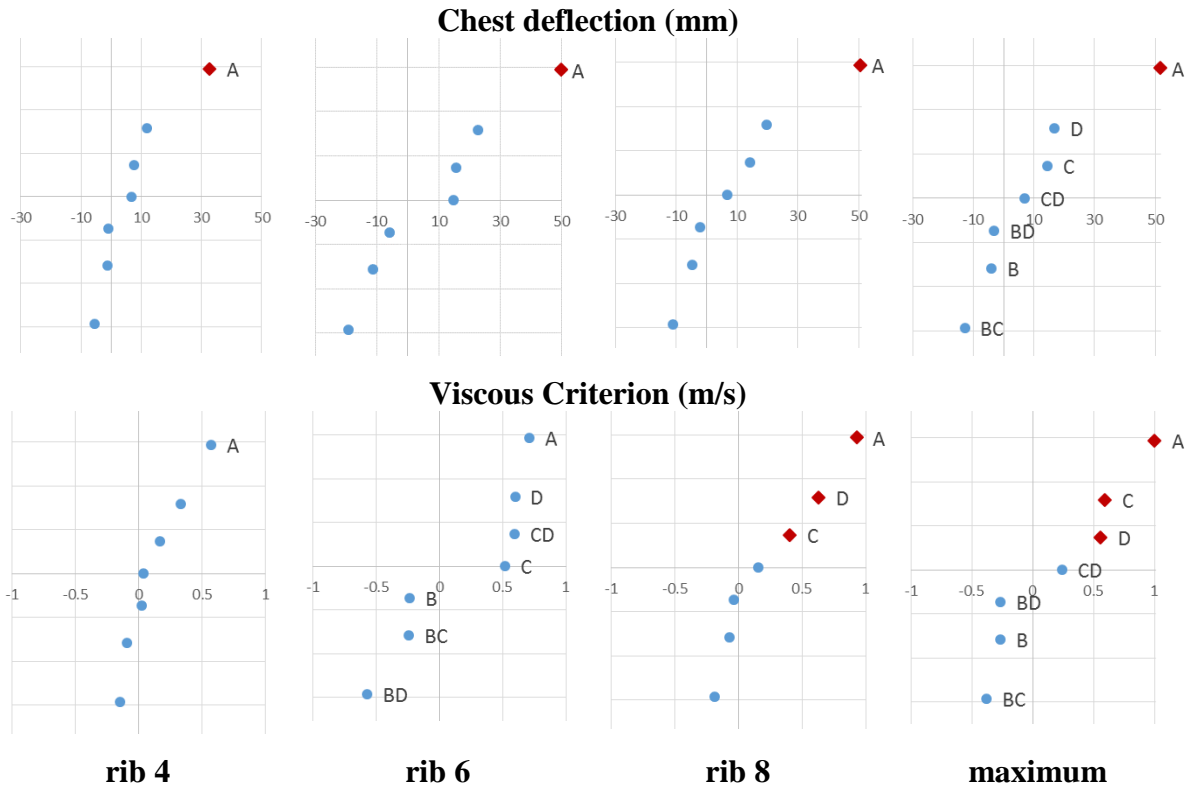


Figure 6.7: Normal plots of the effects at each rib level and maximum overall value, for the UW-HBM model chest deflection response (upper row) and the Viscous Criterion (lower row). Magnitude of the effect plotted on the abscissa for each metric, distinguishable effect marked in red.

Analysis of marginal means plots demonstrated interactions between the tSAB location and pressure (CD and BD). The interactions were the most pronounced at the level of rib 6 for both the chest deflection and VC, which could explain lack of a distinguishable effect at the level of rib 6 (Fig.6.7). The magnitude of the effects associated with each factor was different between the maximum overall values and the three rib levels.

The tSAB performance was dependent on the occupant arm position. While for the vertical arm position finding a combination of tSAB pressure and location that either did not increase or even reduced the occupant response was possible, for the horizontal arm position all considered combinations of tSAB settings increased the predicted occupant injury response (+200% for the maximum chest deflection, +340% for VCmax) (Fig. 6.8). For the horizontal arm position (labeled as ‘H’ in Fig.6.8), the reference scenario without a SAB (‘H no SAB’) was compared to the tSAB location that resulted in the lowest maximum chest deflection and VCmax (‘H with SAB (reduced)’), and to the SAB location that resulted in the highest maximum chest deflection and VCmax values (‘H with SAB (increase)’ (Fig.6.8).

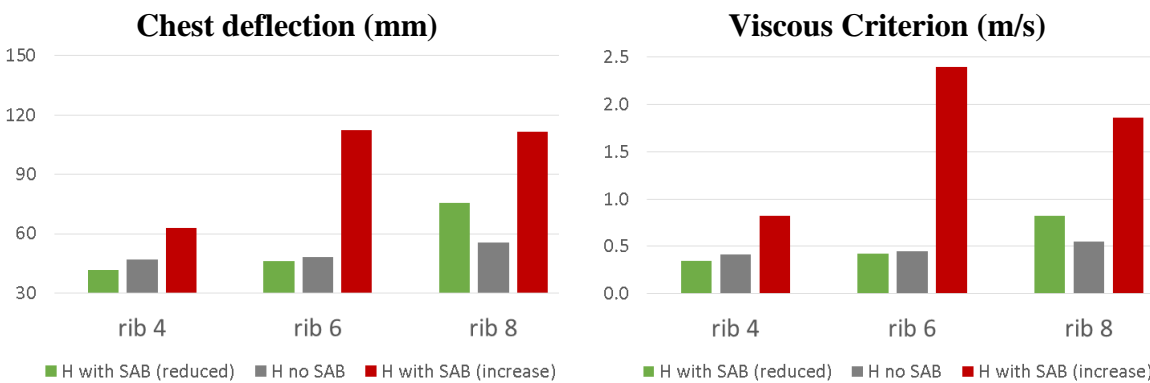


Figure 6.8: UW-HBM response at three rib levels for the horizontal arm position (H), with a tSAB combination that reduced (green) and increased (red) the injury metrics with respect to a case with no tSAB (gray).

For the vertical arm position (labeled as ‘V’ in the graphs, Fig.6.9), the reference scenario without a tSAB (‘V no SAB’) was compared to the tSAB location that resulted in the lowest maximum chest deflection and VCmax (‘V with SAB (reduced)’), and to the tSAB location that resulted in the highest maximum chest deflection and VCmax values (‘V with SAB (increase)’ in the parametric study. Differences between the reference case (no tSAB) and the case with the highest maximum chest deflection and VCmax were less pronounced than in case of the horizontal arm position.

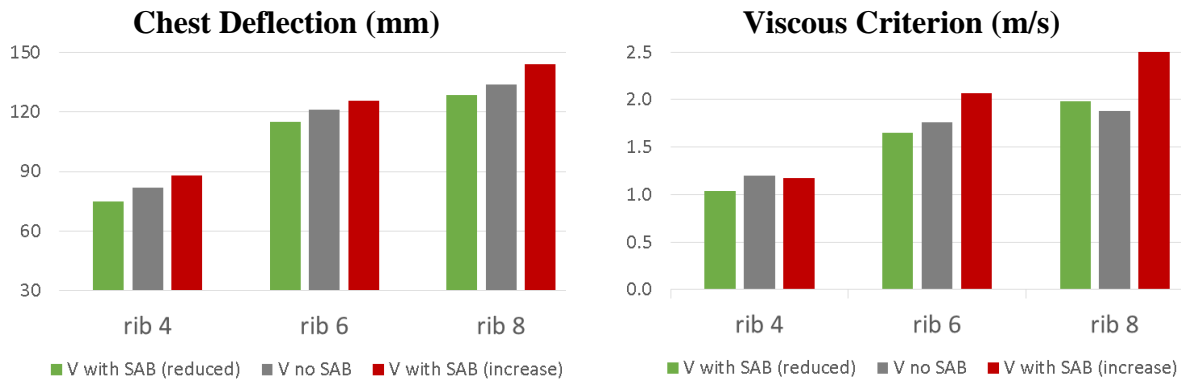


Figure 6.9: UW-HBM response at three rib levels for the vertical arm position (V), with a tSAB combination that reduced (green) and increased (red) the injury metrics with respect to a case with no tSAB (gray).

The contribution of the (A) arm position, (B) longitudinal location of the tSAB, and (C) vertical location of the tSAB to the occupant response was assessed in detail in a full factorial experiment. Factors that contributed more than 5% to the differences in responses amongst the eight experimental runs were marked in red in the normal plots of the effects (Fig. 6.10). For the maximum chest deflection, the highest change in response was attributed the arm position (66%), vertical position of the tSAB (25%), and the interaction between the two (7%) (Fig. 6.10a). For the VCmax, contribution of the vertical tSAB location was the most pronounced (42%), followed by the arm position (32%), and interaction between the two factors (17%) (Fig.6.10b). The number of predicted rib fracture locations was affected by the arm position (62%), followed by the interaction between the arm position and vertical location of the tSAB (16%), and finally the vertical location of the tSAB (11%) (Fig.6.10c). While the predicted contused left lung volume demonstrated noticeable sensitivity to interaction between the arm position and longitudinal location of the tSAB (50%), vertical tSAB location (28%), and interaction between the two (13%), the contused right lung volume was affected almost exclusively by the arm position (89%) (Fig.6.10d). Regardless of the tSAB location (B - longitudinal, C - vertical in Fig. 6.10), the vertical arm position led to approximately 60% more potential rib fractures than the horizontal arm position (average for the horizontal arm

position: 11 locations of eroded rib elements, range 7-12, for the vertical arm position: 17 locations of eroded rib elements, range 17-18 fractures).

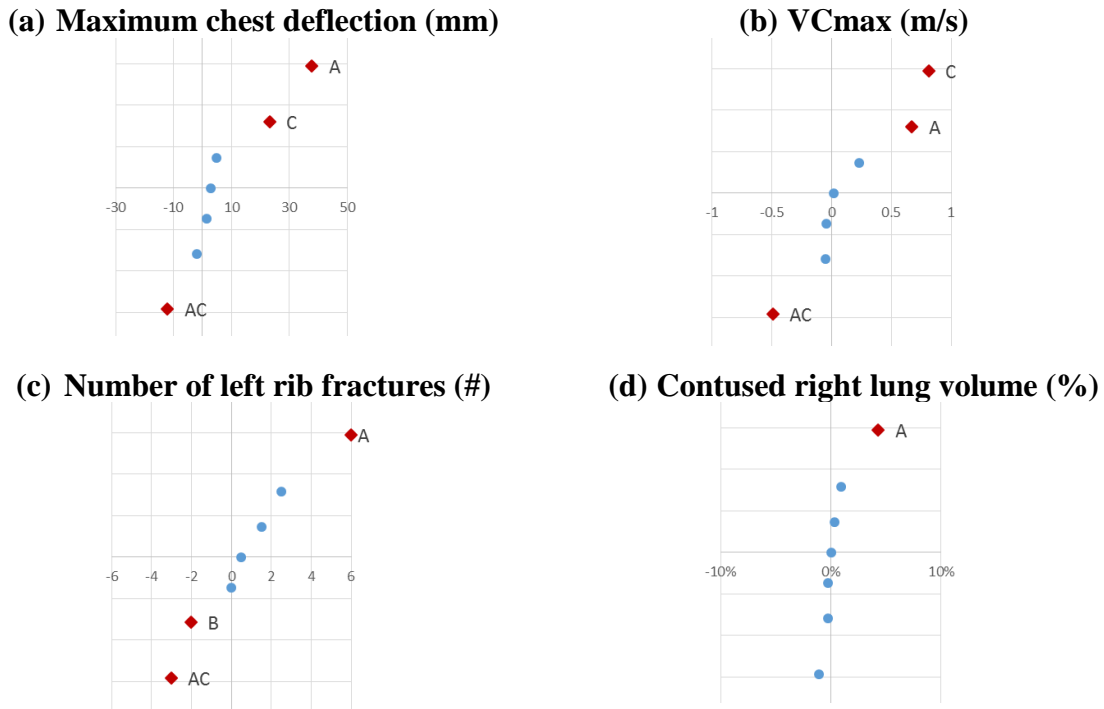


Figure 6.10: Normal plots of the effects, magnitude of the effect plotted on the abscissa for each of the metrics, distinguishable effects marked in red.

An interaction between the arm position and tSAB location (AB) was highlighted for the contused left lung volume (Fig. 6.11a), although the effect was not clearly distinguishable on other plots. No interaction between the arm position and tSAB location was found for the contused right lung volume response, which was expected. An interaction between the arm position and tSAB vertical location (AC) was also predicted for the chest deflection measured at the level of rib 6 (Fig.6.11b), which was even more evident for the VC response at the level of rib 6 (Fig.6.11c) and reflected also by the number of predicted rib fractures locations (Fig.6.11d).

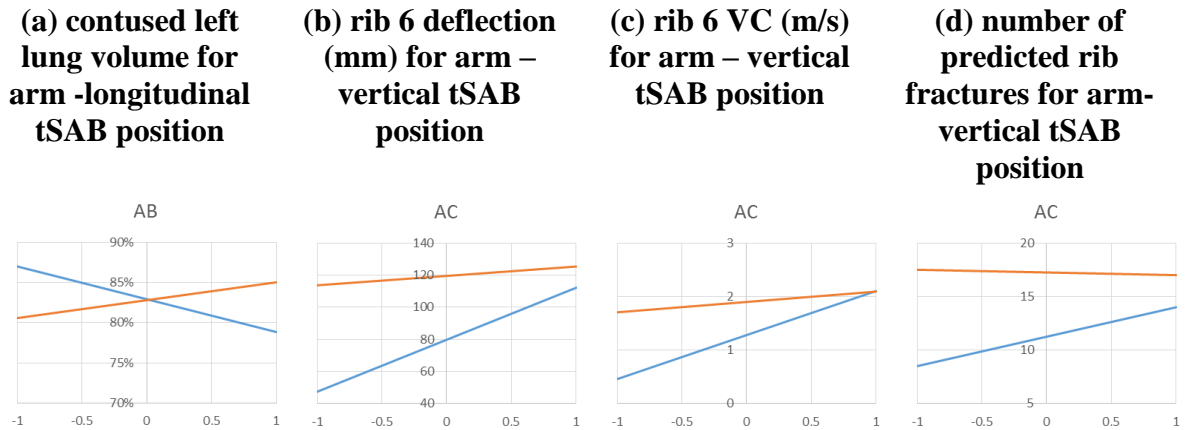


Figure 6.11: Marginal means plots visualizing mean factor effects of two-factor interactions predicted by the UW-HBM.

6.2.2 Interaction with tSAB Depending on Arm Position Predicted by the GHBMC-HBM

The pre-crash position altered the GHBMC-HBM response measured as chest compression, VC, and spine kinematics. For an unbelted case without a tSAB (-B-tSAB), the arm in a vertical position (aV) led to a relative 205% increase of chest compression, compared to the driving arm position (from 16 to 33%). While for the driving arm position the tSAB led to a +75% relative increase of the chest compression, for the vertical arm position the tSAB reduced the chest compression, from 30.2% to 25.8% (lower CB, Fig.6.12). The VC trends were comparable to the chest compression response. When no tSAB was fitted in the vehicle, arm in the vertical position led to a 205% relative increase of VCmax (Table 6.4). With the tSAB, the vertical arm position reduced the VCmax response from 1.38 m/s to 1.21 m/s (relative reduction of 14%), which still remained above the threshold value of 1.0 for the VC (Fig.6.12).

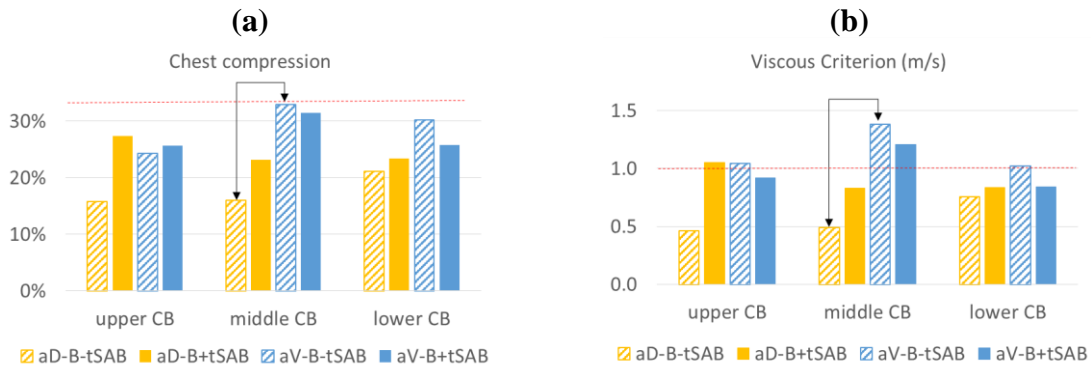


Figure 6.12: Thoracic side airbag (tSAB) effect for a driving (aD) versus vertical (aV) arm position for an unbelted occupant, measured at three chest band (CB) levels: (a) chest compression, and (b) Viscous Criterion (VC). The highest increase in chest compression and VC due to vertical arm position indicated by arrows. Injury criteria threshold values marked with a red dashed line.

Table 6.4: Maximum chest compression and Viscous Criterion results (aD = arms in driving position, aV = arms in vertical position, -B = unbelted, +B = belted, -tSAB = without tSAB, +tSAB = with tSAB deployed) normalized with respect to injury criteria thresholds.

scenario code	aD-B	aD-B	aD+B	aD+B	aV-B	aV-B
	-tSAB	+tSAB	-tSAB	+tSAB	-tSAB	+tSAB
Compression	21.2%	27.4%	24.6%	26.8%	32.9%	31.4%
Compression normalized	0.62	0.81	0.73	0.79	0.97	0.93
VC normalized	0.76	1.05	0.95	0.96	1.38	1.21

6.2.3 GHBMHC-HBM Spine Kinematics Change Due to Arm Position and Restraints Configuration

For the spine kinematics, the smallest overall lateral translation was observed for the unbelted occupant with no tSAB and arms in the driving position (Fig.6.13, aD-B-tSAB), For the driving arm position, when the tSAB was present, the overall lateral translation values increased for all vertebrae and the spine curvature changed more during the impact event. The spine initially translated laterally and vertebrae formed almost a straight line between pelvis centre of gravity (CG) and T1 (Fig.6.13, aD-B+tSAB, 40ms). At 60 ms the upper body interacted with the intruding door (Fig.6.13, aD-B+tSAB, 60ms), increasing relative lateral translation between L3-T11-T6 vertebrae, and causing a change in curvature of the spine, namely change of relative lateral translation between vertebrae.

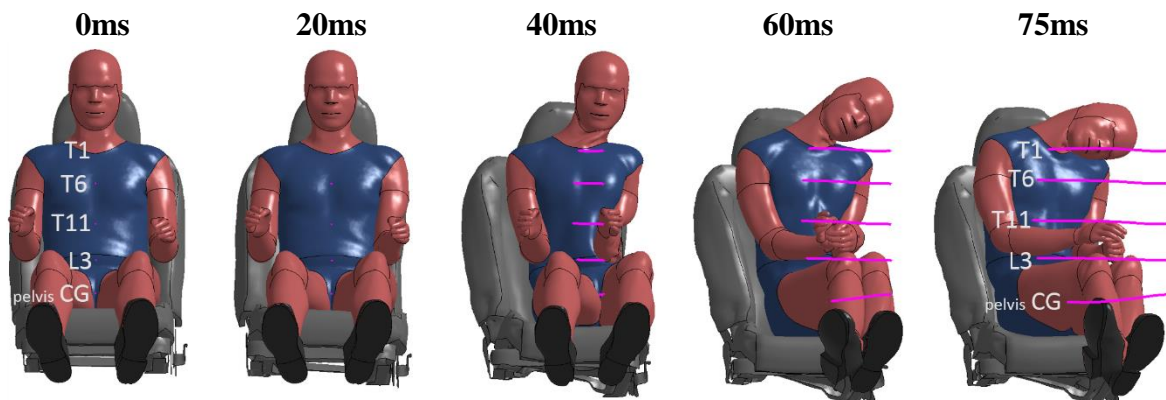


Figure 6.13: Kinematics and visualization of spine tracking of the GHBMHC-HBM during the lateral MDB impact. Unbelted, no tSAB, vertical arm position case (aV-B-tSAB).

Similarly, an increase of relative translation between L3-T11-T6 vertebrae during the crash was observed for the vertical arm position with no tSAB (Fig.6.14, aV-B-tSAB), in addition to an overall increased translation compared to the driving position. For the vertical arm position when the tSAB was present (Fig.6.14, aV-B+tSAB), the change of spinal curvature during the crash was reduced, compared to aV-B-tSAB.

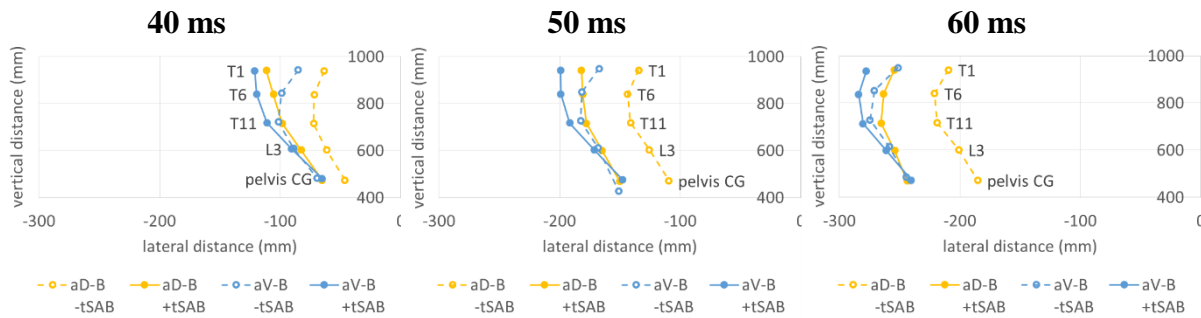


Figure 6.14: Spine kinematics (T1, T6, T11, L3, and pelvis) for four unbelted cases: drive no thoracic side airbag (tSAB), drive with tSAB, vertical no tSAB, vertical with tSAB. Vertical distance was measured from the ground, lateral distance from body centerline (0 at time=0).

In terms of spine kinematics, the unbelted case with no tSAB predicted the smallest overall lateral translation values compared to other restraint configurations for the driving arm position (Fig.6.15). With the seatbelt and no tSAB, although the overall lateral translation values increased for all the vertebrae, the spine curvature remained consistent during the impact event. The relative displacement between T1 and T6, and T11 and L3, was more pronounced in the belted case, compared to the unbelted case. When the tSAB was present, the seatbelt had very little effect on the predicted response, and both the overall lateral translation values and relative translation between vertebrae were similar between the belted and unbelted tSAB configurations (Fig.6.15; aD-B+tSAB and aD+B+tSAB). For the belted occupants, while the L3 and pelvis CG overall lateral translations were comparable between the cases with tSAB and without tSAB, the tSAB reduced the change in spinal curvature during the crash event (Fig.6.15; aD+B+tSAB).

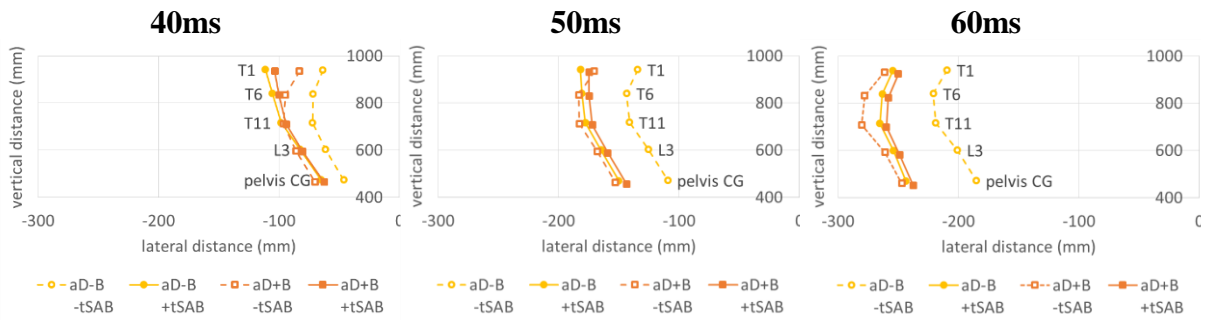


Figure 6.15: Spine kinematics (T1, T6, T11, L3, and pelvis) for driving arm position cases and different restraint combinations: unbelted no tSAB, unbelted with tSAB, belted no tSAB, and belted with tSAB. Vertical distance was measured from the ground, lateral distance from body centerline (0 at time=0).

6.2.4 Side Restraint Combination Effect Assessed with Two Chest Compression Measurement Methods

When no tSAB was fitted in the vehicle, the maximum chest compression measured with rib-deflection (RD) method did not change when the seatbelt was incorporated (20% for both cases) and the deformation pattern was not affected (Fig.6.16). However, the chest band (CB) method predicted an increase of the maximum chest deflection value from 16% to 25% (Fig.6.16) and overall increase of chest compression along the thorax.

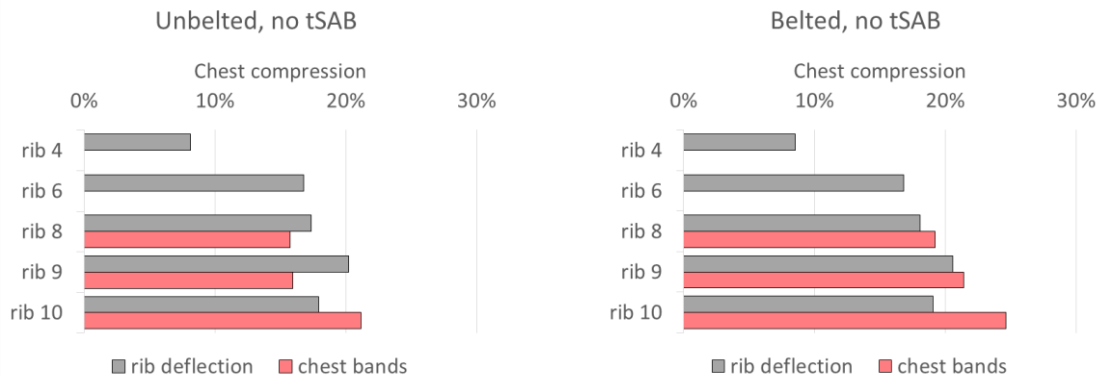


Figure 6.16: Chest compression for unbelted and belted configurations without the tSAB, measured with RD and CB methods.

The GHBMC-HBM predicted more fracture locations (8-9) in the belted, no tSAB case than in the unbelted, no tSAB (4 fracture locations), corresponding to an increased chest compression measured with the CB method. Most of the elements eroded in the vicinity of posterior ends of ribs 9-11 on the left side of the thorax, indicating the highest probability of rib fracture in that area. For the belted case, clusters of eroded elements were predicted in the upper anterior section on the left side of the thorax (ribs 5-6), and in lower anterior section on the right side of the thorax (ribs 7-9), following the seatbelt path (Fig.6.17).

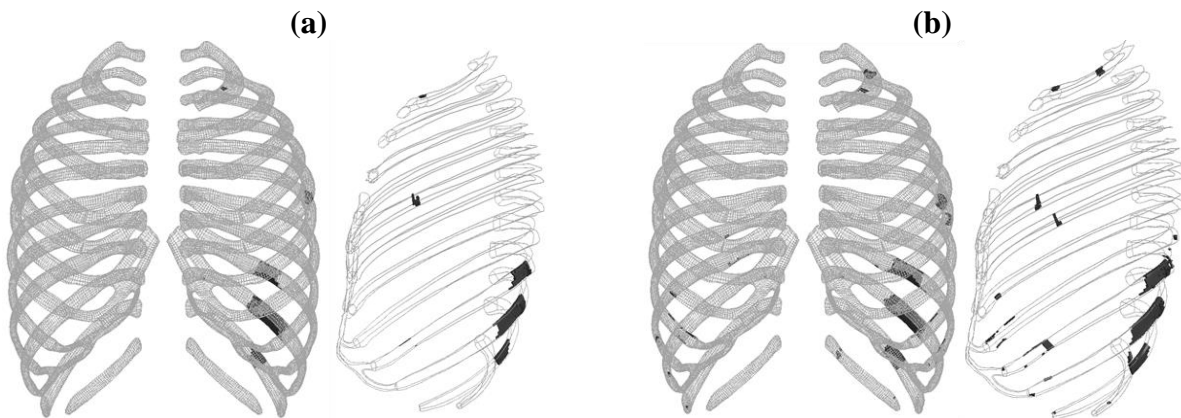


Figure 6.17: Rib fracture locations for the: (a) unbelted, no tSAB, (b) belted, no tSAB. Frontal and lateral view of the GHBMC-HBM ribcage post-crash. Eroded elements marked as black solid.

When the tSAB was fitted in the vehicle, the CB method demonstrated no change in chest compression values and chest compression pattern between belted and unbelted configurations with the tSAB (less than 1% change). In contrast, the RD method demonstrated a decrease in chest compression values for the belted occupant (from 24% to 19%). The maximum chest compression was predicted at the upper CB level (rib 8) for both belted and unbelted configurations with tSAB (Fig. 6.18). When the tSAB was deployed, the belted case predicted fewer fracture locations in the vicinity of the belt compared to the unbelted case (Fig.6.19). The presence of the seatbelt reduced the number of predicted rib fracture locations

from 11 to 6-7, and maximum chest compression predicted by RD method was reduced from 24% to 19%.

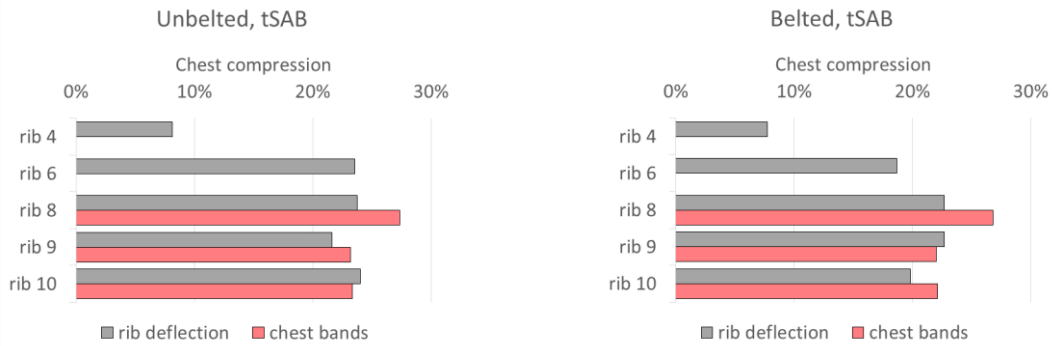


Figure 6.18: Chest compression values for unbelted and belted configurations with the tSAB, measured with RD and CB methods on the GHBCM-HBM.

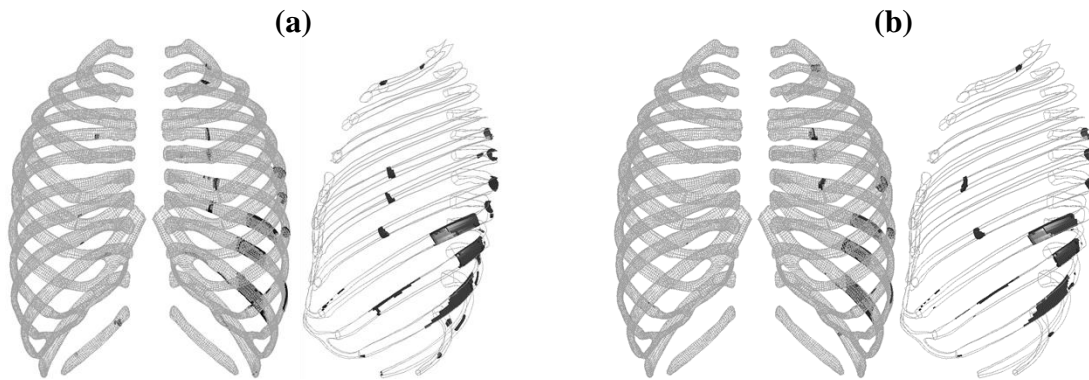


Figure 6.19: Rib fracture locations for the: (a) unbelted, no tSAB, (b) belted, no tSAB. Frontal and lateral view of the GHBCM-HBM ribcage post-crash. Eroded elements marked as black solid.

6.3 Discussion

The pre-crash arm position effect for the UW-HBM responses was observed to dominate over the tSAB location and tSAB maximum pressure. Positioning the arm in the load path, namely the vertical arm position, increased injury metrics in terms of maximum chest deflection, VCmax, number of predicted rib fractures and predicted contused lung volume. When no tSAB was present, the vertical arm position increased maximum chest compression by 140% and VCmax by 428% higher compared to the horizontal arm position. The predicted contused lung volume was in agreement with chest deflection and VC metrics, increasing when the arm was located in the load path.

A slight reduction of the injury metrics was observed for the bottom SAB locations, where it could provide coverage for the lower torso and push the arm away from the load path. The least desired SAB position for both the horizontal and vertical arm positions was in the shoulder and upper torso area, where the deploying SAB would rotate and push the arm towards the torso.

The GHBM-C-HBM demonstrated sensitivity to the pre-crash position of the arm, which was more pronounced (+106% relative increase of the maximum chest compression) than the effect of different combinations of the restraint systems (+75%). In general, the vertically positioned arm in the load path increased the injury metrics, which was in agreement with the earlier findings summarized in Chapters 4 and 5. Importantly, the current study also included a thoracic side airbag (tSAB), which had not previously been investigated.

When the tSAB was fitted in the vehicle, the CB chest compression magnitudes and patterns for the unbelted and belted configurations were comparable. The maximum CB chest compression was predicted at the upper CB level for both the belted and unbelted configurations with tSAB. In contrast, with the RD method the maximum chest compression for the unbelted occupant was evenly distributed across ribs 4–6, while for the belted occupant the maximum chest compression occurred at the level of ribs 8 and 9 only (Table 6.5).

Research on frontal impacts has demonstrated advantages of measuring chest deflection at multiple locations rather than at a few discrete locations (Kemper, 2016), but very few such investigations have been conducted for side impacts. This study demonstrated that

discrete RD measurement locations at the level of ribs 4–8, corresponding to locations of the side-impact ATD ribs, did not capture maximum chest compression locations when they occurred at the level of ribs 9 and 10. Incorporating more measurement locations enabled an identification of the effect of restraint combinations that was not possible using only the three discrete locations. For example, while adding the tSAB increased the maximum chest compression values for the unbelted occupant, it also distributed the load, and therefore the chest compression, more evenly over the torso.

Table 6.5: Effect of the restraints on chest compression for the two measurement methods

Compared configurations	Chest-band method	Rib-deflection method
-B-tSAB and +B-tSAB	Seatbelt increased chest compression (largest increase: from 16% to 25%).	Seatbelt had no effect on chest compression.
-B+tSAB and +B+tSAB	Seatbelt had no effect on chest compression.	Seatbelt reduced chest compression (largest reduction: from 24% to 19%).

Frontal impact studies have also demonstrated that ATD-based metrics implemented in the HBM were less sensitive to different restraint settings than PMHS-based and tissue level predictions, such as CB deflection and rib strain distribution (Danelson 2015). The current study verified Danelson’s observation, but for side-impact scenarios, demonstrating increased sensitivity of the ATD-based metrics (RD method) when the tSAB was present, and increased sensitivity of the HBM-based metrics (CB method) when no tSAB was present in the vehicle.

The response of the GHBMC-HBM was previously compared to PMHS responses by Hayes et al. (2014) in a rigid-wall sled impact at 6.7 m/s. Deformation patterns of the chest bands were comparable between the HBM and three PMHSs (Yoganandan and Pintar 1997)

at the time of maximum loading. The differences between the peak compressions predicted by the GHBMC HBM and the PMHSs varied between 6% and 14%, and Hayes (2014) attributed these differences to the model material properties and differences in rib-cage geometry between the model and the PMHSs. The GHBMC-HBM peak chest compression values predicted by Hayes et al. (2014) were 28%, 26% and 20% for the upper, middle and lower chest band, respectively. Chest compression values reported by Yoganandan and Pintar (1997) were measured as 24% for the CB at the level of rib 8 (upper) and 16% for the CB at the level of rib 10 (lower).

Anthropometric differences between occupants are yet another incentive to include more measurement locations in the injury assessment. In the ATD the ribs are evenly spaced and have the same breadth at all three levels, but in the human thorax the distances between the left and right rib are shorter in the upper thorax (21 cm between apexes of the left and right second rib, measured with the GHBMC-HBM), and greater in the lower thorax (29 cm between left and right eighth rib, measured with the GHBMC-HBM), decreasing again for ribs 9–12. Current side-impact occupant response assessment standards are based on the maximum ATD rib deflection. For the ATD the location of the maximum rib deflection would not affect the chest compression values, but in the human thorax the same magnitude of deflection would yield different (fractional) compression values at different chest levels. Therefore, data should be gathered at all the chest levels where the occupant body contacts the restraints and vehicle interior. A comparison of the outcomes of both CB and RD response measurement methods with use of an HBM would provide a better understanding of the restraint and interior design outcomes for occupant safety than ATD testing alone.

The trends in spine kinematics, assessed using the findings of Shaw (2014) and Kaneko (2007), were consistent with the chest compression and Viscous Criterion (VC) trends. An increase in chest compression and VC was associated with changes in spine curvature during the crash event (i.e. changing from initially straight to curved through interaction with the intruding door). Both an increase in overall lateral displacement and change in the spine curvature during the crash were consistent with the largest increase in chest compression and VC values. Kaneko et al. (2007) in a simulation study with use of ATD models observed that

reducing relative displacements between the vertebrae and ribs decreased chest deflection values, and results of this study are consistent with these findings (Kaneko et al. 2007).

Assessment using lateral displacement of the thoracic spine correlated positively with chest compression and the Viscous Criterion, with the benefit of evaluating the whole thorax response, and provided a useful metric to compare occupant response for different side impact safety systems.

In general, the presence of the thoracic tSAB reduced the chest compression values for the vertical arm position and increased the injury metric values for the driving arm position, for the impact case considered in this study. For configurations with the tSAB, the combined effect of the seatbelt and tSAB reduced the predicted occupant response relative to the case with a tSAB but no seatbelt. The increase in chest compression associated with the seatbelt was related to the shoulder belt engaging the thorax at the location of the lower chest band (CB), where the thorax is more compliant.

The thoracic side airbag was found to increase the chest compression for the driving arm position (+70%), and reduced the injury metrics for the vertical arm position (-17%). It was demonstrated that a tSAB can have both a negative effect and a positive effect on the predicted injury response. For the considered set of parameters and boundary conditions, the pre-crash position of the occupant was a predominant factor for both the UW-HBM and GHBM-HBM injury responses. One potential and important source of ambiguity in epidemiological studies on tSAB effectiveness is the change in tSAB performance due to occupant arm pre-crash arm position.

Limitations

The MDB-to-vehicle impact was a simplified representation of the vehicle-to-vehicle lateral impact. The results and conclusions from this study were related to this specific scenario and should not be extrapolated in general to the passenger vehicle fleet at the current level of knowledge, but the results provide some important insight into the importance of vehicle safety systems and interaction with the occupant. Limitations of the current study include considering only one seat design and restraint system configuration. However, the seat model was validated

with experimental data in a previous study (Watson and Cronin 2011, Campbell and Cronin 2014) and the aim of this study was to demonstrate that arm position could affect the occupant response, rather than to optimize the safety systems for this specific side impact scenario. The importance of this finding is that future research on side impact safety system optimization should consider the effect of occupant posture and position.

Recent studies by Kemper (2013) and Park et al. (2016) have highlighted the importance of biofidelic response of the occupant surrogate arm in side impact. Park et al. proposed enhancements to the GHBMCM50 that could improve the biofidelity of the shoulder area of this HBM, potentially leading to a change in chest deflection on the order of 5% according to the study. However, these further improvements to the HBM are not expected to change the general trends observed in the current study.

The design of the fractional factorial experiment also constituted a limitation of the study. The two-factor interactions were aliased (Table 6.6) hindering the analysis of interactions contribution to the occupant response. However, due to a significantly higher effect of the arm position compared to any other main or interaction effects, for the purpose of this study it was an acceptable compromise. The magnitude of the interaction between the arm position and tSAB location was further examined in a full factorial experiment at the higher tSAB pressure, revealing interactions at the level of rib 6 for the chest deflection, VC, predicted number of rib fracture locations, and volume of contused lungs. The specific location of the interactions further highlights the importance of assessing thoracic response at multiple locations and with use of different methods, beyond discrete locations and maximum values implemented in current safety standards (NHTSA 2012).

Table 6.6: Two-factor interactions aliased due to the experimental design of the fractional factorial experiment.

AB (arm and longitudinal tSAB location)	CD (vertical tSAB location and pressure)
AC (arm and vertical tSAB location)	BD (longitudinal tSAB location and pressure)
AD (arm and tSAB pressure)	BC (longitudinal and vertical tSAB location)

Chapter 7

Conclusions

This study contributes to the existing knowledge on side impact crash scenarios, demonstrating the advantages of integrated numerical vehicle, restraint, and Human Body Models (HBMs) for simulating and understanding occupant thorax response in the crash environment. The benefits of numerical methods include a fully controlled crash environment that assures repeatability and enables detailed parametric studies. This thesis focused on potential contributors to conflicting data on the effectiveness of thoracic side airbags (tsABs) in reducing injury. Four factors examined in this thesis included: 1) the capacity of occupant surrogates to predict changes in measured response due to varying pre-crash parameters; 2) sensitivity of the occupant surrogate to pre-crash parameters in different lateral impact scenarios; 3) influence of the arm position on the effectiveness of tsABs; 4) importance of the occupant response assessment method for predicted outcomes due to varying tsAB and seatbelt settings.

The occupant was modeled with three computational surrogates: a standard ES-2re Anthropometric Test Device (ATD) finite element model, the University of Waterloo HBM (UW-HBM), and the Global Human Body Models Consortium HBM (GHBMC-HBM). For the vertical arm position, an increase of chest compression response was predicted by both HBMs, and the ATD model was not sensitive to varying arm pre-crash orientation (<5% relative change). The VCmax response of the ATD to varying door trim material properties was higher than that of the UW-HBM, owing to a stiffer thorax and a shorter duration between the maximum chest compression and maximum chest compression velocity, attenuated by soft tissues in the UW-HBM. In contrast, the UW-HBM exhibited higher sensitivity to varying door trim material properties in terms of chest compression (+27% relative maximum increase), where the ATD chest compression change remained below 5%. A reduction of the UW-HBM chest deflection at the level of rib 4 was observed with increasing Young's modulus and yield strength of the door trim material, since stiffer door trim properties led to higher contact forces between the intruding door and occupant arm, altering the magnitude of upper arm rotation during crash. Although the UW-HBM predicted potential interactions between

the arm position and door compliance on chest compression, the magnitude of the effect was very low (0-7mm) compared to the effect of arm position itself (83mm).

The UW-HBM predicted an increase of 2.5 times for chest compression (+140%) due to the vertical arm position in the full vehicle scenario, higher than simplified tests such as the rigid-wall sled impacts (+56-69%). Predicted VCmax and number of rib fracture locations were in agreement with chest compression trends, increasing for the vertical arm position. However, the lung contusion response was affected by deformation and load transfer between hard and soft tissues throughout the entire occupant body and depended on the loading type. The pendulum scenarios were relatively insensitive to the arm (-10 to +13% chest compression change), and the UW-HBM confirmed previous observations on protective effect of the arm in velocity-pulse low-severity pendulum impacts.

The effectiveness of a thoracic side airbag (tSAB) was dependent on the occupant pre-crash position. Both HBMs predicted an increase of chest deflection and VC metrics at multiple rib levels due to tSAB deployment for the driving arm position, and a decrease in metrics for the vertical arm position. The pre-crash arm position was more dominant in terms of response metrics compared to the effect of varying tSAB location and pressure for the UW-HBM, and over the effect of any restraint combination for the GHBMC-HBM (+106% increase due to vertical arm position, and +75% increase due to restraints). Lower tSAB locations were found to provide coverage for the lower torso and push the arm away from the load path, and the least desired tSAB position was in the shoulder and upper torso area, where the deploying tSAB would rotate and push the arm towards the torso. Measurement of the spine curvature, namely relative distances between vertebrae during the crash, demonstrated an increase of chest deflection and VC metrics when the overall lateral displacement and change in the spine curvature were the most pronounced, providing a useful metric to compare occupant responses for different side impact safety systems.

Two methods for measuring thorax compression, Post-Mortem Human Surrogate (PMHS) specific, or ATD specific, yielded contrasting results on tSAB and seatbelt effectiveness, as evaluated using the GHBMC-HBM. HBMs provided an improved

understanding of thoracic response, enabling a direct comparison of global, local (measured at multiple rib levels), and tissue level responses.

This study demonstrated that the choice of occupant surrogate, ATD or HBM, to predict changes in injury response affected the outcomes of parametric studies. Sensitivity of the occupant surrogate response to pre-crash parameters was the highest in full vehicle impacts compared to other lateral impact scenarios, and highlighted the importance of replicating real crash conditions for research on further improvement of passive restraints. The arm position of the HBM was observed to affect the effectiveness of tSABs, demonstrating a potential for improvement of occupant safety with multiple pre-crash positions included in vehicle compliance testing. Finally, the HBMs enabled an identification of the effect of restraint combinations beyond the three discrete locations, providing evidence that the effect of passive restraints could be dependent on occupant response assessment method

7.1 Recommendations and Future Work

Future studies should focus on optimization of side restraint systems with HBMs, based on additional insight into the thorax deformation pattern, spine kinematics and change of curvature during impact, and prediction of locations of rib fractures and potential injury to internal organs. A parametric numerical verification of the occupant interaction with safety restraints and vehicle interior in a full vehicle impact would be a beneficial supplement to the physical component-level lateral sled or pendulum impacts. Different impact velocities should be investigated to ensure that the predicted trends for restraint effectiveness follow for higher and lower severity impacts. Additional impact scenarios (impact angle, MDB bumper height) and the effect of occupant position (fore/aft) coupled with arm position for occupant response should be considered. The effect of the arm position should be investigated for rotations in both sagittal and coronal plane, and verified for different door and armrest designs in addition to inflatable restraints (side airbags). Future investigations should consider the interaction of the pelvis and seat to enhance the model validation, and investigation of other HBMs, body anthropometries and postures.

Letter of Copyright Permission



Our Ref: KA/TCRS/P18/1065

13 June 2018

Dear Donata Gierczycka,

Material requested: Donata Gierczycka, Brock Watson & Duane Cronin (2015) Investigation of occupant arm position and door properties on thorax kinematics in side impact crash scenarios – comparison of ATD and human models, International Journal of Crashworthiness, 20:3, 242-269.

Thank you for your correspondence requesting permission to reproduce the above mentioned material from our Journal in your printed thesis to be posted in the university's repository – the University of Waterloo / <https://uwaterloo.ca/>

We will be pleased to grant permission on the sole condition that you acknowledge the original source of publication and insert a reference to the article on the Journals website: <http://www.tandfonline.com>

This is the authors accepted manuscript of an article published as the version of record in International Journal of Crashworthiness © 19 Jan 2015 - <https://www.tandfonline.com/10.1080/13588265.2014.998000>

This permission does not cover any third party copyrighted work which may appear in the material requested.

Please note that this license does not allow you to post our content on any third party websites or repositories.

Thank you for your interest in our Journal.

Yours sincerely

Kendyl

Kendyl Anderson – Permissions Administrator, Journals
Taylor & Francis Group
3 Park Square, Milton Park, Abingdon, Oxon, OX14 4RN, UK.
Tel: +44 (0)20 7017 7617
Fax: +44 (0)20 7017 6336
Web: www.tandfonline.com
e-mail: kendyl.anderson@tandf.co.uk



Taylor & Francis is a trading name of Informa UK Limited,
registered in England under no. 1072954

Bibliography

- Aekbote K, Sundararajan S, Chou CC, Lim GG, and Prater JA, 1999. “A New Component Test Methodology Concept for Side Impact Simulation”. SAE Technical Paper Series, No. 1999-01-0427. Society of Automotive Engineers, Troy, MI.
- Agnew AM, Murach MM, Misicka E, Moorhouse K, Bolte JH IV, and Kang YS, 2017. “The Effect of Body Size on Adult Human Rib Structural Properties”, in *Proceedings of the International IRCOBI Conference*, pp. 728–736, Antwerp, Belgium.
- Albert DL, Beeman SM, Kemper AR, 2018. “Occupant kinematics of the Hybrid III, Thor-M, and postmortem human surrogates under various restraint conditions in full-scale frontal sled tests”, *Traffic Injury Prevention* 19(sup1), pp. S50-S58.
- Arun MWJ, Humm JR, Yoganandan N, and Pintar FA, 2015. “Biofidelity Evaluation of a Restrained Whole Body Model under Frontal Impact using Kinematics Data from PMHS Sled Tests”, in *Proceedings of the International IRCOBI Conference*, Lyon, France.
- ASME V&V 10-2006, 2006. “Guide for Verification and Validation in Computational Solid Mechanics”, the American Society of Mechanical Engineers, NYC.
- Association for the Advancement of Automotive Medicine, 2015. “Abbreviated Injury Scale”. Available at: <https://www.aaam.org/abbreviated-injury-scale-ais/>, AAAM, Chicago, IL.
- Baudrit P, Hammon J, Song E, Robin S, and Le Coz J-Y, 1999. “Comparative Studies of Dummy and Human Body Models Behavior in Frontal and Lateral Impact Conditions”, in *Proceedings of the 43rd Stapp Car Crash Conference*, 99SC05.
- Becher RD, Colonna AL, Enniss TM, Weaver AA, Crane DK, Martin SM, Mowery NT, Miller PR, Stitzel JD, and Hoth JJ, 2012. “An innovative approach to predict the development of adult respiratory distress syndrome in patients with blunt trauma”. *Journal of Trauma and Acute Care Surgery* 73 (5), pp. 1229–1235.

Bédard M, Guyatt GH, Stones MJ, and Hirdes JP, 2002. “The Independent Contribution of Driver, Crash, and Vehicle Characteristics to Driver Fatalities”. *Accident Analysis and Prevention* 34 (6), pp. 717–727.

Berg FA, Schmitt B, Epple J, Mattern R, and Kallieris D, 1998. “Results of full-scale crash tests, stationary tests and sled tests to analyse the effects of air bags on passengers with or without seat belts in the standard sitting position and in out-of-position situations”. In *Proceedings of the International IRCOBI Conference*, pp.1055–1070, Gothenburg, Sweden.

Bhalsod D, Krebs J, 2008. “214 Shell Barrier Documentation”. Livermore Software Technology Corporation. Livermore, CA.

Campbell B, Cronin DS, 2014. “Coupled Human Body and Side Impact Model to Predict Thoracic Response”, *International Journal of Crashworthiness* 19 (4), pp. 394-413.

Campbell BM, 2009. “A Numerical Side Impact Model to Investigate Thoracic Injury in Lateral Impact Scenarios”. MAsc thesis, University of Waterloo, Waterloo, ON, Canada.

“Canadian Motor Vehicle Traffic Collision Statistics: 2016”, 2017. Retrieved from <https://www.tc.gc.ca/eng/motorvehiclesafety/canadian-motor-vehicle-traffic-collision-statistics-2016.html>

Carter PM, Flannagan CAC, Reed MP, Cunningham RM, Rupp JD, 2014. “Comparing the effect of age, BMI, and gender on severe injury (AIS 3+) in motor-vehicle crashes”. *Accident Analysis & Prevention* 72, pp. 146-160.

Cavanaugh JM, 2002. “Biomechanics of Thoracic Trauma”. In *Accidental Injury, Biomechanics and Prevention*, ed. Nahum AM, Melvin JW, Springer, New York, NY.

Cavanaugh JM, Walilko TJ, Malhotra A, Zhu Y, and King AI, 1990a. “Biomechanical Response and Injury Tolerance of the Pelvis in Twelve Sled Side Impacts,” in *Proceedings of the 34th Stapp Car Crash Conference*, 902305.

- Cavanaugh JM, Walilko TJ, Malhotra A, Zhu Y, and King AI, 1990b. “Biomechanical Response and Injury Tolerance of the Thorax in Twelve Sled Side Impacts,” in *Proceedings of the 34th Stapp Car Crash Conference*, 902307.
- Cavanaugh JM, Zhu Y, Huang Y, and King AI, 1993a. “Injury and Response of the Thorax in Side Impact Cadaveric Tests”, in *Proceedings of the 37th Stapp Car Crash Conference*, 933127.
- Cesari D, Ramet M, and Bloch J, 1981. “Influence of Arm Position on Thoracic Injuries in Side Impact”, in *Proceedings of the 25th Stapp Car Crash Conference*, 811007.
- Chang F, 2001. “The Development and Validation of a Finite Element Human Thorax Model for Automotive Impact Injury Studies”, in *Proceedings of the 2001 ASME International Mechanical Engineering Congress and Exposition*, AMD Vol. 251, pp. 103–111.
- Cheng H, Obergefell L, and Rizer A, 1994.”Generator of Body (GEBOD) Manual”.
Armstrong Laboratory, Air Force Materiel Command. Wright-Patterson Air Force Base, OH.
- Choi H-Y, Eom H-W, Kho S-T, and Lee I-H, 1999. “Finite Element Human Model for Crashworthiness Simulation”, SAE Paper No. 1999-01-1906.
- Chung J, Cavanaugh JM, King AI, Koh S-W, and Deng Y-C, 1999. “Thoracic Injury Mechanisms and Biomechanical Responses in Lateral Velocity Pulse Impacts”, in *Proceedings of the 43rd Stapp Car Crash Conference*, 99SC04.
- Cohen J, 1988. “Statistical Power Analysis for the Behavioral Sciences”. Lawrence Erlbaum Associates, Mahwah, NJ.
- “Crash Injury Research (CIREN), case number #831030778”, 2018. Retrieved from [https://one.nhtsa.gov/Research/Crash-Injury-Research-\(CIREN\)](https://one.nhtsa.gov/Research/Crash-Injury-Research-(CIREN)).
- Cronin DS, 2011. “Explicit Finite Element Method Applied to Impact Biomechanics Problems”, Keynote Lecture, *International IRCOBI Conference*. Krakow, Poland.

- Cummings JR, Osterholt GD, Van Calhoun D, Biller BA, 2009. "Occupant Friction Coefficients on Various Combinations of Seat and Clothing". *SAE Technical Paper Series*, No. 2009-01-1672, 1–11. SAE International, Troy, MI.
- D'Elia A, Newstead S, and Scully J, 2013. "Evaluation of vehicle side airbag effectiveness in Victoria, Australia". *Accident Analysis and Prevention* 54, pp. 67–72.
- Danelson KA, Stitzel JD, 2015. "Finite Element Model Prediction of Pulmonary Contusion in Vehicle-to-Vehicle Simulations of Real-World Crashes". *Traffic Injury Prevention* 16, pp. 627–636.
- Danelson KA, Golman AJ, Kemper AR, Gayzik FS, Gabler HC, Duma SM, and Stitzel JD, 2015. "Finite Element Comparison of Human and Hybrid III Responses in a Frontal Impact". *Accident Analysis and Prevention* 85, pp. 125–156.
- De Moya M, Manolakaki D, Chang Y, Amygdalos I, Gao F, Alam HB, and Velhmahos GC, 2011. "Blunt Pulmonary Contusion: Admission Computed Tomography Scan Predicts Mechanical Ventilation". *Journal of Trauma, Injury, Infection, and Critical Care* 71 (6), pp. 1543–1547.
- Deng Y-C, 1989. "The Importance of the Test Method in Determining the Effects of Door Padding in Side Impact", *SAE Technical Paper Series* No. 892429.
- Deng Y-C, Kong W, and Ho H, 1999. "Development of a Finite Element Human Thorax Model for Impact Injury Studies", *SAE Technical Paper Series* No. 1999-01-0715.
- Dischinger PC, Ho SM, Kerns TJ, and Brennan MS, 1996. "Patterns of injury in frontal collisions with and without airbags", in *Proceedings of the International IRCOBI Conference*, pp. 311–319, Dublin, Ireland.
- Donlon JP, Poulard D, Lessley D, Riley P, and Subit D, 2015. "Understanding how Pre-Impact Posture can Affect Injury Outcome in Side Impact Sled Tests using a New Tool for Visualization of Cadaver Kinematics." *Journal of Biomechanics* 48 (3), pp. 529–533.

- Donnelly BR, Rhule HH, Moorhouse KM, Kang YS, and Stammen JA, 2007. “An Improved Deflection Energy Method to Normalize PMHS Thoracic Response Data”, in *Proceedings of the International IRCOBI Conference*, pp. 728–736, Antwerp, Belgium.
- Economic Commission for Europe (ECE), 1995. ”Agreement Concerning the Adoption of Uniform Conditions of Approval and Reciprocal Recognition of Approval for Motor Vehicle Equipment and Parts – Addendum 95: Regulation No. 95”.
- El-Jawahri RE, Laitury TR, Ruan JS, Rouhana SW, and Barbat SD, 2010. “Development and Validation of Age-Dependent FE Human Models of a Mid-Sized Male Thorax”. *Stapp Car Crash Journal*, Vol. 54 (November 2010), pp. 407–430.
- EuroNCAP, 2018: <https://www.euroncap.com/en/for-engineers/protocols/adult-occupant-protection/>
- “Fatal Accident Reporting System”, 2016. Retrieved from www-FARS.nhtsa.dot.gov
- “Fatality Facts 2016”, Insurance Institute for Highway Safety, 2017. Retrieved from <http://www.iihs.org/iihs/topics/t/general-statistics/fatalityfacts/overview-of-fatality-facts>.
- Fitzharris M, Fildes B, Newstead S, and Logan D, 2004. “Benefits of Australian Design Rule 69 (full frontal crash protection) and airbags in frontal crashes in Australia”, in *Proceedings of the 48th Annual Conference of the Association for the Advancement of Automotive Medicine*, Miami, FL.
- Forbes PA, Cronin DS, and Deng Y-C, 2006. “Multi-Scale Human Body Model to Predict Side Impact Thoracic Trauma”. *International Journal of Crashworthiness*, Vol.11 (3), pp. 203–216.
- Forbes PA, Cronin DS, Deng Y-C, and Boismenu M, 2005. ”Numerical Human Model to Predict Side Impact Thoracic Trauma”, in *IUTAM Proceedings on Impact Biomechanics: From Fundamental Insights to Applications*, pp. 441–450.

- Gayzik FS, Hoth JJ, Daly M, Meredith JW, and Stitzel JD, 2007. “A Finite Element-Based Injury Metric for Pulmonary Contusion: Investigation of Candidate Metrics through correlation with computed tomography,” *Proceedings of 51st Stapp Car Crash Conference*, pp. 189–209.
- Gayzik FS, 2008. “Development of a finite element based injury metric for pulmonary contusion”. *Ph.D. Dissertation*, Virginia Tech-Wake Forest University, Winston-Salem, NC.
- Gayzik FS, Hoth JJ. And Stitzel JD, 2011. “Finite-element based injury metrics for pulmonary contusion via concurrent model optimization”. *Biomechanics and Modeling in Mechanobiology* 10, pp. 505–520.
- Gehre C, Praxl N, Stahlschmidt S, and Fressman D, 2013. “Evaluation of a Dummy by Using a Human Body Model”. *4th International Symposium on Human Modeling and Simulation in Automotive Engineering*, CARHS, 2013.
- Gierczycka D, Cronin DS, 2014. “Investigation of Injury Metrics Sensitivity to Thorax Impact Loading Using a Detailed Human Body Model”, in *Proceedings of the International IRCOBI Conference*. Berlin, Germany.
- Gierczycka D, Cronin DS, 2015a. “Investigation of Human Body Model Response to Different Lateral Loading Conditions”, in *Proceedings of the IRCOBI Conference*, Lyon, France.
- Gierczycka D, Watson B, and Cronin DS, 2015b. Investigation of Occupant Arm Position and Door Properties on Thorax Kinematics in Side Impact Crash Scenarios- Comparison of ATD and Human Models. *International Journal of Crashworthiness* 20 (3), pp. 242–269.
- Gierczycka D, Cronin DS, 2017. “Occupant Thorax Response Variations Due to Arm Position and Restraint Systems in Side Impact Crash Scenarios”. *Accident Analysis and Prevention* 106, pp. 173–180.

- Gierczycka D, Cronin DS, 2018. "Influence of the chest compression measurement method on assessment of restraint performance in side-impact crash scenarios". *Journal of Biomechanics* 75, pp. 53–57.
- Global Human Body Models Consortium, GHBM, 2014. "User Manual: M50 Occupant, Version 4.3 for LS-DYNA". Elemance, LLC.
- Gray H, 1918. "Anatomy of the Human Body". Gramercy Books, New York.
- Griffin R, Huisingh C, McGwin G, and Reiff D, 2012. "Association between side-impact airbag deployment and risk of injury: a matched cohort study using the CIREN and the NASS-CDS". *Journal of Trauma and Acute Care Surgery* 73 (4), pp. 914–918.
- Haland Y, Lindqvist M, 1994. "Sensor for a Side Airbag: Evaluation by a New Subsystem Test Method", in *Proceedings of the 14th ESV Conference*. Paper No. 94-S6-W-26, pp.1-12. Munich, Germany.
- Hayes AR, Vavalle NA, Moreno DP, Stitzel JD, and Gayzik SF, 2014. Validation of Simulated Chestband Data in Frontal and Lateral Loading using a Human Body Finite Element Model. *Traffic Injury Prevention* 15 (2), pp. 181–186.
- Heron M, 2017. "Deaths: Leading Causes for 2015". U.S. Department of Health and Human Services, *National Vital Statistics Reports* 66 (5), pp. 1-76. Retrieved from https://www.cdc.gov/nchs/data/nvsr/nvsr66/nvsr66_05.pdf
- Huang Y, King AI, and Cavanaugh JM, 1994. "A MADYMO Model of Near-Side Human Occupants in Side Impacts". *Journal of Biomechanical Engineering* 116, pp. 228–235.
- Hwang E, Hu J, Chen C, Klein KF, Miller CS, Reed MP, Rupp JD, Hallman JJ, 2016. "Development, evaluation, and sensitivity analysis of parametric finite element whole-body human models in side impact". *Stapp Car Crash Journal* 60 (November), pp. 473-508.

- Insurance Institute for Highway Safety, 2017. "Side Impact Crashworthiness Evaluation Crash Test Protocol", IIHS, Ruckersville, VA. Retrieved from <http://www.iihs.org/iihs/about-us/vrc>
- ISO/TR 9790:1999, "Road vehicles – Anthropomorphic Side Impact Dummy – Lateral Impact".
- Iwamoto M, Kisanuki Y, Watanabe I, Furusu K, Miki K, and Hasegawa J, 2002. "Development of a Finite Element Model of the Total Human Model for Safety (THUMS) and Application to Injury Reconstruction", in *Proceedings of the International IRCOBI Conference*. Munich, Germany.
- Jordan A, 1974. "Test Sled Simulation of Crash Induced Yaw and Pitch", in *Proceedings of the 3rd International Conference on Occupant Protection*, Troy, MI.
- Kahane CJ, 2004. "Lives Saved by the Federal Motor Vehicle Safety Standards and Other Vehicle Safety Technologies, 1960-2002". *NHTSA Technical Report* No. DOT HS 809 833. NHTSA, Washington, DC.
- Kahane CJ, 2007. "An Evaluation of Side Impact Protection. FMVSS 214 TTI(d) Improvements and Side Air Bags". (Report No. DOT HS 810 748). National Highway Traffic Safety Administration.
- Kahane CJ, 2014. "Updated Estimates of Fatality Reduction by Curtain and Side Air Bags in Side Impacts and Preliminary Analyses of Rollover Curtains". (Report No. DOT HS 811 882). National Highway Traffic Safety Administration.
- Kaneko N, Taguchi S, Motoki M, and Ogawa S, 2007. "Optimization of the Side Airbag System using MADYMO Simulations." *SAE Technical Papers*: 2007-01-0345.
- Kemper AR, McNally C, Kennedy EA, Manoogian SJ, and Duma SM, 2008. "The Influence of Arm Position on Thoracic Response in Side Impact". *Stapp Car Crash Journal* 52, Paper No. 08S-02.

- Kemper AR, Santago AC, Stitzel JD, Sparks JL, and Duma SM, 2012. "Biomechanical response of human spleen in tensile loading". *Journal of Biomechanics* 45 (2), pp. 348–355.
- Kemper AR, 2013. "Response Corridors for the Medial-Lateral Compressive Stiffness of the Human Arm: Implications for Side Impact Protection." *Accident Analysis and Prevention* 50, pp. 204-222.
- Kemper AR., Beeman SM, Porta DJ, and Duma SM, 2016. "Non-censored Rib Fracture Data during Frontal PMHS Sled Tests". *Traffic Injury Prevention* 17 (S1), pp. 131–140.
- Kim T, Shaw G, Lessley D, Park G, Crandall J, Svendsen A, Whitcomb B, Ayyagari M, Mishra P, and Markusic C, 2016. "Biofidelity Evaluation of WorldSID and ES-2re under Side Impact Conditions with and without Airbag." *Accident Analysis and Prevention* 90, pp. 140-151.
- Klaus G, Kallieris D, 1983. "Side Impact – A Comparison between HSRI, APROD and HYBRID II Dummies and Cadavers". *SAE Technical Paper Series* No. 831630, SAE, Troy, MI.
- Kroell CK, Schneider DC, and Nahum AM, 1971. "Impact Tolerance and Responses of the Human Thorax", in *Proceedings of the 15th Stapp Car Crash Conference*, 710851.
- Kroell CK, Schneider DC, and Nahum AM, 1974. "Impact Tolerance and Response of the Human Thorax II", in *Proceedings of the 18th Stapp Car Crash Conference*, 741187.
- Kuppa S, 2004. "Injury Criteria for Side Impact Dummies". National Highway Traffic Safety Administration, Washington, DC.
- Kuppa S., Eppinger RH, McKoy F, Nguyen T, Pintar FA, and Yoganandan N, 2003. "Development of Side Impact Thoracic Injury Criteria and their Application to the Modified ES-2 Dummy with Rib Extensions (ES-2re)." *Stapp Car Crash Journal* 47, pp. 189–210.

- Lau IV, Viano DC, 1986. “The Viscous Criterion - Bases and Applications of an Injury Severity Index for Soft Tissues”, in *Proceedings of the 30th Stapp Car Crash Conference*, 861882.
- “Leading causes of death, total population, by age group”, 2018. Statistics Canada, retrieved from <https://www150.statcan.gc.ca/t1/tbl1/en/tv.action?pid=1310039401>
- Lessley D, Shaw G, Parent D, Arregui-Dalmases C, Kindig M, Riley P, Pursetzov S, Sochor M, Gochenour T, Bolton J, Subit J, Crandall J, Takayama S, Ono K, Kamiji K, and Yasuki T, 2010. “Whole-Body Response to Pure Lateral Impact”. *Stapp Car Crash Journal* 54, pp. 289–336. The Stapp Association, Ann Arbor, MI.
- Leveau GD, 1903. “Protective straps for automobiles and other vehicles”, patent No.FR331926A.
- Lizee E, Robin S, Song E, Bertholon N, Le Coz J-Y, Besnault B, and Lavaste F, 1998. “Development of a 3D Finite Element Model of the Human Body”. *SAE Technical Paper Series*, No. 983152.
- Lobdell TE, Kroell CK, Schneider DC, Hering WE, and Nahum AM, 1973. “*Impact response of the human thorax*”. In “*Human Impact Response, Measurement and Simulation*”, King WF and Mertz HJ Ed. Plenum Press, New York-London.
- Lockhart P, Cronin DS, and Watson B, 2013. “Frontal Impact Response for Pole Crash Scenarios”, *Traffic Injury Prevention* 14 (5), pp. 509-519.
- Loftis KL, Weaver AA, and Stitzel JD, 2011. “Investigating the Effects of Side Airbag Deployment in Real-World Crashes Using Comparison Techniques”, *Annals of Advances of Automotive Medicine* 55, pp. 81-90.
- Lorenzo L, Burr S, and Fennessy-Ketola K, 1996. “Integrated Inner Door Panel/Energy Absorber Designs for Side Impact Occupation Protection”. *SAE Technical Series Paper Series* No. 960151.
- “LS-Dyna Keyword User’s Manual”, Livermore Software Technology Corporation, Livermore, CA, 2016. Retrieved from lsc.com/pdf/ls-dyna_971_manual_k.pdf

- LSTC, Livermore Software Technology Corporation, 2018: <http://www.lstc.com/>
- Luzon-Narro J, Arregui-Dalmases C, Hernando LM, Core E, Narbona A, and Selgas C, 2014. "Innovative Passive and Active Countermeasures for Near Side Crash Safety." *International Journal of Crashworthiness* 19 (3), pp. 209–221.
- McCartt AT, Kyrychenko SY, 2007. "Efficacy of Side Airbags in Reducing Driver Deaths in Driver-Side Car and SUV Collisions." *Traffic Injury Prevention* 8 (2), pp. 162–170.
- Mendoza-Vazquez M, Jakobsson L, Davidsson J, Brodin K, and Ostmann M, 2014. "Evaluation of thoracic injury criteria for THUMS finite element human body model using real-world accident data", in *Proceedings of the International IRCOBI Conference*, Berlin, Germany.
- Mertz H, Irwin AL, and Prasad P, 2003. Biomechanical and scaling bases for frontal and side impact injury assessment values. *Stapp Car Crash J.* 47, pp. 155–188.
- Miller CS, Rupp JD, 2011. "PMHS Impact Response in Low and High-Speed Nearside Impacts", *University of Michigan Transportation Research Institute Report No. UMTRI-2011-10*, Ann Arbor, MI.
- Montgomery DC, 2012. "Design and Analysis of Experiments" 8th ed., John Wiley and Sons, Danvers, MA.
- Moore KL, Agur AMR, Dalley AF, 2011. "Essential clinical anatomy". Lippincott Williams & Wilkins, Baltimore MD.
- Morris AP, Hassan AM, and Mackay M, 1997. "Chest Injuries in Real-World Side Impact Crashes – An Overview", in *Proceedings of the International IRCOBI Conference*. Hanover, Germany.
- NHTSA, 1996. "Report No.: 214D-MGA-97-04". National Highway Traffic Safety Administration. Retrieved from <http://www.safercar.gov/Vehicle+Shoppers/5-Star+Safety+Ratings/1990-2010+Vehicles/Vehicle-Detail?vehicleId=4362>, accessed June 27, 2014.

- NHTSA, 2001. “A Compilation of Motor Vehicle Crash Data from the Fatality Analysis Reporting System and the General Estimates System”, in *Traffic Safety Facts 2001*, NHTSA Report No. DOT HS 809-484
- NHTSA Biomechanics Test Database, 2009-2018, 2018. Retrieved from <https://www-nrd.nhtsa.dot.gov/database/bio/information.htm>
- NHTSA Vehicle Crash Test Database, 2009-2018, 2018. Retrieved from <https://www-nrd.nhtsa.dot.gov/database/veh>
- NHTSA, 2006. “Laboratory Test Procedure for FMVSS No. 214 Dynamic Side Impact Protection”, Document Number TP214D-08 Part 1. National Highway Traffic Safety Administration, Washington, DC.
- NHTSA, 2006: *Traffic Safety Facts 2006: A Compilation of Motor Vehicle Crash Data from the Fatalities Analysis Reporting System and General Estimates System*, Washington, DC, US Department of Transportation.
- NHTSA, 2012a. “Laboratory Test Procedure for the New Car Assessment Program Side Impact Moving Deformable Barrier Test”. National Highway Traffic Safety Administration, Washington, DC.
- NHTSA, 2012b. “Laboratory Test Procedure for the New Car Assessment Program Side Impact Rigid Pole Test”. National Highway Traffic Safety Administration, Washington, DC.
- O’Connor JV, Kufera JA, Kerns TJ, Stein DM, Ho S, Dischinger PC, and Scalea TM: Crash and Occupant Predictors of Pulmonary Contusion. *The Journal of Trauma Injury, Infection, and Critical Care* 66, pp. 1091–1095.
- Opiela KS, 2008. “Finite Element Model of Ford Taurus. NHTSA Finite Element Model Archive”. Retrieved from <http://www.ncac.gwu.edu/vml/archive/ncac/vehicle/taurus-v3.pdf>, accessed June 3, 2011.

- Oshita F, Omori K, Nakahira Y, and Miki K, 2001. "Development of a finite element model of the human body". *Proceedings of the 7th International LS-Dyna Users Conference*, Detroit, MI.
- Otte D, Sferco R, Schafer R, Eis V, Thomas P, and Welsh R, 2009. "Assessment of Injury Severity of Nearside Occupants in Pole Impacts to Side of Passenger Cars in European Traffic Accidents – Analysis of German and UK in-depth Data". *Proceedings of the International Technical Conference on the Enhanced Safety of Vehicles*, Stuttgart, Germany.
- "Overview of materials for Acrylonitrile Butadiene Styrene (ABS), Molded", MatWeb, 2010. Retrieved from <http://www.matweb.com/search/DataSheet.aspx?MatGUID=eb7a78f5948d481c9493a67f0d089646>
- Park G, Kim T, Crandall JR, Svendsen A, Saunders N, and Markusic C, 2014. "Evaluation of Biofidelity of Side Impact Computational Surrogates (ES-2re, WorldSID, GHBMC)". *SAE Technical Paper Series*, No. 2014-01-0541.
- Park G, Kim T, Panzer MB, and Crandall JR, 2016. "Validation of Shoulder Response of Human Body Finite-Element Model (GHBMC) Under Whole Body Lateral Impact Condition." *Annals of Biomedical Engineering*, pp. 1–19.
- Pintar FA, Yoganandan N, Hines MH, Maltese MR, McFadden J, Saul R, Eppinger R, Khaewpong N, and Kleinberger M, 1997. "Chestband Analysis of Human Tolerance to Side Impact". *Proceedings of the 41st Stapp Car Crash Conference*, Paper No. 973320, Lake Buena Vista, FL.
- Pipkorn B, Haland Y, 1996. "A Side Airbag System to Meet Chest Injury Measures: Evaluation by Mathematical Simulations". *International Journal of Crashworthiness* 1 (1), pp. 145–161.
- Plank GR, Kleinberger M, and Eppinger RH. 1998. "Analytical Investigation of Driver Thoracic Response to Out of Position Airbag Deployment". *SAE Technical Paper Series*, No. 983165.

- Pyttel T, Floss A, Thibaud C, and Goertz C, 2007. “Realistic Simulation Models for Airbags and Humans – New Possibilities and Limits of FE Simulation”. *International Journal of Crashworthiness* 12(5), pp. 481-492.
- Ratingen M, 2001. “Development and Evaluation of the ES-2 Side Impact Dummy. Response Requirements to Assess the Biofidelity of the Dummy”. *Proceedings of the 17th Conference on Enhanced Safety of Vehicles*, Paper No. 336. Amsterdam, Netherlands.
- Reed MP, Ebert SM, Park B-K D, Jones MLH, 2018. “Passenger Kinematics during Crash Avoidance Maneuvers”. *Final Report UMTRI-2018-5*. University of Michigan Transportation Research Institute.
- Reed MP, Ebert SM, 2016. “Upper-Extremity Postures and Activities in Naturalistic Driving”. *Final Report UMTRI-2016-20*, University of Michigan Transportation Research Institute.
- Rhule H, Suntay B, Jerriott R, Ameson T, Stricklin J, and Bolte IV JH, 2011. “Response of PMHS to High- and Low-Speed Oblique and Lateral Pneumatic Ram Impacts”. *Stapp Car Crash Journal* 55, pp. 281–315.
- Richardson DC, 2010. “Relationship between Speed and Risk of Fatal Injury: Pedestrians and Car Occupants”. *Road Safety Web Publication* No. 16, Department of Transport, London, UK.
- Robin S, 2001. “HUMOS: Human Model for Safety – a Joint Effort Towards the Development of Refined Human-Like Car Occupant Models”, in *Proceedings of the 17th International Technical Conference on the Enhanced Safety of Vehicles*. Paper No. 297.
- Ruan J, El-Jawahri R, Chai L, Barbat S, and Prasad P, 2003. “Prediction and Analysis of Human Thoracic Impact Responses and Injuries in Cadaver Impacts Using a Full Human Body Finite Element Model”. *Stapp Car Crash Journal* 47, pp. 299–321.

- Rupp JD, Miller CS, Reed MP, Klinich KD, and Schneider LW, 2011. "Comparison of WorldSID and Cadaver Responses in Low-Speed and High-Speed Nearside Impact", in *Proceedings of the 22nd International Technical Conference on the Enhanced Safety of Vehicles*. Paper No. 11-0080.
- Samaha RR, Maltese M, and Bolte J, 2001. "Evaluation of the ES-2 Dummy in Representative Side Impacts", in *Proceedings of the 17th International Technical Conference on the Enhanced Safety of Vehicles*, Paper No. 2001-06-0096.
- Scherer R, Bortenschlager K, Akiyama A, Tylko S, Hartlieb M, and Harigae T, 2009. "Worldsid Production Dummy Biomechanical Responses". *Proceedings of the International Technical Conference on the Enhanced Safety of Vehicles*, Stuttgart, Germany.
- Schneider S, Niwa M, Koyama T, Tanase T, Sato Y, Sakamoto M, and Asaoka M, 2005. "Effectiveness of Thorax and Pelvis Side Airbag for Improved Side-Impact Protection". National Highway Transport Safety Administration, Washington, DC.
- Shaw G, Lessley DJ, Ash JL, Sochor MR, Crandall JR, Luzon-Narro J, and Arregui-Dalmases C, 2014. "Side impact PMHS thoracic response with large-volume air bag", *Traffic Injury Prevention* 15, pp. 40–47.
- "Side Impact Crash Test Dummies", Humanetics Innovative Solutions, Farmington Hills, MI, 2018, retrieved from <http://www.humaneticsatd.com/crash-test-dummies/side-impact/>
- "Side Impact Dummy Models", DYNAmore GmbH, Stuttgart, Germany, 2015. Retrieved from <https://www.dynamore.de/en/products/models/side>
- Snyder RG, 1969. "A Survey of Automotive Occupant Restraint Systems: Where We've Been, Where We Are, and Our Current Problems". *SAE Technical Paper Series* No. 690243, SAE International, Troy, MI.

- Stalnaker RL, Tarriere C, Fayon A, Walfisch G, Balthazard M, Masset J, Got C, and Patel A, 1979. "Modification of Part 572 Dummy for Lateral Impact According to Biomechanical Data". *SAE Technical Paper Series* No. 791031. Troy, MI.
- Stapp JP, 1947. "Human Exposures to Linear Acceleration: Part II. The Forward - Facing Position and Development of a Crash Harness". Dayton, Ohio: *AF Technical Report* No. 5912
- Stapp JP, 1949. Human Exposures to Linear Deceleration I, "Preliminary Survey of Aft-Facing Seated Position". Dayton, OH. *AF Technical Report* No. 5915.
- Stricklin J, Rhule D, 2009. "Biofidelity Analysis of WorldSID and ES-2re". Government/Industry Meeting February 5, 2009 (Society for Automotive Engineers and NHTSA).
- Strother CE, Smith GC, James MB, and Warner CY, 1984. Injury and Intrusion in Side Impacts and Rollovers. *SAE Technical Paper Series* No. 840403. Troy, MI.
- Tamura A, Watanabe I, and Miki K, 2005. „Elderly Human Thoracic FE Model Development and Validation”, in *Proceedings of the 19th International Technical Conference on the Enhanced Safety of Vehicles*. Paper No. 05-0229.
- Tencer A, Kaufman R, Mack C, and Mock C, 2005. "Factors Affecting Pelvis and Thoracic Forces in Near-Side Impact Crashes: a Study of US-NCAP, NASS and CIREN Data". *Accident Analysis and Prevention* 37, pp. 287–293.
- Tencer A, Kaufman R, Huber P, and Mock C, 2005. "The Role of Door Orientation on Occupant Injury in a Nearside Impact: a CIREN, MADYMO Modeling and Experimental Study". *Traffic Injury Prevention* 6, pp. 372–378.
- Thomas P, Frampton R, 1999. "Injury Patterns in Side Collisions - A New Look with Reference to Current Test Methods and Injury Criteria" *SAE Technical Paper Series* No. 99SC01.
- Thunert C, 2012. "CORA Release 3.6 User's Manual". Retrieved from <http://www.pdb-org.com/en/information/18-cora-download.html>

- Thunnissen J, Wismans J, Ewing CL, and Thomas DJ, 1995. "Human Volunteer Head-Neck Response in Frontal Flexion: A New Analysis". In *Proceedings of the 39th Stapp Car Crash Conference*, Paper No. 952721, San Diego, CA.
- Trosseille X, Baudrit P, Leport T, and Vallancien G, 2008. "Rib Cage Strain Pattern as a Function of Chest Loading Configuration." *Stapp Car Crash Journal* 52, pp. 205–231.
- Trosseille X, Baudrit P, Leport T, Petitjean A, Potier P, and Vallancien G, 2009. "The Effect of Angle on the Chest Injury Outcome in Side Loading". *Stapp Car Crash Journal* 53, pp. 403–419.
- Trosseille X, Petitjean A, 2010. "Sensitivity of the WorldSID 50th and ES-2re Thoraces to Loading Configuration". *Stapp Car Crash Journal* 54, pp. 259–287.
- United States Federal Code, 2008 "Title 49: Transportation, Part 572 – Anthropometric Test Devices". *United States Code of Federal Regulations*. Retrieved from www.access.gpo.gov/nara/cfr/waisidx_08/49cfr572_08.html
- "U.S. Environmental Protection Agency's Smart Way Partnership Program: Recommendations and Findings". U.S. EPA, 2014. Retrieved from <https://www.epa.gov/sites/production/files/2014-09/documents/smartway-wkgrp-report-042014.pdf>
- Viano DC, Lau IV, Andrzejak DV, and Asbury C, 1989. "Biomechanics of Injury in Lateral Impacts". *Accident Analysis and Prevention*, Vol. 21 (6), pp. 535–551.
- Viano DC, Parenteau CS, 2016. "Difference in Dummy Responses in Matched Side Impact Tests of Vehicles with and without Side Airbags". *Traffic Injury Prevention* 17 (5), pp. 524–529.
- Viano DC, Patel M, and Ciccone MA. 1989b. "Patterns of Arm Position during Normal Driving." *Human Factors* 31 (6), pp. 715–720.

- Viano DC 1991. "Evaluations of Injury Risks by Armrest Loading in Side Impacts".
Proceedings of the 35th Stapp Car Crash Conference, SAE Technical Paper Series,
No. 912899. Society of Automotive Engineers, Troy, MI.
- Viano DC 1994. "Comparison of Arm Up and Down in Side Impacts with BioSID and
Different Armrests". *Journal of Biomechanical Engineering* 116, pp. 271-277.
- Vilhena L, Ramalho A, 2016. "Friction of human skin against different fabrics for medical
use". *Lubricants* 4, pp. 1–10.
- Wang HC, 1995. "Development of a Side-Impact Finite Element Human Thoracic Model".
PhD dissertation, Wayne State University, Detroit, MI.
- Wang JT, 2014. "Phase II Plan and Status of the Global Human Body Model Consortium",
2014 Government and Industry Meeting, Jan 22-24, Washington DC.
- Watson B, 2010. "Evaluation of Thoracic Response in Side Impact Crash". *MASc thesis*,
University of Waterloo, Waterloo, ON, Canada.
- Watson B, Cronin DS, 2011. Side impact occupant response with varying positions.
International Journal of Crashworthiness 16 (5), pp. 569–582.
- Weaver AA, Danelson KA, Armstrong EG, Hoth JJ, and Stitzel JD, 2013. "Investigation of
pulmonary contusion extent and its correlation to crash, occupant, and injury
characteristics in motor vehicle crashes". *Accident Analysis and Prevention* 50, pp.
223–233.
- Welsh R, Morris A, and Hassan A, 2007. "Injury Outcomes in Side Impacts Involving
Modern Passenger Cars", in *Proceedings of the 20th International Technical
Conference on the Enhanced Safety of Vehicles*, Paper No. 07-0097.
- Wismans J, Happee R, and van Dommelen JAW, 2005. "Computational human body
models", in *IUTAM Proceedings on Impact Biomechanics: From Fundamental
Insights to Applications*, Michael D. Gilchrist, ed., Springer Academic Publishers,
Dordrecht, pp. 417–429.

- Wismans J, van Oorschot H, and Woltring HJ, 1986. "Omni-Directional Human Head-Neck Response", in *Proceedings of the 30th Stapp Car Crash Conference*, Paper No. 861893, San Diego, CA.
- "WorldSID 50th Dummy", Hi-Tech, 2018. Retrieved from <https://hitech.com.sg/products.php?type=Dummy>
- Yen RT, Fung YC, and Liu SQ, 1988. "Trauma of Lung Due to Impact Load", *Journal of Biomechanics* 21(9), pp. 745–753.
- Yoganandan N, Pintar FA, 1997. "NHTSA Test Reports: Side Impact Test with Human Surrogate: B3120, B3122, B3155, B3588, B3663, B3664, B3700, B3276, B3277, and B3719". National Highway Transport Safety Administration, Washington, DC.
- Yoganandan N, Pintar FA, Stemper BD, Gennarelli TA, and Weigelt JA. 2007. "Biomechanics of Side Impact: Injury Criteria, Aging Occupants, and Airbag Technology." *Journal of Biomechanics* 40 (2), pp. 227–243.
- Yoganandan N, Humm JR, Pintar FA, and Brasel K, 2011. Region-Specific Deflection Responses of WorldSID and ES2-re Devices in Pure Lateral and Oblique Side Impacts. *Stapp Car Crash Journal*, 55, pp. 351–378.
- Yuen KF, Cronin DS, and Deng YC, 2008. "Lung Response and Injury in Side Impact Conditions," *Proceedings of the International Research Council on Biomechanics of Injury (IRCOBI) Conference*, Bern, Switzerland.
- Yuen KF, 2010. "The Development of a Numerical Human Body Model for the Analysis of Automotive Side Impact Lung Trauma". *MASc thesis*, University of Waterloo, Waterloo, ON, Canada.

Appendix A

Supplementary figures for Chapter 4

Two-level interactions between the door trim material properties were assessed through marginal means plots (Montgomery 2012) of chest deflections predicted at three rib levels of the ATD (Fig. A.1). Sensitivity of the ATD model to the parametric changes was very low, and responses predicted for different combinations of the door material properties were returning similar responses. The similarity of the responses was reflected by overlapping results of chest deflection predicted in runs with different door material properties.

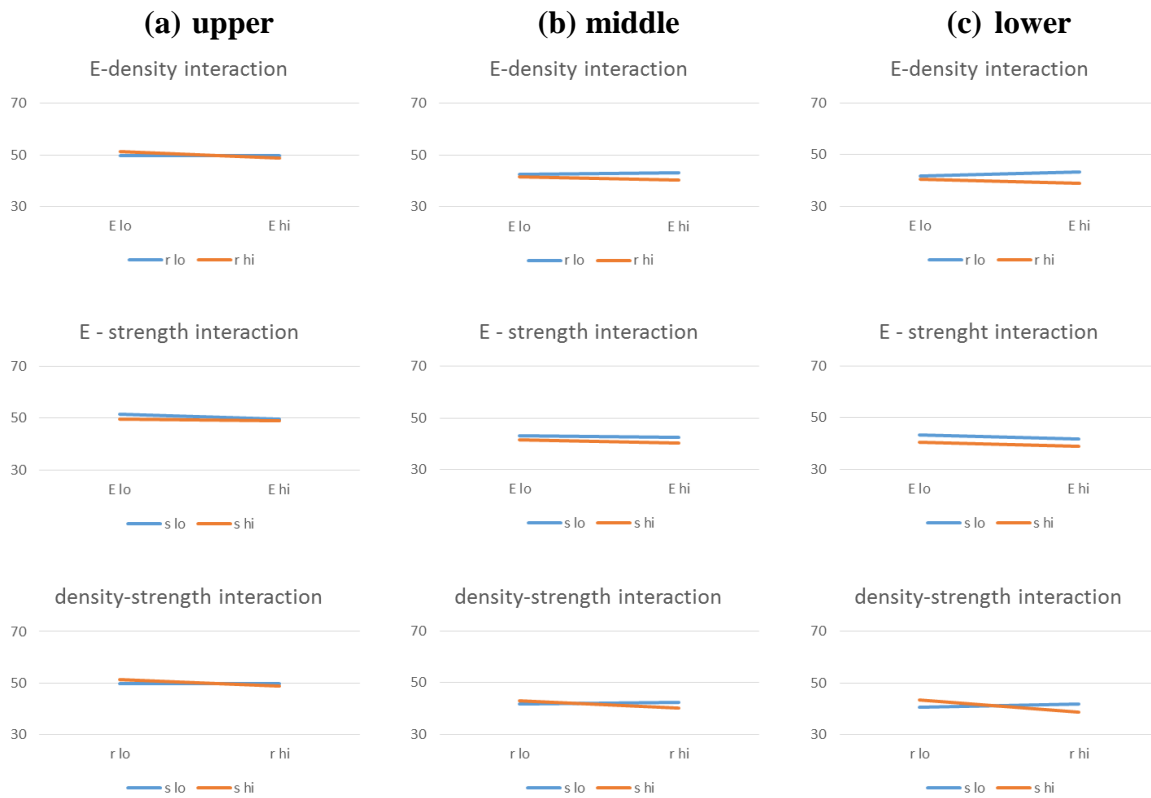


Figure A.1: Marginal means plots visualizing mean factors effects and two-factor interactions between the Young's modulus, density, and yield strength, predicted by the ATD at the three rib levels.

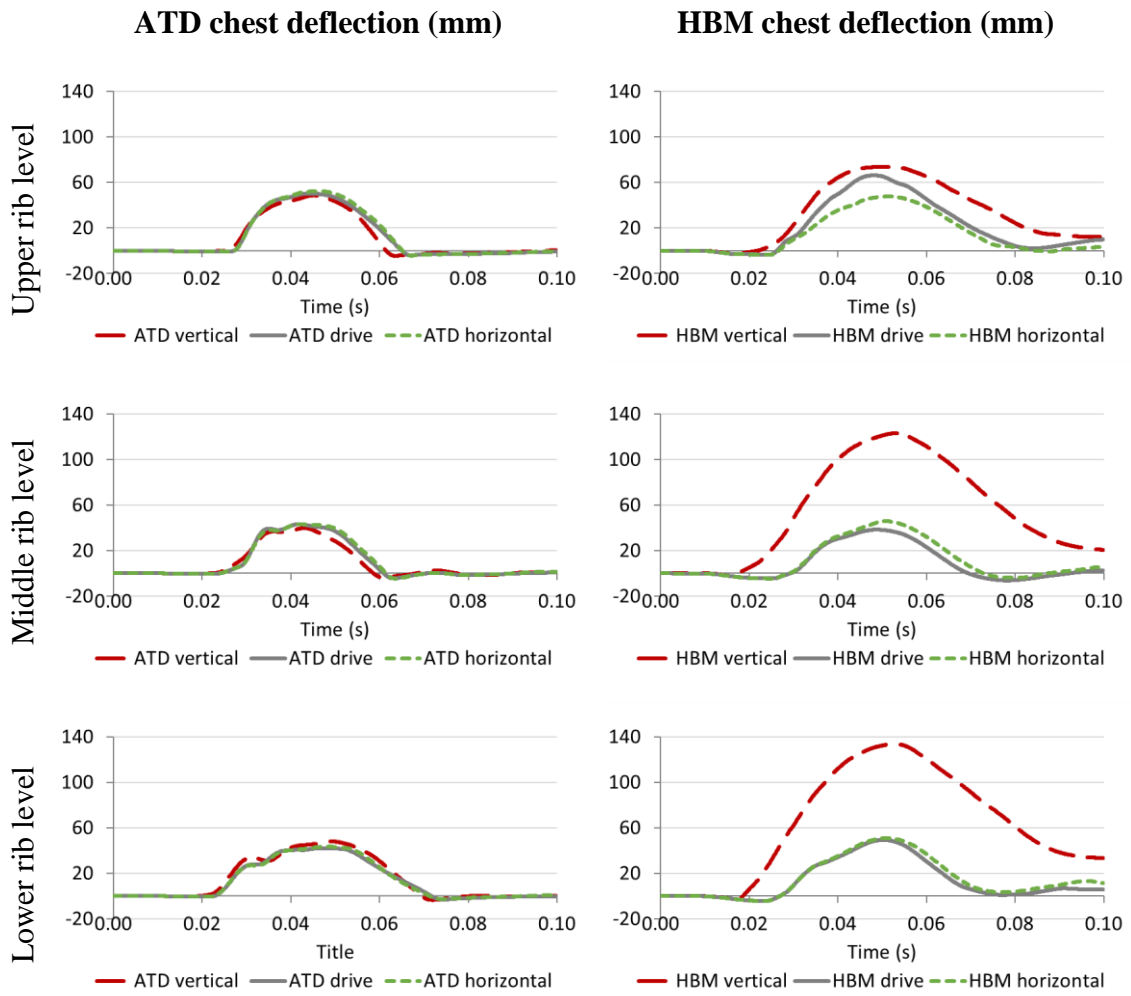


Figure A.2: Comparison of chest deflection time histories of the UW-HBM and ATD at three rib levels.

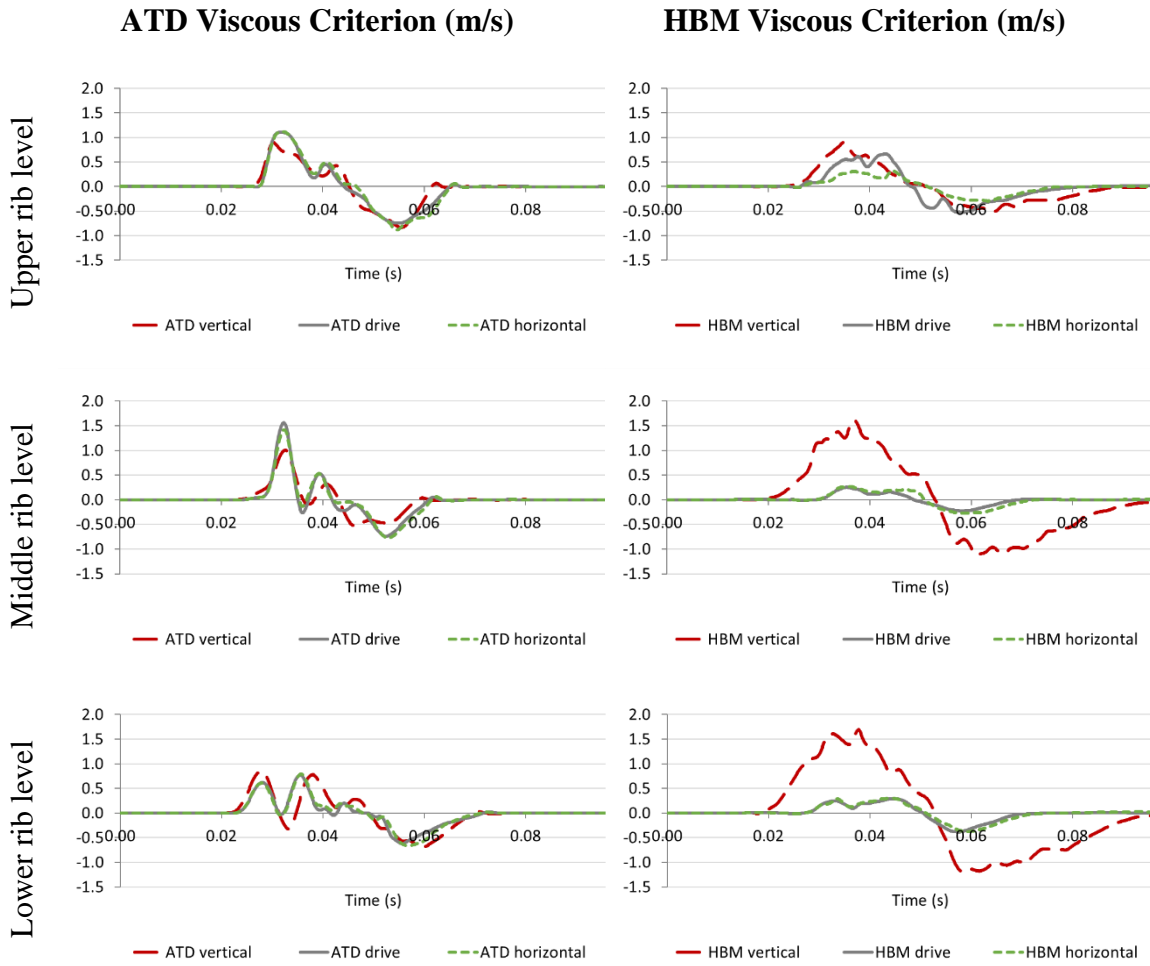


Figure A.3: Comparison of Viscous Criterion time histories of the UW-HBM and ATD at three rib levels.

Table A.1: Chest deflection and VC response on different chest band levels. Base – baseline material properties. Low – lower boundary for material properties. High – upper boundary for material properties.

Arm position							Density						
defl max [mm]	ATD			HBM			defl max [mm]	ATD			HBM		
	vertical	driving	horizontal	vertical	driving	horizontal		low	base	high	low	base	high
up	49	50	52	79	66	47	up	51	50	51	62	66	55
mid	40	43	43	123	38	46	mid	44	43	43	38	38	36
low	48	42	43	134	49	51	low	43	42	43	51	49	42

Arm position							Density						
VC max [m/s]	ATD			HBM			VC max [m/s]	ATD			HBM		
	vertical	driving	horizontal	vertical	driving	horizontal		low	base	high	low	base	high
up	0.90	1.11	1.12	0.90	0.67	0.32	up	1.03	1.11	1.05	0.64	0.67	0.67
mid	1.00	1.56	1.42	1.62	0.25	0.27	mid	1.53	1.56	1.48	0.28	0.25	0.33
low	0.84	0.77	0.79	1.69	0.29	0.30	low	0.89	0.77	0.81	0.33	0.29	0.46

Young's modulus							Yield strength						
defl max [mm]	ATD			HBM			defl max [mm]	ATD			HBM		
	low	base	high	low	base	high		low	base	high	low	base	high
up	51	50	50	62	66	56	up	52	50	50	66	66	52
mid	43	43	42	38	38	37	mid	45	43	42	37	38	35
low	45	42	40	48	49	49	low	41	42	42	50	49	39

Young's modulus							Yield strength						
VC max [m/s]	ATD			HBM			VC max [m/s]	ATD			HBM		
	low	base	high	low	base	high		low	base	high	low	base	high
up	1.06	1.11	1.01	0.70	0.67	0.69	up	1.14	1.11	1.06	0.76	0.67	0.59
mid	1.34	1.56	1.38	0.32	0.25	0.27	mid	1.51	1.56	1.47	0.30	0.25	0.35
low	0.93	0.77	0.70	0.50	0.29	0.34	low	0.91	0.77	0.77	0.44	0.29	0.43

Table A.2: Correlation ratings on three rib levels: d – driving position, h – horizontal position, v – vertical position. Base – baseline material properties, low – lower boundary for material properties, high – upper boundary for material properties.

Arm position							Density						
deflection	ATD			HBM			deflection	ATD			HBM		
	correlation	d-v	d-h	h-v	d-v	d-h		h-v	correlation	base-low	base-high	high-low	base-low
up	0.95	0.97	0.89	0.85	0.85	0.76	up	1.00	0.98	0.99	0.96	0.92	0.95
mid	0.92	0.98	0.87	0.55	0.90	0.64	mid	1.00	0.99	1.00	0.99	0.94	0.95
low	0.93	0.99	0.94	0.64	0.95	0.69	low	0.99	1.00	0.99	0.95	0.96	0.92

VC							Density						
deflection	ATD			HBM			deflection	ATD			HBM		
	correlation	d-v	d-h	h-v	d-v	d-h		h-v	correlation	base-low	base-high	high-low	base-low
up	0.93	0.96	0.90	0.90	0.71	0.68	up	0.98	0.98	0.99	0.93	0.70	0.83
mid	0.84	0.97	0.85	0.60	0.85	0.65	mid	1.00	0.99	0.99	0.98	0.91	0.92
low	0.85	0.96	0.88	0.64	0.97	0.65	low	0.97	0.97	1.00	0.97	0.55	0.73

Young modulus							Yield strength						
deflection	ATD			HBM			deflection	ATD			HBM		
	correlation	base-low	base-high	high-low	base-low	base-high		high-low	correlation	base-low	base-high	high-low	base-low
up	1.00	0.99	1.00	0.95	0.93	0.97	up	0.97	0.99	0.97	0.92	0.90	0.98
mid	1.00	1.00	1.00	0.97	0.99	0.99	mid	0.96	0.99	0.95	0.94	0.93	0.99
low	0.97	0.97	0.94	0.95	0.99	0.95	low	0.97	1.00	0.97	0.96	0.95	0.99

VC							Yield strength						
deflection	ATD			HBM			deflection	ATD			HBM		
	correlation	base-low	base-high	high-low	base-low	base-high		high-low	correlation	base-low	base-high	high-low	base-low
up	0.99	0.98	0.97	0.93	0.84	0.90	up	0.96	0.98	0.94	0.99	0.69	0.77
mid	0.95	0.93	0.98	0.94	0.98	0.95	mid	0.98	0.97	0.96	0.98	0.91	0.94
low	0.93	0.94	0.88	0.92	0.92	0.91	low	0.98	0.98	0.99	0.88	0.81	0.83

